(2)

Thermo Electron Technologies Corporation

TTC-2459-R
17 June 92
Copy No. 11

TRANSVERSE DIODE PUMPING OF SOLID-STATE LASERS

Final Technical Report

Contractor:
Thermo Electron Technologies Corporation
9550 Distribution Avenue
San Diego, CA 92121-2305

Contract Number:
N00014-87-C-2412

Effective Date of Contract:
24 September 87

Expiration Date of Contract:
31 March 92

Reporting Period:
24 September 87 - 31 March 92,
CLINS 0001 & 0002,
CLINS 0003 & 0004,
CLINS 0005 & 0006

Principal Investigator:
Eric Korevaar
(619) 578-5885

Sponsored By:
Naval Research Laboratory
4555 Overlook Avenue, S.W/
Washington, DC 20375-5000

SECURITY CLASSIFICATION OF THIS PAGE

REPORT DOCUMENTATION PAGE

1a. REPORT SECURITY CLASSIFICATION Unclassified	1b. RESTRICTIVE MARKINGS
2a. SECURITY CLASSIFICATION AUTHORITY	3. DISTRIBUTION / AVAILABILITY OF REPORT
2b. DECLASSIFICATION / DOWNGRADING SCHEDULE	
4. PERFORMING ORGANIZATION REPORT NUMBER(S) TTC-2459-R	5. MONITORING ORGANIZATION REPORT NUMBER(S) N00014-87-C-2412
6a. NAME OF PERFORMING ORGANIZATION Thermo Electron Technologies Corporation 6b. OFFICE SYMBOL (*if applicable*) TTC	7a. NAME OF MONITORING ORGANIZATION DCMAO, San Diego
6c. ADDRESS (*City, State, and ZIP Code*) 9550 Distribution Avenue San Diego, CA 92121-2305	7b. ADDRESS (*City, State, and ZIP Code*) 7675 Dagget Street, Suite 200 San Diego, CA 92111-2241
8a. NAME OF FUNDING / SPONSORING ORGANIZATION Naval Research Laboratory 8b. OFFICE SYMBOL (*if applicable*) NRL	9. PROCUREMENT INSTRUMENT IDENTIFICATION NUMBER
8c. ADDRESS (*City, State, and ZIP Code*) 4555 Overlook Avenue, S.W. Washington, D.C. 20375-5000	10. SOURCE OF FUNDING NUMBERS PROGRAM ELEMENT NO. / PROJECT NO. / TASK NO. / WORK UNIT ACCESSION NO.

11. TITLE (*Include Security Classification*)
Transverse Diode Pumping of Solid-State Lasers

12. PERSONAL AUTHOR(S)
Eric Korevaar

13a. TYPE OF REPORT	13b. TIME COVERED	14. DATE OF REPORT (*Year, Month, Day*)	15. PAGE COUNT
Final Report	FROM 9/24/87 TO 3/31/92	5/29/92	95 pages

16. SUPPLEMENTARY NOTATION

17. COSATI CODES			18. SUBJECT TERMS (*Continue on reverse if necessary and identify by block number*)
FIELD	GROUP	SUB-GROUP	Diode Pumped Lasers; Tm,Ho:YAG Lasers; Nd:YAG Lasers; Diode Pumping Geometry

19. ABSTRACT (*Continue on reverse if necessary and identify by block number*)

The transverse pumping of solid-state lasers in a cylindrical rod configuration has been explored both analytically and experimentally. The pumping configuration coupled diode laser arrays to the laser rod through slits in a geometrically reflecting chamber using simple lenses. 50 W of diode lasers in the form of ten 5 W, 1 cm bars were used to pump 2 cm of a Nd:YAG rod. Output powers for 3 mm and 4 mm diameter rods were compared with and without the reflecting multi-pass pump cavity. An increase in output power of 35% was achieved by using the multi-pass cavity, approximately in agreement with expectations. Although threshold pump powers agreed with our analysis, slope efficiencies were much lower than expected, and output powers seemed to saturate at 2.5 W with 35 W incident on the rod. Detailed data on the beam profiles and wavelength distributions of the diode laser bars is also presented.

20 DISTRIBUTION / AVAILABILITY OF ABSTRACT ☒ UNCLASSIFIED/UNLIMITED ☐ SAME AS RPT. ☐ DTIC USERS	21. ABSTRACT SECURITY CLASSIFICATION Unclassified
22a. NAME OF RESPONSIBLE INDIVIDUAL Eric Korevaar	22b. TELEPHONE (*Include Area Code*) (619) 578-5885 22c. OFFICE SYMBOL

DD FORM 1473, 84 MAR 83 APR edition may be used until exhausted. All other editions are obsolete.

SECURITY CLASSIFICATION OF THIS PAGE

SUMMARY

The transverse pumping of solid-state lasers in a cylindrical rod configuration has been explored both analytically and experimentally. This work is a continuation of, and expansion on, earlier geometrical optics and wave optics analyses of similar geometries. The prior work was documented and reported in TTC Technical Report TTC-1529-R, dated 6 January, 1989.

The emphasis of this phase of the project is to demonstrate experimentally the performance of a Nd:YAG laser transversely pumped with commercially available diode lasers, and to compare the results with analyses and models developed under the program. Because of the current cost of suitable commercial diode lasers, these experiments were carried out with Nd:YAG rods of 3- and 4-mm diameter, and a pumped length of 2 cm. Ten 1-cm long diode arrays, each rated at 5 watts output, provide 50 watts of total pump light. We measured laser performance as a function of laser rod diameter, single- or multi-pass pump geometry, and pump power. A preliminary measurement of thermal lensing in the laser rod was consistent with analytic expectations.

A novel aspect of analyses and experiments is the use of a solid pump cavity, as opposed to a conventional gas-filled pump cavity. The multi-pass pump cavity was fabricated by plating the reflector on the outside of a solid cylinder of clear fused quartz, and boring a clearance hole through the center for the laser rod and coolant channel. The resultant device is rugged and the pump cavity reflecting surface is protected from oxidation, atmospheric attack, and accidental coolant spills. Extension of this configuration to militarized systems could include mounting of the laser resonator optics to the ends of the pump cavity, providing a single, rigid structure that could be inherently thermally compensated.

Initial alignment stability of the pump diode lenses proved inadequate, leading to non-reproducible and inconsistent laser performance data. Accordingly, issuance of this report has been delayed until some of the data could be retaken under more controlled conditions. This report revision incorporates these latest results.

Transverse-pumped cylindrical solid-state laser designs are intermediate in average power between face- or side-pumped slab geometries and end-pumped rod geometries. Slab geometries have shorter thermal diffusion paths than equal-volume rod geometries, and thus should be capable of extrapolation to higher power operation. Issues of utilization of the pump light, and limiting degradation of the laser beam quality in the slab geometry are being actively addressed by other organizations. Slab-laser geometries will especially benefit from the future development of two-dimensional diode laser arrays.

The second alternative, end-pumped geometries provide ease of shaping the radial gain profile in the laser medium for control of the laser modes generated. However, end pumping results in significant longitudinal gain variation if the available pump light is to be efficiently utilized. End pumping geometries incur significant limitations in the utilization of linear diode arrays, the most common form of high power diode lasers. Also, the fact that both the pump light and the intra-cavity laser field must share one or more common apertures (laser rod end and cavity end mirror) leads to a thin-film coating damage issue. The transverse pumped geometry avoids the longitudinal gain profile problem and coating damage issues, allowing extension of the rod-geometry solid-state laser to higher power operation than end-pumped geometries are able to achieve. These benefits come at the expense of increased difficulty controlling the radial gain profile and laser transverse mode structure, and require more attention to assure efficient utilization of the available pump light.

Transversely pumped rod geometries may have the pumping diode-laser arrays located either close to the laser rod, or remotely. Close coupling reduces the need for optics in the pump paths, but makes multiple-pass pumping for efficient utilization of the pump light difficult. Moving the pumping diodes away from the rod, as TTC and NRL have chosen for this demonstration program, provides several advantages, at the cost of increased complexity of the optics in the pump paths. The greatest advantage is the ability to introduce a pump reflector and utilize multi-pass absorption of the pump light, increasing efficiency while providing greater ability to shape the pump distribution and radial gain profile in the rod. Moving the diodes a few centimeters away also provides the laser system engineer with greater flexibility in routing cooling for both the laser rod and the diodes, as well as for bringing electrical power leads to the diodes. These advantages will become more apparent as devices are incorporated into systems and realistic maintenance and repair strategies developed.

We demonstrated that low cost Fresnel lenses provide an attractive alternative meeting the pump optics requirements in this geometry. Simple, replaceable, diode-lens modules will significantly simplify field laser maintenance.

The use of low-cost liquid coolers for the diode arrays was also demonstrated. Their use reduces system cost and potentially leads to substantial improvement in over-all system efficiency. We utilized a TTC proprietary one-half inch square cooler developed for high-power adaptive optics mirror applications.

The laser performance observed, with up to 35 watts of pump light, is consistent with most of our expectations. Both 3- and 4-mm diameter rods were used in single pass and our unique multi-pass pumping geometry. The near-threshold performance of the 4-mm rod was as expected, while the 3-mm results show effects of pumping non-uniformity. The 4-mm rod geometry showed performance improvement with multi-pass pumping consistent with calculations. Performance of both rods substantially above threshold is below expectations, the 4-mm rod giving a peak of 2.94 watts output with 35 watts of pump light available. We attribute this low output to gain depletion by an unidentified mechanism. The far-field mode pattern observed, although not optimal, is consistent with these preliminary experiments. Thermal lensing observed in the rod also is consistent with predictions, based on the low heat deposition in the laser medium by the diode laser pump sources. Follow-on experiments need to identify the cause of the gain roll-over, optimize the gain profile, improve the diode light utilization with improved collimation optics, and refine the experimental technique, set up, and data.

The following were explicitly demonstrated:

- The diode-lens pairing allows standing off the diodes from the rod while maintaining efficient utilization of the diode light. In these first demonstrations, approximately 70 percent of the diode light was incident on a 3-mm diameter rod more than 5 cm away.

- The multi-pass pump cavity geometry allows efficient pumping of small rods in the transverse geometry. The multi-pass geometry demonstrated approximately a 35 percent increase in pumping efficiency, despite the fact that our first pumping cavity had an internal reflectivity of only about 80 percent.

- Linear diode arrays can be effectively water cooled, with sufficient heat removal and temperature stability to effectively pump Nd:YAG, eliminating the significant system losses associated with thermoelectric cooling.

Some problems were identified, as follows:

- The losses from the diodes to the rod on the first pass were excessive, approaching 25 percent. This requires improvement.

- The internal reflectance of our pump cavity was below expectations, just exceeding 80 percent. This requires improvement.

- We had inadequate pump power available to adequately explore thermal limitations and effects.

- Some mechanism, not unambiguously identified, limited the unsaturated gain and resultant output power to very low levels.

- Our 4-mm rod threshold data were generally consistent with our analyses, but insufficient above-threshold data were available to fully verify the calculated power flows in the laser oscillator.

- Our 3-mm rod experiments were not optimized and suffered from inconsistencies, perhaps due to alignment.

The following specific experiments and analyses are recommended in order to exploit the results of this work:

- Identify and solve the gain-depleting mechanism limiting the laser output power.

- Evaluate point designs utilizing improved optics for collimation of the diode output light into the laser rod.

- Improve the pumping wheel design to increase the internal reflectivity, anti-reflection coat the entrance windows, and match the size of the windows to the diode-lens configuration to minimize losses.

- Performance of lasers with limited available pump power is critically sensitive to passive losses. Our rods, especially the 4-mm diameter rod, had excessive losses, limiting the efficiency and output power. The full significance of this work will not be apparent until we obtain a truly low-loss rod with excellent AR coatings, and repeat the experiments.

- Extend the analysis of multiple pump diode arrays beyond the upper limit of 11 examined in our calculations to date.

Table of Contents

	Summary	iii
	Contents	vi
	List of Figures	vii
I.	Introduction	1
II.	Previous Results	10
III.	Laser Design and Pumping Analysis	13
IV.	Diode Laser Characteristics	36
V.	Experimental Results and Comparison with Analyses	57
VI.	Laser System Design Considerations	73
VII.	Conclusions and Recommendations	81
	Appendices	84

List of Figures

1	Multipass Transverse Pumping Geometry	2
2	A Diode-Pumped, Cylindrically Symmetric Laser Geometry	11
3	Geometrical Optics Approximation and Diffraction Integral Calculation of Pump Light Intensity in a Caustic Region	11
4	Efficiency versus Available Power and Output Coupler, 3-mm Rod	15
5	Efficiency versus Available Power and Output Coupler, 4-mm Rod	16
6	Efficiency versus Output Coupler and Available Power Times Induced Emission Cross Section, 3-mm Rod	17
7	Thermal Lensing versus Dissipated Power	18
8	Ray Paths Inside YAG Laser Rod	21
9	A Non-Uniform First-Pass Pump Intensity Profile	22
10	Uniformity versus Number of Diodes, RMS and Average Error from the Mean	24
11	Uniformity versus Number of Diodes, Peak-to-Valley Ratio	24
12	Uniformity versus Focusing Delta, RMS and Average Error from the Mean	25
13	Uniformity versus Focusing Delta, Peak-to-Valley Ratio	25
14	Uniformity versus Sigma-R Product, Peak-to-Valley Ratio for Five Diodes	26
15	Uniformity versus Sigma-R Product, Peak-to-Valley Ratio for Eleven Diodes	26
16	Pump Intensity Profile, 5 Diodes, 4-mm Rod, $\sigma = 4$ cm^{-1}, $\delta = 0.67$	27
17	Pump Intensity Profile, 11 Diodes, 4-mm Rod, $\sigma = 4$ cm^{-1}, $\delta = 1.0$	27
18	Relative Absorption for Multiple Passes versus Delta, Five Diodes	29
19	Relative Absorption for Multiple Passes versus Cavity Reflectivity	29
20	AR-coated Cylindrical Collimating Lens	32
21	Diode-Lens Losses versus Temperature, Initial Data, 2.85-mm Slit	32
22	Diode-Lens Loss Versus Divergence, New Data, 4-mm Slit	32
23	Slit Transmission, New Data, Diode to Rod-Center ≅ 6 cm	32
24	Diode Operating Parameters	34
25	Pumping Ray Trace Through 3-mm Rod	34

List of Figures (continued)

26	Witness Reflectivity versus Wavelength	36
27	SDL-3480-L Typical Input-Output Curve	39
28	SDL-3480-L Package Outline	39
29	Measured Transmission Through 0.292-cm Rod Diameter	39
30	Multi-Mode Spectrum, One of 20 Lasers	41
31	Diode Wavelength versus Temperature	42
32	Diode Laser Wavelength versus Position Along Bar	44
33	Change in Spectral Width with Temperature	45
34	Diode Efficiency versus Output Power at Room Temperature	45
35	Diode s/n 45 Efficiency versus Temperature at 4.0 Watts Output	45
36	Diode Current versus Age and Temperature	46
37	Diode Laser Power versus Input Current at Room Temperature	47
38	Diode Laser Efficiency versus Serial Number	47
39	Horizontal Diode Beam Profiles with Gaussian Fits	48
40	Diode Horizontal Beam Divergence versus Serial Number	49
41	Horizontal Beam Profile at Three Positions Along Array	50
42	Vertical Beam Profile versus Distance, Diode s/n 39	51
43	Diode Laser Vertical Beam Profiles	52
44	Diode Mounting on TTC Cooler	54
45	Cross-sectioned Liquid Cooler and Views of Mounted Diodes	54
46	Tin Plated Over Failed Diode Facet	56
47	Single-Pass Experimental Setup	57
48	Rod Mounted in Cooling Jacket for Single-Pass Pumping	58
49	Silver-Coated, Fused Silica Multi-Pass Pumping Cavity	58
50	Assembled Multi-Pass Experiment	59
51	Laser Cavity Configuration	59
52	4-mm Rod, Single-Pass Pumping	60
53	4-mm Rod, Multi-Pass Pumping	60
54	4-mm Rod Fluorescence Output	62
55	Circumferential Parasitic Mode	62

List of Figures (continued)

56	Fraction of YAG Rod Swept by Circumferential Mode	62
57	Diode Pump Power Through 4-mm Slit	64
58	Laser Performance, 4-mm Rod, Single-Pass Pumping	64
59	Laser Performance, 4-mm Rod, Multi-Pass Pumping	64
60	Calculated and Experimental Laser Thresholds, 4-mm Rod, 3.25- and 0.4-Percent Round Trip Loss	66
61	4-mm Laser Output Performance, Calculation and Experiment	69
62	3-mm Rod, Single-Pass Pumping	70
63	3-mm Rod, Multi-Pass Pumping	70
64	Diode Pump Power Through 3-mm Slit	71
65	Laser Performance, 3-mm Rod, Single-Pass Pumping	71
66	Laser Performance, 3-mm Rod, Multi-Pass Pumping	71
67	Laser Thresholds with 3-mm Rod	72

SECTION I

INTRODUCTION

This section discusses the background and rationale for interest in pumping solid-state lasers with diode laser pump sources. Also discussed is the variety of pump geometries being explored by different investigators, where this TTC-NRL transversely pumped geometry fits into the over-all picture of choices available to future system designers, and significant issues amenable to analysis and experimental verification.

This report covers the second and third years of the program. The results of the analysis performed during the first year are summarized in Section II, which immediately follows.

Section III discusses the design of the laser experiments and the pumping analysis. Section IV discusses the diode lasers used to provide the pump light. Section V discusses the experimental results and comparisons with the analyses.

Section VI discusses system implications of the use of laser diodes to transversely pump solid-state lasers. Finally, Section VII summarizes the conclusions and recommendations for continued experiments and design effort.

Description of System

TTC is examining, analytically and experimentally, a transverse pumping geometry suitable for the application of linear array diode laser technology to the pumping of a variety of solid-state lasers. The geometry is believed to be suitable for a range of applications intermediate in power, being able to operate at higher total pump power than can end pumped geometries, but lower than achievable with slab geometries. Figure 1 shows a cross section through the geometry analyzed and tested. This geometry differs slightly from that analyzed during the first year, which is discussed in Section II.

A total of 60 watts of diode laser arrays were purchased, with 50 watts used to pump 2 centimeters of the laser rods in the experimental effort. Nd:YAG rods of 3- and 4-mm diameters, were used. All rods had a nominal 1.1 atomic percent Nd concentration.

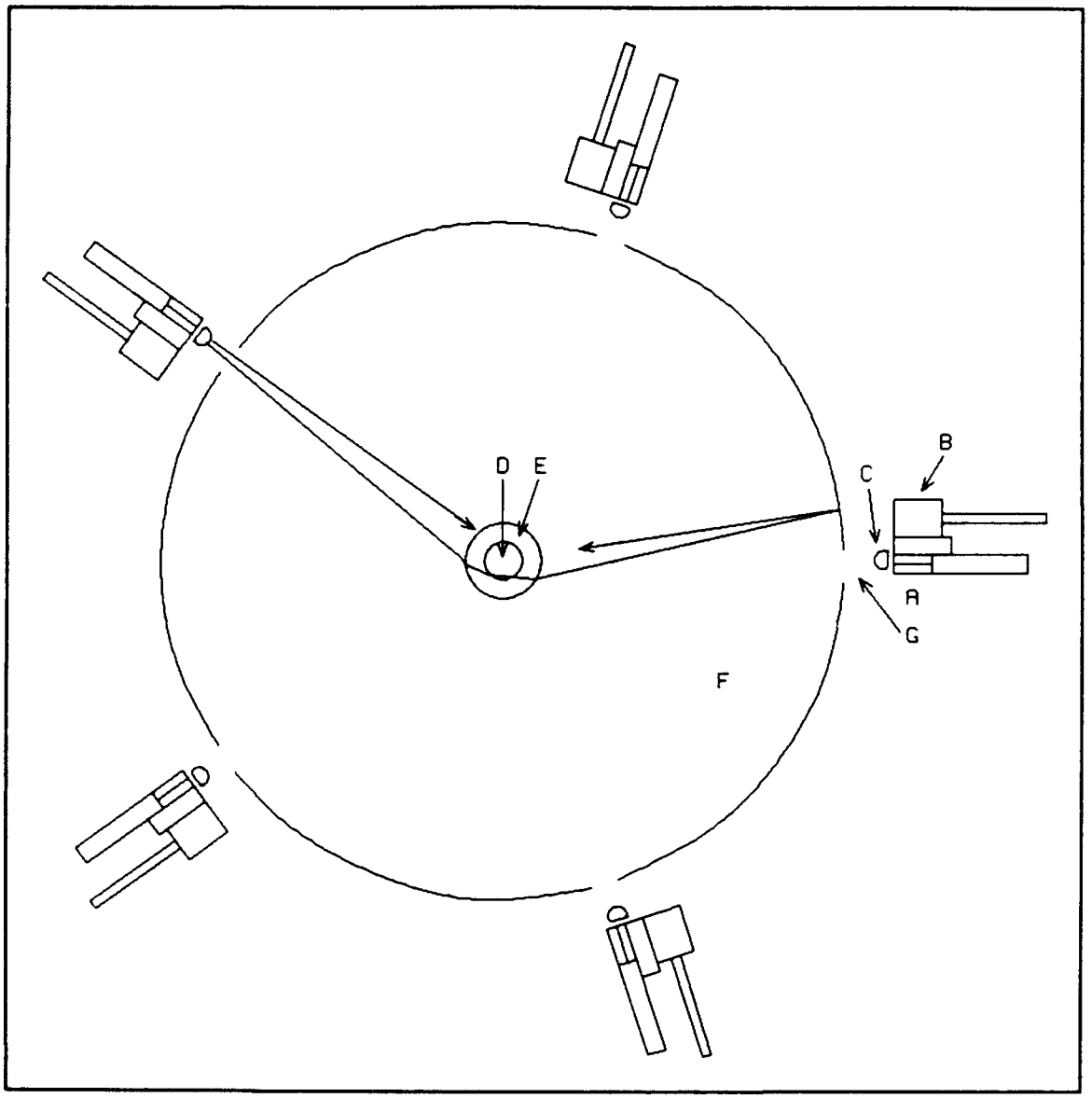

FIGURE 1
Multipass Transverse Pumping Geometry

Components include (A) Diode Laser, (B) TTC Liquid Cooling Unit, (C) Diode Light Collimating Lens, (D) Laser Rod, (E) Coolant Channel, (F) Internally Reflecting Pump Cavity, and (G) Entrance Windows

Major features of the geometry in Figure 1 include the following:

- Multiple linear diode arrays are located around the periphery of the solid-state laser rod, aligned with their axes parallel with the rod axis.

- The diodes are located sufficiently far from the laser rod that there is room to introduce a reflecting cavity to allow multiple pass absorption of the pump light, improving efficiency.

- The system designer is able to take advantage of the multiple-pass pump geometry to tailor the absorption depth in the laser rod to achieve a specified radial gain profile.

- With the diodes spaced away from the rod, adequate space is available to route cooling and power.

- The pump cavity, a solid piece of fused silica, makes a rugged, monolithic structure possible, and protects the pump cavity reflecting surface from oxidation and damage.

- The rod is pumped with a uniform longitudinal profile.

- The geometry is generally applicable to a variety of other solid-state laser systems, including Ho:Tm:YAG (or YLF), Nd:YLF, and Nd:BEL.

Background: Diode Pumping

Diode pumping of Nd:YAG attracts attention due to theoretical advantages in efficiency. This higher efficiency derives from the narrow spectrum of the diode emission, which can be tuned to an absorption peak of the laser material, eliminating the non-useful energy dominating flashlamp output spectra. The elimination of spurious light absorption in the laser host reduces its thermal loading, potentially increasing laser output power. Higher device efficiencies also portend higher system efficiencies and lower weights, although practical systems have not, to date, necessarily demonstrated these advances. Longer system lifetimes or maintenance intervals, or greater system reliability, are also anticipated with diode-pumped systems.

Diode pumping shows a considerable cost disadvantage compared to flashlamp pumping, due to the high, but decreasing, cost of the diodes. There are two major application areas where other considerations can out-weigh the cost premium: applications requiring laser output power or beam quality unachievable with the

additional heat loading inherent to flashlamp-pumped systems, and applications where weight and efficiency issues are paramount, as in space.

The system efficiency advantage has not materialized so far, primarily because of a relative lack of sophistication in diode cooling systems. Although diodes are more efficient light sources than flashlamps, they represent concentrated heat loads requiring comparatively complex cooling technology. Also, while flashlamp performance is relatively temperature independent, the narrow spectral output of diodes must be held closely on the absorption line of the laser material being pumped. Although injection locking techniques are being developed to ease requirements, to date this spectral control has been achieved by close temperature control, of the order of a degree Celsius. Heat removal and temperature control are often achieved with thermoelectric coolers, which erode the over-all system efficiency and raise the weight.

Although Thermo Electron Corporation is a long-time leader in thermoelectric cooling technology, the elimination of thermoelectric cooling was a high priority in this effort. We chose to use direct liquid cooling of the diodes, reducing cost and weight. TTC has developed, for other optical applications, a small liquid heat exchanger of suitable performance. We are aware Lawrence Livermore National Laboratory is also pursuing liquid cooling for similar reasons. They have pursued very high heat transfer coefficient devices, using microchannel technology evolved from integrated circuit cooling developments at Stanford University. The microchannel technology may easily be over-optimized for heat transfer rate, leading to potential channel blockage problems in military field applications.

Practical direct liquid cooling benefits from reduction of the sensitivity to diode emission wavelength. The TTC-NRL transverse-pumped geometry with multi-pass absorption, shown in Figure 1, directly supports this design objective. By allowing multiple passes for the pump light, the wavelength does not have to be closely held right on a narrow absorption peak. Indeed, slight detuning allows better control of the radial gain profile, reduced sensitivity to system environment, and independent optimization of laser doping, without unacceptable degradation of pump light utilization efficiency. YAG is the worst-case laser host for this constraint, having the narrowest pump absorption lines. Other hosts of interest to the Navy will ease the temperature control requirements. The multi-pass pumping geometry allows use of lasers with lower pump band absorption coefficients than would be otherwise satisfactory for transverse pumping.

System cost is also driven by whether the application is cw, quasi-cw, or pulsed. For a given investment in gallium arsenide, the cost minimizes if the maximum average power is extracted from the diodes. The cw case probably always wins here, but it constrains the system pulse repetition frequency (PRF) to be of the order of or greater than the reciprocal of the laser's storage lifetime. Nd:YAG is again a bad

choice, having typical storage lifetimes of 100 to 230 microseconds, and considerable interest has focused on holmium systems in search of multi-millisecond storage lifetimes. Recent progress in quasi-cw diodes indicates that average output power can be maintained for duty cycles as low as perhaps 20 percent. Depending on the pulse widths for which this is true, it relaxes the minimum system PRF requirement by the same factor (in this case, five) before incurring a cost penalty from underutilization of the diodes. The cost penalty for underutilization of the diodes is not necessarily as bad as linear with the reciprocal of the fraction of the available average power used. Devices become cheaper as average heat flows reduce, and heatsink requirements obviously reduce as device average power decreases, with concurrent reduction of weight. Detailed system design tradeoffs are required to assess these factors.

If the pulse width becomes shorter than the thermal equilibration time across the diode's lasing channel (about a microsecond), then a substantially different class of diode designs becomes optimum, usually referred to as pulsed devices. It is unlikely that pulsed diodes will find large application as pumping devices in weight and cost constrained systems. Although their peak powers are substantial, achievable average powers are less than for equivalent cw designs. A rule of thumb is that it never pays to not take advantage of the storage properties of the laser medium.

Background: Transverse-Pumped Rod Geometry

Three geometries have received attention for diode-pumped solid state lasers: end-pumped rods, side- (transverse-) pumped rods, and edge-pumped slabs. Each has its best area of application.

End-pumped geometries allow long absorption lengths in the rod, improving the utilization of the available pump photons. This is especially critical when pump diodes and power are at a premium cost. End pumping also allows careful tailoring of the radial gain profile in the laser rod, often negating the need for mode selection elements in the lasing cavity. It is not, however, without its drawbacks. The longitudinal pump uniformity obviously suffers, a price of good absorption efficiency. All the pump power, plus the laser field, must share one face of the rod, leading to a damage-imposed limitation of the total pumping. Just as there must be a longitudinal pumping nonuniformity, there will also be a longitudinal temperature gradient, as well as a radial one. These limit end pumping to relatively low power applications.

Transverse-pumped rod geometries offer significantly greater surface for admission of the pump light. The remaining limits to the laser power are energy storage density and the resultant radial temperature gradient to the cooling channel. Transverse-pumped rod geometries have been explored by FiberTek, Herndon, VA. As mentioned above, transverse pumping suffers from the limited absorption depth,

which decreases the efficiency of utilization of pump photons. This drives the designer to one or more of the following: higher than optimum doping, poor radial gain profile, excessively tight wavelength and temperature specifications on the diodes, and/or suboptimal efficiency. The TTC-NRL multi-pass pumping is an approach to alleviate these constraints.

Slab lasers attempt to alleviate the temperature gradient problem by geometries with larger surface-to-volume ratios than rods have. In a rectangular slab, the cooling can be applied to the largest faces, while the laser beam propagates through the smallest faces. The pump light can enter through either the cooled faces or the intermediate-sized faces orthogonal to the laser axis and the temperature gradient. Although the latter geometry offers a smaller surface area for getting the pump light in, it also offers a greater absorption depth within the slab, improving efficiency. McDonnell-Douglas and Lawrence Livermore National Laboratory have shown the greatest interest in the slab geometry, because of its significantly higher average power potential.

End pumping is most applicable to low power oscillators, while transverse pumping is more relevant to intermediate-to-high power oscillators and amplifiers, up to perhaps 1 to 2 kilowatts of average laser power. Slab geometries are the only approach for multi-kW amplifiers. Achievement of high beam quality increases in difficulty as average power increases because of thermal and gain profile reasons.

The pumping geometry selected interacts with the selection of the pumping diode. End pumping is best accomplished with diodes with relatively few lasing channels, using fiber-optic coupling. Transverse-pumped geometries naturally lend themselves to linear diode arrays, which, conveniently, offer the higher power output required. Slab geometries will benefit most from the development of face-emitting diodes, a technology under active development by several diode manufacturers.

Significant Issues

The biggest single issue is the efficiency of utilization of the available pump photons, since they come from the diodes at a dear price. To the first order the system input power, weight, and cost will scale inversely with this efficiency. The TTC-NRL multi-pass geometry is 40 to 45 percent more efficient in its utilization of pump light than single-pass transverse geometries.

The absorption path available per pass is limited to the rod diameter. Practically, the average pathlength in the rod is a large fraction of the diameter, perhaps 80 percent of the diameter. Higher power applications with more pump diodes arrayed around the periphery of the rod favor increasing this fraction. The

pumping uniformity increases with an increasing ratio of pathlength to absorption depth, that is, as the absorption coefficient increases. This drives the design to operation on the peak of absorption lines, and increasing doping levels, both of which have significant detrimental side effects. As discussed earlier, operation on absorption peaks requires greater, even unreasonable, temperature control of the diodes, and resultant sensitivity of performance to environment. Increasing doping decreases storage lifetime, which decreases efficiency at a fixed repetition rate in repetitively pulsed applications.

The design of the pumping cavity involves several tradeoffs. The hollow cavity analyzed during the first phase of this program saves weight, while the solid cavity tested in the second phase provides greater protection to the reflecting surface and provides a stronger, simpler mechanical configuration. With the solid cavity, silver is an acceptable reflector, while the open cavity design requires a more inert surface, such as gold. The larger the pumping cavity diameter, the less light is lost out of the slits where the pump light enters, but the alignment is more difficult, the weight and size greater, and the light lost by missing the rod increases. There obviously is a diameter that maximizes the efficiency, although we did not look for it either analytically or experimentally.

Of concern is the formation of caustics in the pumping field within the rod, near its periphery. Caustics are regions where the geometrical optics approximation has a pole, i.e., predicts infinite pump intensity. Considerable analytical effort was spent calculating the locations of the caustics and calculating their true intensities using Fresnel's diffraction principles. Avoiding pump caustics drives one toward more costly diode collimation optics and possibly smaller pump cavity diameters. With the low power available in the experimental program, formation of pump caustics were ignored, based on the from-first-principles Fresnel calculations performed in the analytical effort.

Diode arrays have large divergences in their transverse direction, across the rod, requiring use of collimating optics at the large standoff distances involved in the TTC-NRL multi-pass pump geometry. We used simple cylindrical lenses. More complex focusing optics, including reflective optics, AR-coated Fresnel lenses, or acylindrical optics, need further analysis and thought.

Efficient utilization of the laser volume and stored energy requires control of the radial gain profile. We analyzed many of the variables involved, but were unable to experimentally explore this parameter within the scope of the contracted effort. The 4-mm diameter rod geometry showed no gross effects of radial nonuniformity, while the less-optimum 3-mm rod in the same pump cavity showed performance consistent with nonuniform pumping.

Suppression of parasitic modes is essential to avoid depletion of the stored energy and subsequent loss of efficiency. Our experimental data showed classic symptoms of gain saturation due to parasitic limiting, despite the low pump power available. Reasonable experiments ruled out longitudinal parasitic modes, and transverse modes are unrealistic. Thus, by elimination, we deduce the parasitic mode limiting the gain was circumferential. Our rod geometry is particularly susceptible to this mode. The problem is not unique, and control techniques include improving the index matching of the coolant to the YAG rod and sawing small longitudinal grooves in the rod. Solving the problem was not within the available scope of the contract, so the maximum output powers observed were less than they could have been.

Diode emission spectral widths are of the same order as the widths of single peaks in the YAG absorption spectrum. If the diode emission is to be held on an absorption peak, especially critical in single-pass transverse-pumped geometries, the permissible scatter in emission peaks between diodes in a system, and the tolerable drift of the emission peaks with time, are essentially zero. The TTC-NRL multi-pass transverse-pumped geometry described here relaxes these tolerances slightly. All emission control schemes require the diodes lase at approximately the same wavelength under similar conditions. The diodes utilized here, from Spectra Diode Laboratories, were hand selected to the tightest wavelength specification SDL would accept at reasonable prices, within a 5-nm band. This comparatively large spread was accommodated by individually temperature tuning each diode, a technique incompatible with significant system applications. LLNL has reported success obtaining unselected devices within a 1 nm spread from another vendor, a much more satisfactory situation.

NRL has performed numerous experiments on injection-locking diode arrays for the purposes of either wavelength control or far-field radiation pattern shaping. Eventual systems may utilize some technique of injection locking the diodes for wavelength control, relaxing the requirements for system temperature control. There will obviously be a tradeoff space between injection locking subsystem complexity and cooling subsystem complexity. Injection locking and its tradeoffs were not explored by TTC under this program.

Because the emission wavelength is bandgap dependent, and the bandgap is temperature dependent, diodes must typically be held to within a fraction of a degree Celsius when pumping YAG without injection lock control of their wavelength. The TTC-NRL multipass geometry relaxes this requirement, although the exact functional relationship between temperature drift and system efficiency was not determined. Conventionally, diodes have been thermoelectrically cooled, with closed-loop control, to meet temperature and wavelength stability requirements. This imposes unacceptable system penalties in weight, complexity, and efficiency. We chose to use direct liquid cooling, as LLNL also has done. We feel direct liquid cooling, although

not achieving theoretically maximum pump photon utilization efficiency, has significant positive system implications. We chose to use lower heat transfer rate coolers than LLNL has been developing for four reasons: TTC already had developed them for another optics application, they are cheap, our commercial SDL diodes have lower power density and heat transfer requirements than LLNL is designing to, and we are skeptical of the long-term utility of the fine cooling passages in LLNL's latest microchannel coolers.

Whereas flashlamp-pumped lasers allow system designers important flexibility in the location of subsystem components, diode-pumped systems are not as forgiving. The diodes require significant cooling and electrical connections, providing a challenge for the designer. An advantage of the multi-pass geometry described herein is that the designer has greater latitude in locating the diodes with respect to the laser rod.

The spatial emission patterns of linear diode arrays are usually narrow in the direction parallel with the axis of the array, that is, parallel with the axis of the laser rod. In the transverse direction the emission patterns are much broader, tens of degrees half angle. Without coupling optics, the diodes must be located directly adjacent to the laser rod in order for the rod to intercept an acceptable fraction of the pump light. In the NRL-TTC multi-pass geometry, the diodes are located further away, and collimating optics must be used with the diodes. Although these optics are not ideal (not all rays pass through the rod) and introduce additional losses due to surface reflections and scatter, they are essential. In the multi-pass geometry, any ray which misses the rod on a pass will continue to miss the rod on all future passes across the pump cavity. We used fused-silica cylindrical singlet lenses cut from rods and AR coated. We also tried commercial acrylic cylindrical Fresnel lenses. Additional improvements can be made, including evaluation of reflective coupling optics, development of acylindrical corrections to the simple lenses, and/or AR coating of the acrylic Fresnel lenses. Development of a sealed, prealigned, field replaceable module incorporating diode, collimating lens, and integral low-cost cooler would be valuable.

All the normal parameters of laser optimization, including extraction efficiency and optical beam quality also must be addressed in designing diode-pumped solid-state systems. Because of the high cost of diode pump sources, matching of the system repetition rate, upper state energy storage lifetime, and diode power cycle are comparatively more critical than in flashlamp-pumped systems.

All of these design factors combine to make the design of optimal diode-pumped systems non-trivial exercises. Multiple approaches will be required, in order to meet differing systems applications and requirements. And initial designs will fall below expectations, but will benefit from continuing design iterations, refinements, and development. Also, as diode technology improves and costs come down, optimum design points and rules of thumb will become out-dated and require revision.

SECTION II

PREVIOUS RESULTS

This report describes the progress and results of the second year of the NRL-TTC transverse diode-pumped solid-state laser demonstration program. This section summarizes the results of the prior (first year's) results, which were reported more completely in Technical Report TTC-1529-R, Transverse Pumping with Diode Lasers, 6 January 1989.

Uniformity and Caustics in Transversely Pumped Geometries

The transverse pumping of a cylindrical laser rod (such as YAG) by an arrangement of diode laser arrays equally spaced in angle around the rod was analyzed using both geometrical and wave optics. Figure 2 shows an example of the geometry analyzed. The analysis accommodates an arbitrary number of concentric media, transparent to the pump light, between the diodes and the laser rod. Additional optics to modify the laser diodes' far-field radiation patterns are also required and are accommodated by the analysis, even when the optics do not image the diode emission pattern to line foci. It is sufficient to be able to describe the intensity and ray directions in finite apertures concentric with the rod.

One result of the cylindrical geometry with simple cylindrical optics is formation of caustics having, in the geometrical optics approximation, infinite intensity. It is thus necessary to develop a wave optics theory to predict the pump intensity in the neighborhood of the caustic edge of the illuminated region inside the laser rod. The wave theory developed first uses geometrical optics to calculate the amplitude and phase just inside the rod surface, which serves as an aperture distribution function describing the source of Huygens wavelets in the computation of a diffraction integral. The resultant calculation, with no free parameters, yields with fractional percent accuracy the same results as the geometrical optics approximation in regions where the latter is valid. An alternate approximation considered, which assumed constant amplitude and cubic phase distributions along the source surface, yields an Airy function description of the caustic intensities that is useful for relating this problem to other physical phenomena, but which over-estimates the intensity peak. Thus computation of the diffraction integral was the preferred method of estimating the peak intensity near caustics in the pump intensity distribution. Figure 3 illustrates how diffraction effects reduce the intensity in the region of a caustic.

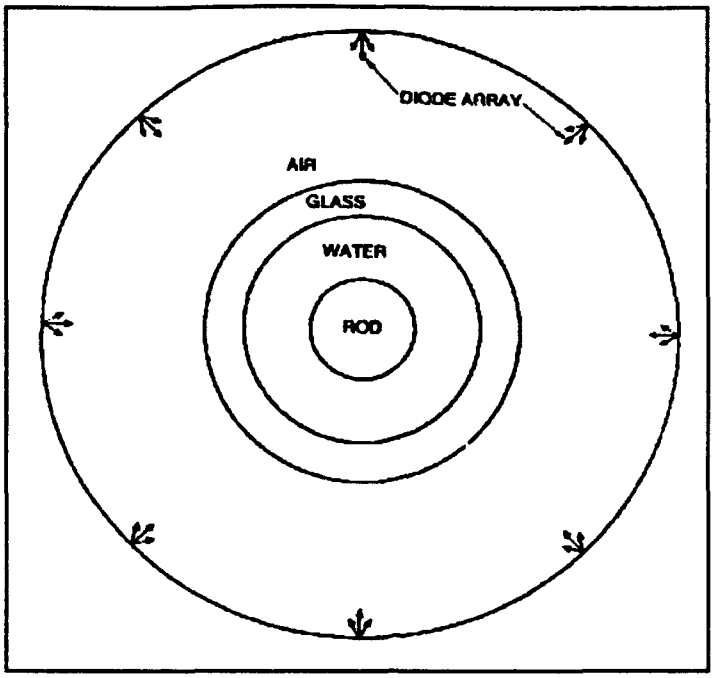

FIGURE 2
A Diode-Pumped Cylindrically Symmetric Laser Geometry

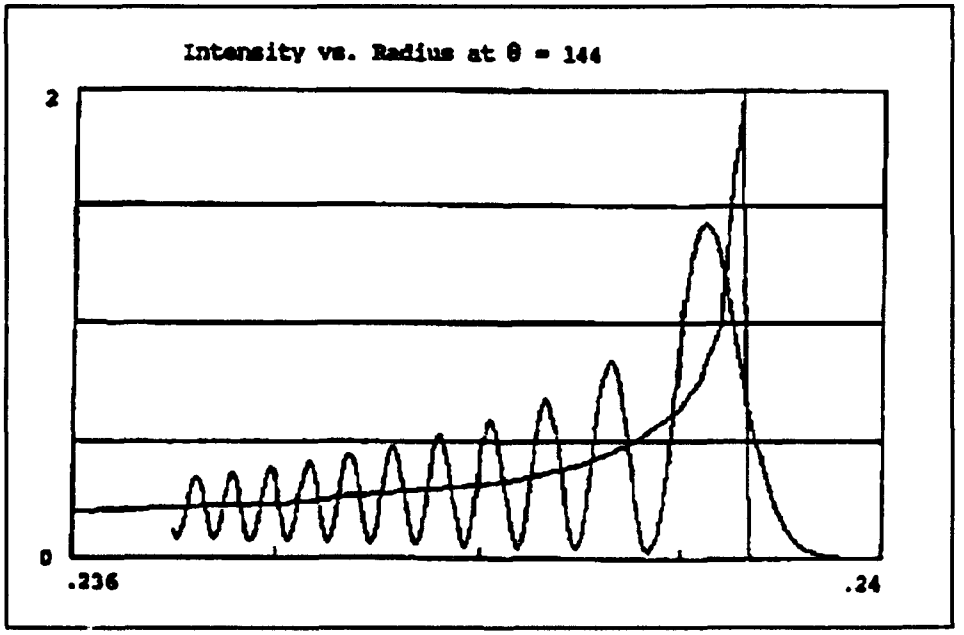

FIGURE 3
Geometrical Optics Approximation and Diffraction Integral Calculation of Pump Light Intensity in a Caustic Region

The use of small-diameter laser rods and practical pump-light absorption coefficients results in a significant fraction of the pump light being transmitted through the laser rod on the first pass. Effective utilization of the transverse pumping geometry with small-diameter laser rods requires reflecting this transmitted light back into the rod. We assumed that the reflecting surface is at the same radius as the source images or source apertures. The analysis showed that this leads to high pumping efficiency, defined by the fraction of the total available pump light that is absorbed in the laser rod. All of the computations assumed a Gaussian profile for the source radiation pattern, which is typical for linear diode arrays in the direction perpendicular to their axes. The principal efficiency-limiting mechanism is edge rays grazing or missing the rod on the first pass, as their energy is wasted. This points to the need for optics near the pump diodes to efficiently direct the pump radiation into the laser rod.

The computations were simplified in several ways to provide the maximum insight without becoming lost in detail. The principal simplification was that the longitudinal components of the pump intensity were not accounted for, although a method of doing so was presented. The two-dimensional approximation utilized is adequate for most laser design optimization and for convenient numerical investigation of some of the relationships amongst design parameters.

The second year effort, reported in this report, had the following objectives:

- furthering the analyses performed during the first year,
- providing a laboratory demonstration of a transverse-pumped Nd:YAG laser similar to the geometry described, and
- comparing the experimental and analytical results for this geometry.

SECTION III

LASER DESIGN and PUMPING ANALYSIS

This section first discusses the analysis of the demonstration laser constructed for the experimental program. The laser design discussion is followed by a discussion of the pumping analysis, which is an extension of the work reported last year (see Section II, "Previous Results"). The pumping analyses focus on the geometry of the laboratory demonstration laser, but are extensible to, and more generally applicable to, diode-pumped solid-state lasers of similar (transverse-pumped rod) geometry. The experimental data are reported in Section V and compared to these analyses.

Cases Considered

The most severe limitation on the experimental program was the limited amount of pump power that could be purchased within the project budget. Preliminary estimates showed that 50 watts of pump light would be the minimum useful. By purchasing this as ten 1-cm diode arrays of 5 watts each, two experimental configurations were envisaged, as follows:

- pumping 2 cm of rod from each of 5 directions, and
- pumping 1 cm of rod with all 10 devices.

The first configuration is superior for experiments relating to the gain of the laser. Illumination from 5 directions is the minimum predicted to give useful pump uniformity in the rod, and the 2-cm pumped length is not ridiculously short in view of the amount of unpumped rod required to mount it and the associated cooling jacket.

Conversely, pumping only 1 cm of rod would maximize the pump power density for thermal experiments. However, this option did not get used during the experimental program. The limited amount of pump power available this year was insufficient to do credible thermal experiments, except simple thermal lensing measurements, which could be done equally well with the 2-cm set up. No additional analysis or experimental effort is planned on the 1-cm pumped-length configuration.

Rods of two diameters, 3 and 4 mm, were used in the analyses and experiments. They had distinctly different roles in understanding the scaling and modeling. It is anticipated that additional analysis and experiments with both will be productive, but the longer-term interest is on 4-mm and larger diameter rods.

It is necessary to get sufficiently over threshold in order to do meaningful experiments to determine the absorbed power density and distribution. This dictated that most of the experimental work be done with laser rods of 3-mm diameter and that much of the analysis was devoted to 3-mm diameter rods. High-power operation may require use of 4-mm diameter, or larger, rods. Larger rods also have a larger range of design space available for optimization of the energy deposition. There are two positive effects of the larger rod from a pumping view point: the larger diameter reduces the power required in the diode focusing cylindrical optics, and the increased thickness provides the designer with a better ability to optimize the first-pass absorption of the pump light. Since much of the analysis was devoted to the 4-mm rod case, because of its longer-term usefulness, the preliminary pumping experiments (principally non-lasing) were performed with a 4-mm rod for comparison.

Laser output power, for the 3- and 4-mm rods, is calculated as a function of the available pump power and the output coupler reflectivity. Both of these parameters were experimentally variable. Pump power was adjustable up to a maximum of 50 watts out of the diodes, and couplers of nominally 90, 92.5, 95, and 97.5 percent reflectivity (91.7, 94.0, 97.5, and 98.2 measured, respectively) were available.

Laser Performance Prediction

As mentioned, the laser performance is dominated by the shortage of pump power, leaving us in a very low-gain situation sensitive to small variations in the laser parameters. As a result, experimental comparison with these analyses, important in verifying the predictive nature of the calculations, is bound to be less than ideal.

Figures 4 and 5 show the predicted laser efficiency versus absorbed power, laser cavity losses, and output coupler reflectivity for two rod diameters, 3 and 4 mm. The following are assumed: a pumped length of 2.5 cm, wavelength of 1.064 μm, induced emission cross section of 3.4E-19 cm^2, and effective upper-state lifetime is 230 microseconds. The efficiency is the total laser output available as a fraction of the available power at upper laser level. The formulation by Rigrod given as Equation 52 of Siegman's Lasers is used in the following form:

$$\eta \equiv \frac{I_{out}}{I_{avail}} = \frac{1 - R_2}{(1+\sqrt{R_2/R_1})\,(1-\sqrt{R_1 R_2})}\left[1+\frac{\ln\sqrt{R_1 R_2}}{\ln G_0}\right]$$

where R_2 is the output coupler reflectivity, R_1 is 1 minus all the other round-trip losses, and G_0 is the unsaturated single-pass gain. The experimental results are presented in Section V.

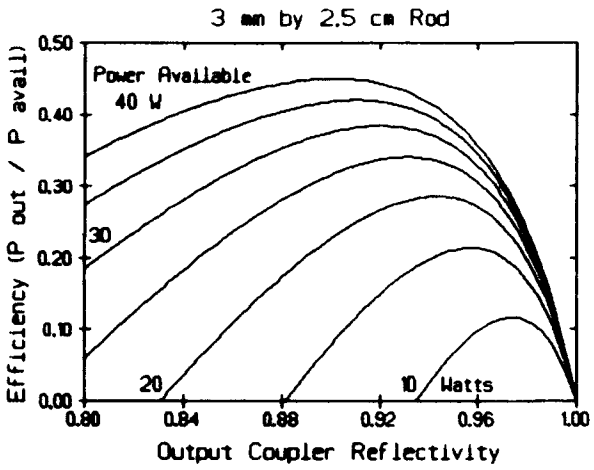

5 Percent Losses

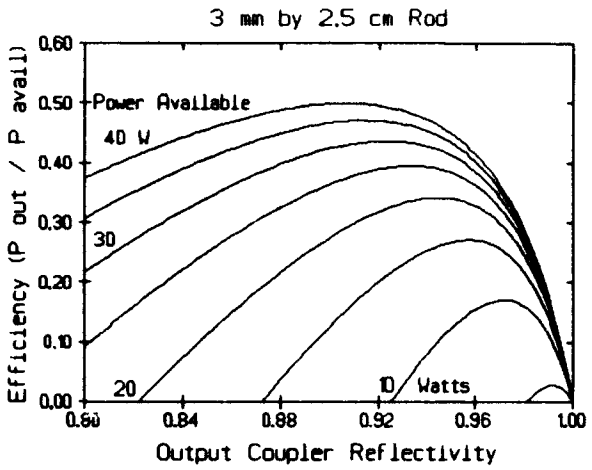

4 Percent Losses

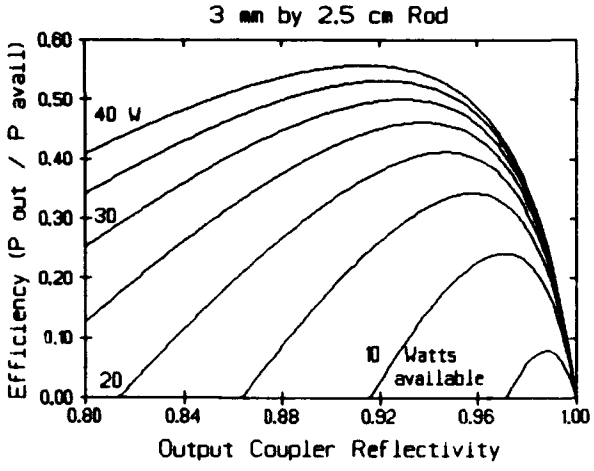

3 Percent Losses

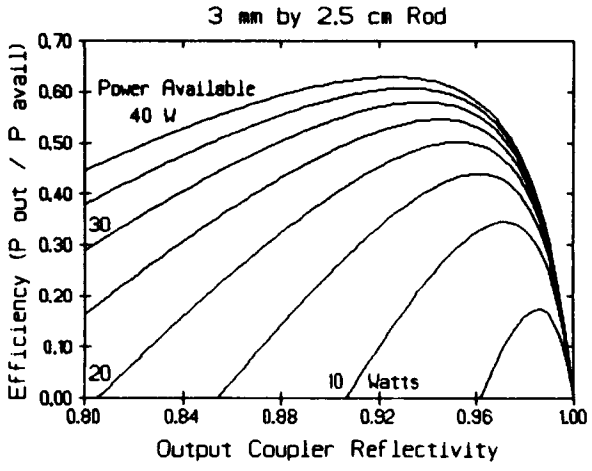

2 Percent Losses

FIGURE 4
Efficiency versus Available (Upper-Level) Power and Output Coupler, 3-mm Rod

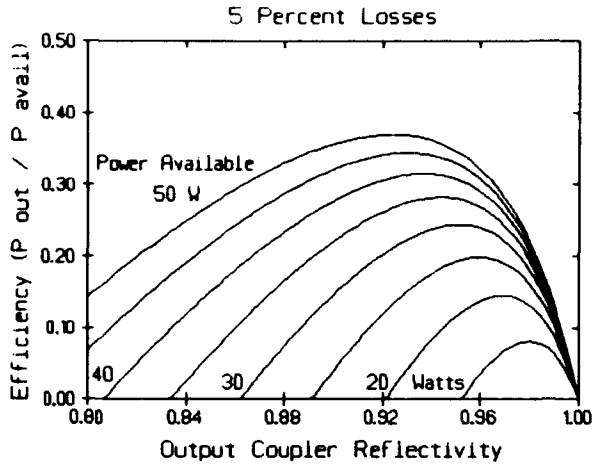

5 Percent Losses

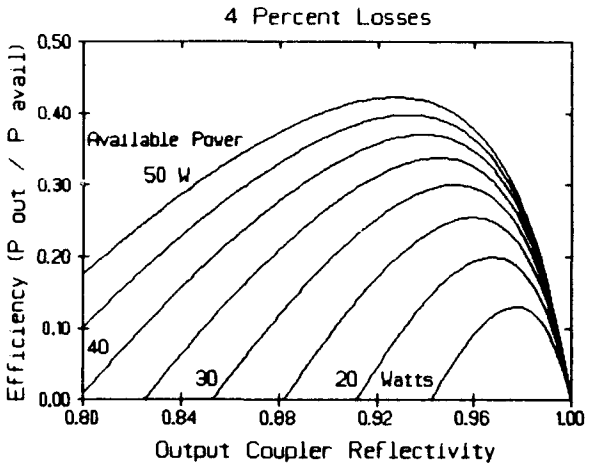

4 Percent Losses

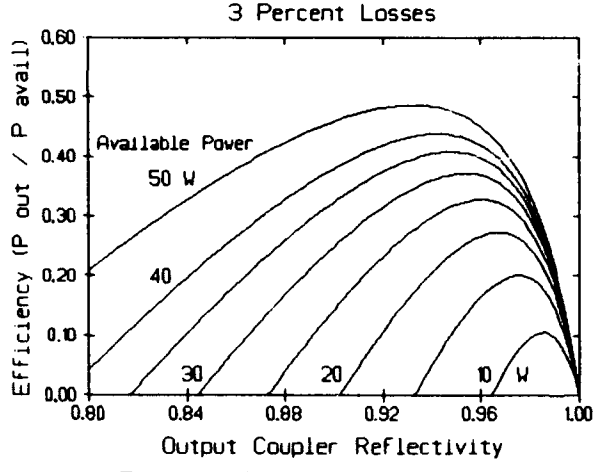

3 Percent Losses

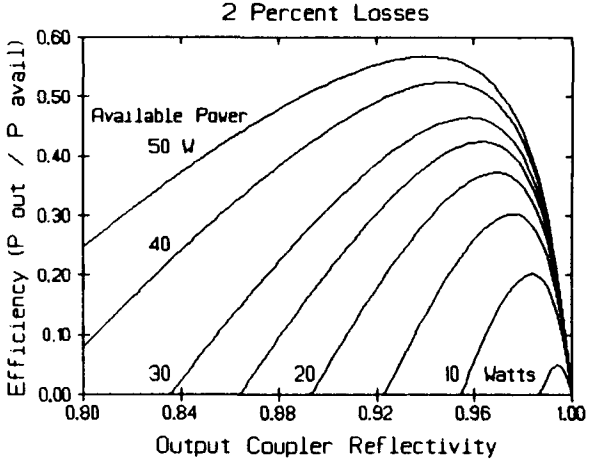

2 Percent Losses

FIGURE 5
Efficiency versus Available (Upper-Level) Power and Output Coupler, 4-mm Rod

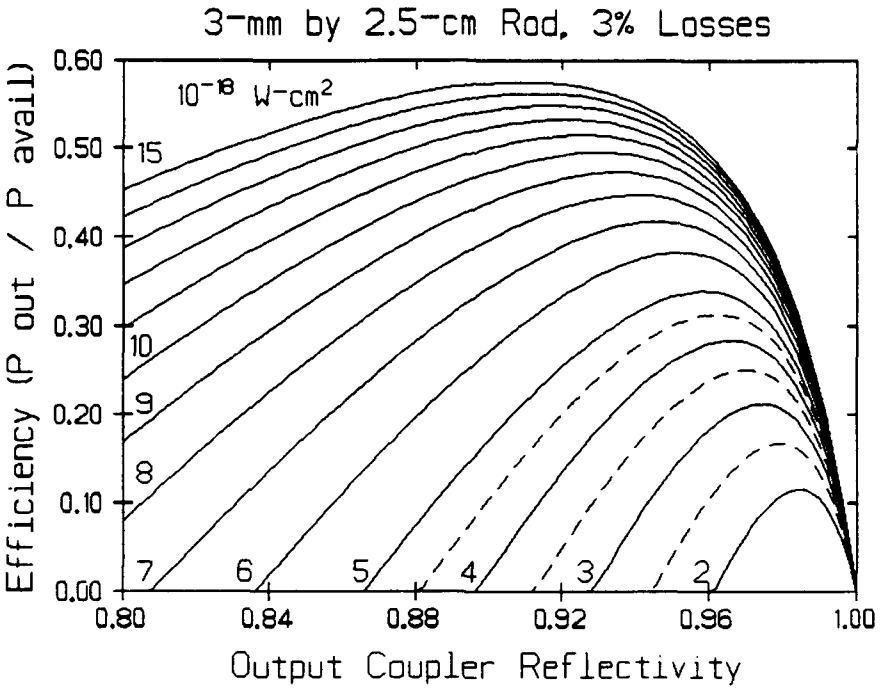

FIGURE 6
Efficiency versus Output Coupler Reflectivity and
Available (Upper-Level) Power times Induced Emission Cross Section,
3-mm Rod, 3-Percent Round-Trip Losses

The curves plotted in Figures 4 and 5 are really contours of constant absorbed power times induced emission cross section. Since there is considerable uncertainty in the value of the latter for cw YAG under these conditions, the value of 3.4E-19 cm^2 assumed in these figures may be low. Figure 6 shows the 3-percent loss case from Figure 4 replotted in terms of power times cross section, in units of 10^{-18} watts-cm^2. Data with laser operation substantially above threshold are required to deconvolve these two variables of the experiments.

Thermal Lensing

Figure 7 shows the calculated focal length of the laser rod from thermal lensing. Curves are shown for 3- and 4-mm diameter YAG rods of 2.5-cm length. The calculation presumes a uniform pump distribution within the rod and a resultant quadratic temperature profile. Neither of these assumptions are applicable to the experiments here, but they represent reasonable approximations to the conditions being sought. The curves plotted

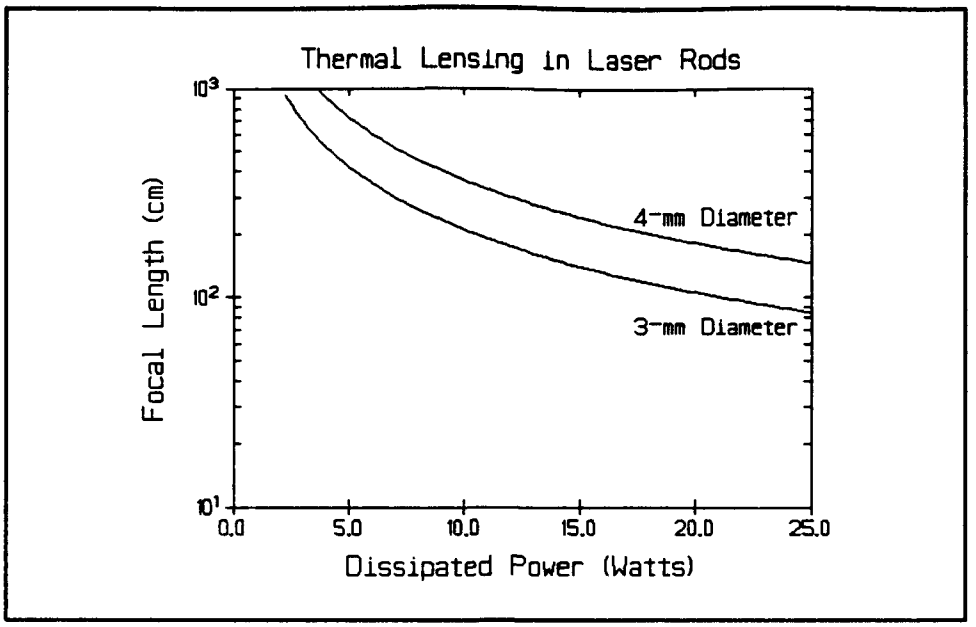

FIGURE 7
Thermal Lensing versus Dissipated Power

are the average of the focal lengths for the radially and azimuthally polarized components. The program used to generate the plot is in the appendices; it calculates the two components independently. A complete calculation incorporating the actual pump absorption profile would require at least two dimensions, and would be premature.

Laser Pumping--Comments

The geometry analyzed during the first contract year (see Section II) was an air-filled pump cavity. The analysis included extensive, generalized geometrical optics calculations and diffraction calculations of the intensity in the region of caustics, but simplified the diode coupling optics. This year the diffraction integral evaluation program was generalized to incorporate lenses collimating the diode emission. The effects on the calculated intensity in the caustic regions are insufficient to merit further treatment at this time during the program. The focus of the work during this contract period has been on the fused silica pump cavity previously shown in Figure 1 (Section I) and minimizing of caustic formation in the pumping geometry.

There are two major parts to analyzing the pumping of the laser rod by the diode arrays in the pump geometry of interest: the general case of how well you can do and what the trade-offs are, and specific case of modeling the laboratory experiments done during

this period of the program. In both cases the problem is realistically two dimensional, although in real systems with multi-cm length laser rods it may be possible to reduce the problem to being only one dimensional. The two-dimensionality of the problem arises from the fact that the diodes do not uniformly illuminate the periphery of the rod, so the pump-light distribution has an azimuthal component as well as a radial component. In a long assembly it should be possible to average out the azimuthal variation of the pumping by staggering the positions of the diode arrays around the rod, but mechanical design complexities might dictate not doing so. Conversely, fine-tuning the performance of a design may require modeling the longitudinal variations in pumping, specifically the effects near the ends of the rod. Accordingly, the analyses during the first phase of the program, and those during this phase, have been two dimensional, in polar radius and azimuth.

The generalized case is simpler, although not trivial. This results primarily from the assumption that the diodes are all the same, and it is left to the system designer to figure out how to couple the diode emission into the laser rod in the desired manner. But the general case must be carried further, to include realistic sensitivity analyses for production variables. And it must be constrained to reasonably achievable design details. Actually, for this contract period, the general case analyzed closely resembles the laboratory setup, and serves as a basis for the comparison calculations.

The specifics of modeling the experiments are more challenging. As will be seen in Section IV, the diodes available to use were all individuals, varying in beam divergence, spectrum, and efficiency. There are too few of them, preventing some generalizations and averaging. YAG is far from the ideal host for diode pumping under these conditions; its absorption spectrum is highly structured. And there were several variables: two laser rod diameters, three sets of diode collimation lenses, and both single-pass and multiple-pass pumping geometries. The calculations will be presented only for those cases in which sufficient experimental data are available to permit meaningful comparisons. The experimental results and comparisons are in Section V.

Laser Pumping--Generalized Case

The general case examined is of the geometry illustrated in Section I, Figure 1. The analyses look at the pump-light distributions in the rod for the first pass and for the first two passes, as a function of the number of diode arrays around the periphery, the degree of collimation of the diode light in the rod, and the absorption coefficient (which can be generalized to the product of absorption coefficient and diameter). The laser rod is presumed to be 3-mm in diameter, located in an 8-mm diameter hole in a 10-cm OD pump cavity of fused silica.

The detail omitted from the generalized calculations is the optical system coupling the diode emission to the laser rod. The diodes' transverse emission patterns are presumed to be Gaussian, and the same for all diodes. The optics are presumed to map rays from the diodes to the periphery of the rod without distortion, although the intensity distribution presumed to be modified by four interface transmission functions. These four functions are as follows:

- the light leaving the diode is presumed to refract through a first surface with an angle of incidence equal to the departure angle from the diode,
- it then refracts through another surface at an angle of incidence equal to one-half of that on the first surface, and
- it refracts through the quartz-to-water and water-to-YAG interfaces.

All other surfaces are presumed to be sufficiently normal to the rays that the intensity distribution is not altered in shape. Of course there is a multiplicative factor, of less than unity, that must be applied for the other surfaces, in order to account for the Fresnel losses. In these calculations that factor is taken to be 1.00.

The diode emission is presumed to be Gaussian in the transverse direction with a full angle between the e^{-2} intensity points of 44 degrees and a maximum useful collection full angle (95 percent of the light) of 60 degrees. The polarization is defined by the E vector being parallel with the diode axis, so the pump light is "S" polarized at the optics interfaces between the diode and the rod.

The assumption that the pump-light optics map the rays from the diode to the rod without distortion prevents the formation of caustics during the first pass through the rod. The angular extent around the periphery of the rod of the light arriving from each diode is limited to slightly less than that angle at which the rays would totally reflect from the rod rather than enter it, or to a lesser angle if necessary to prevent the formation of caustics on the second pass. The calculation was not carried beyond the second pass during this contract period. The intensity on the third and subsequent passes are sufficiently low that caustic formation is not likely to be a practical concern.

The coolant is presumed to be water. For the second-pass calculations the reflectivity of the pump cavity reflector is presumed to be 92 percent. Since the results are not a strong function of this reflectance, other values were not examined during this contract period. Under certain conditions some of the rays may exit through the windows in the pump reflector that let the pump light in from the diodes. This effect seldom occurs between the first and second passes, but since the rays still carry a significant fraction of the total diode light at this first reflection, this effect is accounted for. This loss becomes

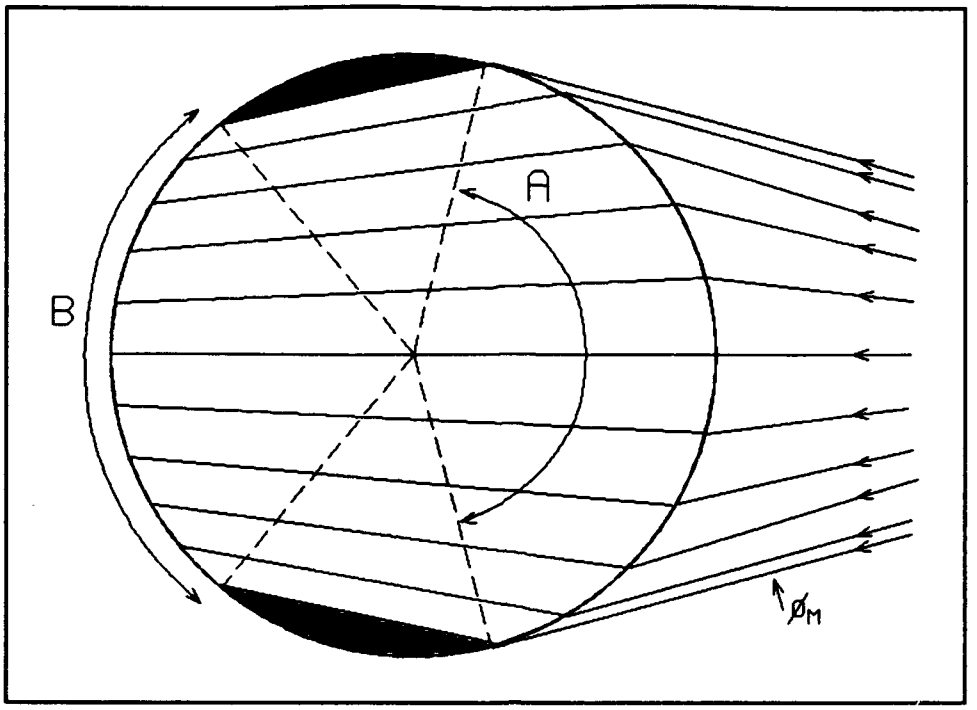

FIGURE 8
Ray Paths Inside YAG Laser Rod
$\delta = B/A$

more significant on subsequent passes, at least in terms of the numbers of rays lost, but no estimate is made here of its significance in terms of energy loss after the second pass. The ratio of the pump wheel periphery occupied by the pump windows, times the total power reaching the pump cavity perimeter after the second pass through the rod, would be a conservative upper bound on this loss on these additional round-trips through the rod and pump cavity.

Figure 8 shows the rays from one diode traversing the rod on the first pass. The ray ϕ_M is the marginal ray; all rays beyond totally reflect at the water-YAG interface. An important parameter of the analysis is the factor δ, which is the reciprocal of the ratio of the angular extent around the periphery of the rod of the rays entering from the diode to their angular extent exiting the rod after the first pass. If $\delta = 1$, the rays are all parallel inside the rod, while $\delta = 0$ corresponds to the rays focusing at the exit face and $\delta = -1$ corresponds to the rays focusing at the center of the rod. Values of $\delta > 1$ correspond to the rays diverging as they pass through the rod the first time.

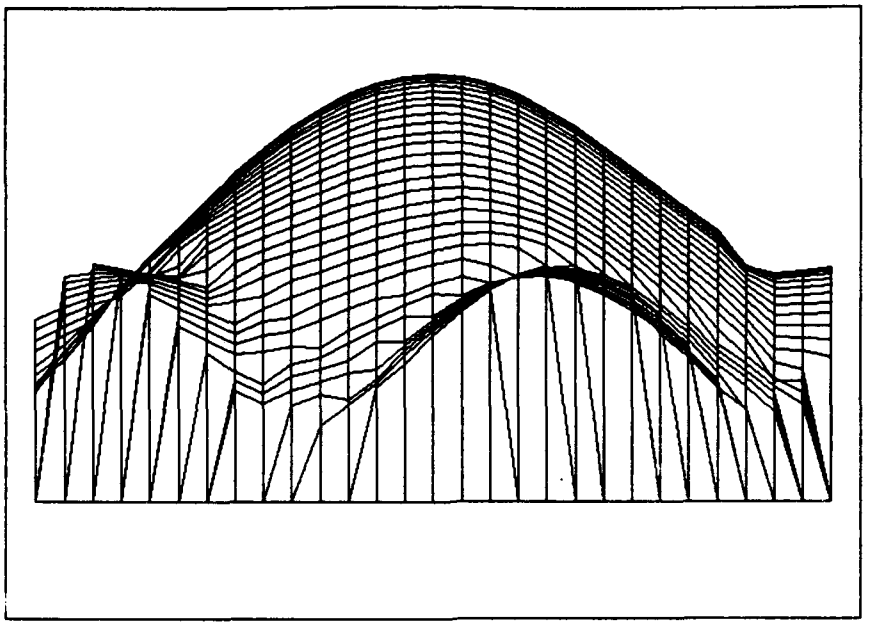

FIGURE 9
A Non-Uniform First-Pass Pump Intensity Profile

The focusing, and potentially defocusing, of the rays during their first pass through the laser rod is somewhat under the designer's control. However, the rays are always strongly focusing during their second and subsequent passes through the rod. Thus the parameter δ is meaningfully defined only for the first pass absorption.

Figure 9 shows a three-dimensional surface plot of the pump-light absorption with the features exaggerated to aid in the explanation. This is a case in which there are five diodes. You, the observer, are sitting on a plane through the rod, with diode number 1 entering from 90 degrees to your right and exiting 90 degrees to your left. With five diodes, they are spaced 72 degrees apart, so diode number 2 is entering from 18 degrees to your right, and diode 3 is entering from 54 degrees to your left. In this particular case the rod is 3 mm in diameter and the absorption coefficient, σ, is 4 cm^{-1}. Only the first pass absorption is shown. The factor δ = 1.5, so the rays are strongly diverging while passing through the rod. This leads to the pronounced dips in intensity around the periphery of the rod between the entering beams, because the exiting beams are so defocused that they do little to fill in the valleys between the entering beams. For this profile the average absolute error between the intensity curve and its average value is 30 percent, the RMS error is 36 percent, and the peak-to-valley ratio is 6.06. Appearances are deceiving, however. Despite the obvious ripple around the periphery of the rod, the statistics are dominated by the central peak. As we shall see, reducing the ripple around the periphery fills in the valleys, but does little to reduce the mean or RMS error from a uniform profile.

The method used to calculate these ideal pumping cases is as follows. The number of diodes, rod diameter, absorption coefficient, δ factor, and number of passes (1 or 2) is selected. The marginal ray is identified, that is, the angle A corresponding to ray ϕ_M in Figure 8 is found. If the incident patterns from adjacent diode arrays overlap on the rod, the angle A may be reduced to eliminate the overlap, but, normally the overlap is beneficial. If two passes are to be analyzed, the ray bundle is propagated through the rod, pump cavity, and back through the rod. The angle A is then reduced, if necessary, to avoid the formation of caustics in the rod on the second pass. With the angle A thus determined, and the factor δ preset, the angle B (in Figure 8) is determined and the first pass energy deposition is mapped. If the second pass is to be analyzed, the rays are propagated back through the rod for the second pass and the energy deposition mapped. The deposition from the two passes is then summed for the total. As mentioned earlier, the Fresnel losses are accounted for at all of the interfaces, as is the leakage out of the windows in the pump reflector that admit the diode emission. The programs are too lengthy to include in the appendices, but are available on request. One program, in MathCAD 2.5, analyzes the first pass. A second, in QuickBasic 4.00b, does both the first and second passes. A third, also in MathCAD 2.5, does surface plots like Figure 9. Surface contour interval plotting is also available, but was not integrated into the package this year.

It is obvious that all the major parameters of the system are inter-related. The following discussion looks at each separately, because single-variable analyses are sufficient to elucidate the significant trends. Most of the discussion will be based on analysis of the first-pass energy deposition. We will see that the later passes do not significantly alter the pump uniformity, although they do improve the efficiency.

Number of Diodes: Figure 10 shows the average absolute error and the RMS error from the mean value of the pump intensity, for the first pass, through a 3-mm rod. The independent variable is the number of diode arrays symmetrically arranged around the periphery of the rod. The constraints are that $\delta = 1$ (rays are parallel in the rod) and $\sigma = 4$ cm^{-1}. Figure 11 shows the peak-to-valley ratio for the same case. The conclusions from these data are two-fold:

- the minimum number of diode arrays for useful experiments is five, which is what we used, and

- there is no significant difference in pumping uniformity for seven or more arrays around the rod periphery.

Note that we use an odd number of arrays in order to reduce the loss, after the first pass through the rod, out the windows in the pump reflector. The windows are necessary for the pump light to enter from the diodes (See Figure 1, Section I).

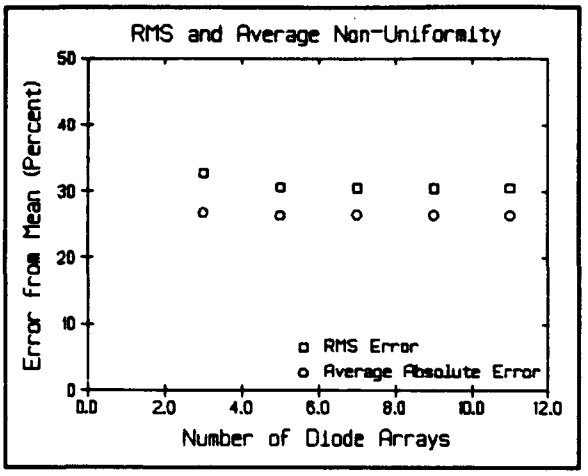

FIGURE 10
Uniformity versus Number of Diodes
RMS and Average Error from the Mean

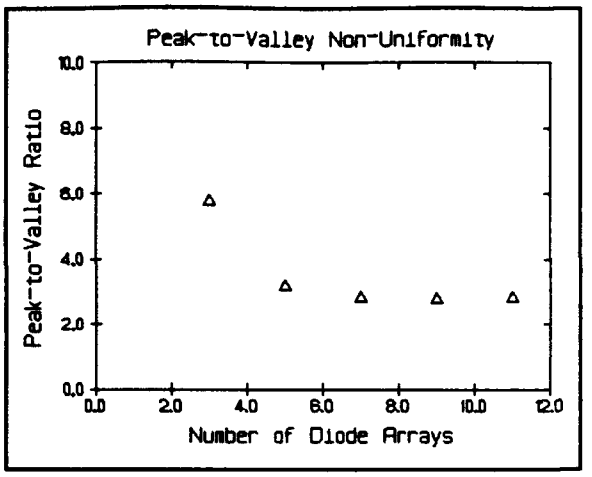

FIGURE 11
Uniformity versus Number of Diodes
Peak-to Valley Ratio

Variation of δ: Figures 12 and 13 show the first pass non-uniformity as a function of the ray collimation parameter δ. The constants are 5 diode arrays, a 3-mm rod, and an absorption coefficient of 4 cm^{-1}. The RMS error from the mean, and the average absolute error from the mean, both go through broad minima for values of δ between about 1.0 and 1.5, while the peak-to-valley ratio has a minima for values of δ between about 0.75 and 1.0. As discussed earlier in the definition of the parameter δ, most realistic optical configurations are expected to have the rays focusing as they pass through the rod the first time, corresponding to $\delta < 1$. Also shown in these figures is the effect of increasing the number of diode arrays around the rod periphery to 11.

The effects of increasing the number of diode arrays from 5 to 11 depends on the measure of the non-uniformity being plotted. For example, in Figure 12, it has no effect at all on the average absolute error as a function of δ. Why? Because it simply smoothes out the ripples around the periphery of the rod, lowering the peaks and filling the valleys, so the average error from the mean intensity is essentially invariant. However, since the extremes of the error surface are smoothed, the RMS error is reduced slightly, as shown in Figure 12, especially for large (and thus unrealistic) values of δ. Both measures of non-uniformity plotted in Figure 12 are dominated by the central, on-axis peak of the pumping intensity. Thus, it is reasonable that increasing the number of diode arrays arranged around the periphery of the rod should have little, or even no, effect on these results.

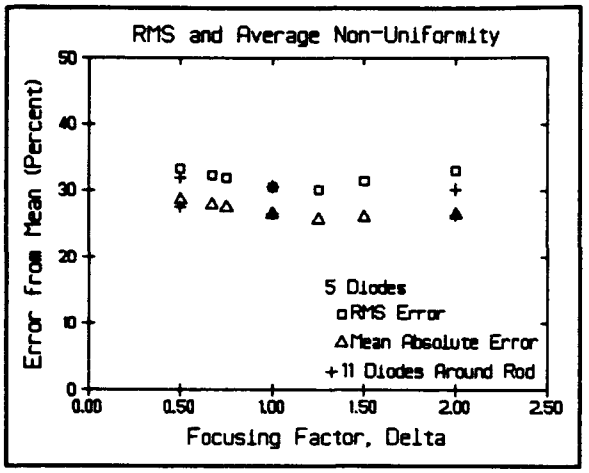

FIGURE 12
Uniformity versus Focusing Delta
RMS and Average Error from the Mean

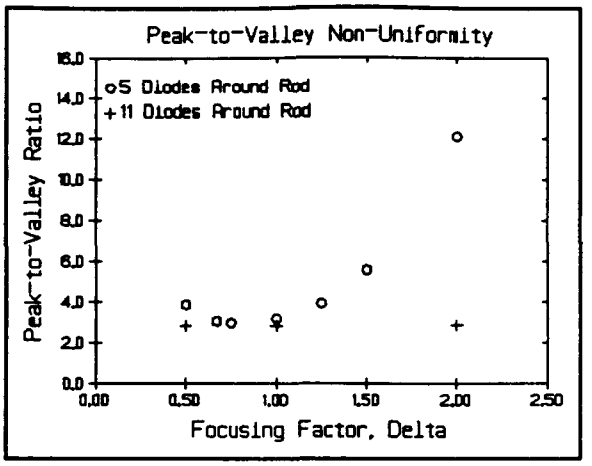

FIGURE 13
Uniformity versus Focusing Delta
Peak-to-Valley Ratio

Conversely, if we measure the non-uniformity by the peak-to-valley ratio, as shown in Figure 13, increasing the number of diode arrays dramatically changes the shape of the non-uniformity versus δ. Whereas the 5-diode case shows a distinct minimum for values of δ between about 0.75 and 1.0, with 11 diodes the peak-to-valley ratio is essentially independent of δ. Over the range of δ from 0.5 to 2.0, the peak-to-valley ratio varies between 2.80 and 2.88 . The good news is that the designer need not worry about optimizing the value of δ to minimize the non-uniformity, while working with higher power systems pumped by a large number of arrays arranged around the rod. The bad news is that adding diode arrays around the rod doesn't reduce the minimum peak-to-valley ratio. That is, you can do just as well with 5 diodes as with more; the design space is simply more restricted. Why? Because the on-axis peak dominates the non-uniformity. The only way to reduce the on-axis peak is to absorb more of the pump light at the rod periphery on the first pass, which means significantly increasing the product of the rod diameter times the absorption coefficient. Adding diodes won't substitute, nor will adjustments to the focusing or defocusing of the pump light in the rod. And, as we will see, neither will reducing the absorption coefficient, at least within practical limits.

Sigma-Radius (σ-r) Product: Figures 14 and 15 show the peak-to-valley ratio for 5 and 11 diodes arrayed around the rod, as a function of both the focusing parameter, δ, and the product of the absorption coefficient times the radius, σ-r. This is for the geometry, i.e., the first pass through a 3-mm diameter rod. What we see in Figure 15 is that for the 11 diode case, increasing σ from 4 to 10 cm^{-1} decreases the peak-to-valley ratio from about 2.8 to about 1.6, and it remains independent of δ.

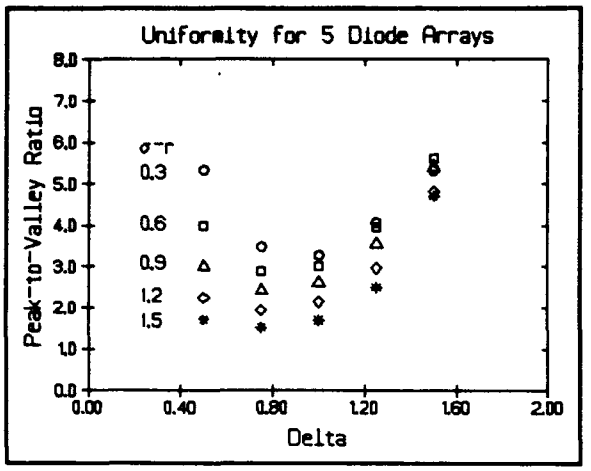

FIGURE 14
Uniformity versus Sigma-R Product
Peak-to-Valley Ratio for Five Diodes

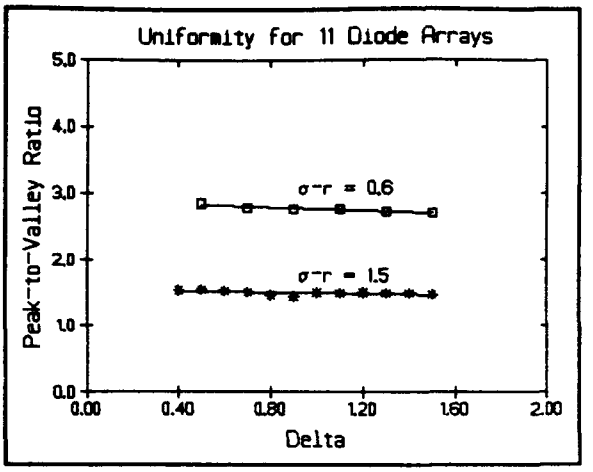

FIGURE 15
Uniformity versus Sigma-R Product
Peak-to-Valley Ratio for Eleven Diodes

The five-diode case in Figure 14 is more complex. In Figure 13, the peak-to-valley ratio goes through a minimum for values of δ slightly less than unity, i.e., for the rays slightly focusing on the first pass. In Figure 14, as σ increases from 2 to 10 cm^{-1}, the minimum peak-to-valley ratio decreases from about 3.1 to about 1.5. The minimum also shifts from δ of about 1.0 to about 0.75, and becomes broader. This is advantageous, since stronger focusing of the rays on the first pass of the light through the rod is the natural tendency from the geometry of the pump cavity and coolant layer. This avoids focusing of the pump light in the fused silica before the first pass through the rod, but it tends to tread into the design space that leads to the formation of caustics, either on the second, or worse, first, pass of the rays through the rod.

Figures 14 and 15 reiterate a previous point. Increasing the number of diodes arrayed around the rod does not significantly alter the minimum achievable peak-to-valley ratio. Instead, it allows the designer to reach the minimum value independent of the selection of the ray focusing parameter, δ. Conversely, increasing the absorption coefficient improves the uniformity, almost unconditionally. Figure 14 shows that for all values of $\delta < 1.5$, the peak-to-valley ratio is a monotonically decreasing function of σ.

Single-Pass Pumping, Additional Notes: Figure 8 intentionally illustrates a particularly bad pump intensity profile. Figures 16 and 17 illustrate two more realistic profiles. Figure 16, like Figure 8, has 5 diode arrays around the periphery, but with the first-pass light converging, rather than diverging, in the rod. Observe that the peaks in the peripheral pumping profile correspond to the exiting rays, whereas in Figure 8 the peaks were where the rays entered. Figure 17 shows the smoothing with 11 arrays, which is nearly independent of the value of δ.

Avoiding a focus within the rod on the first pass is both necessary and easy. A second-pass focus can be avoided by improving the collimation of the rays at the rod before the first pass. By the third pass, a focus is difficult to avoid, but it may be of little consequence because of two factors: there is not much power left in the pump field by the third pass, and the aberrations are so severe that the focal line size is large and fuzzy. Several additional factors can contribute to reducing the intensity in this focus, including using more arrays of lower power each and collimating the diode light to increase the value of δ on the first pass.

If they occur (low values of δ), first-pass caustics are not shown in these figures. (See the first-year report for their cause, location, and intensity.) The techniques which reduce the third-pass focal-spot intensity also help avoid formation of caustics or reduce their peak intensity. The use of regular polygonal rods instead of circular cross-section rods is effective for elimination of first-pass caustics with small numbers of diode arrays, as with a pentagonal rod and five arrays. As the number of arrays increases, this technique becomes less attractive, because the light from each diode array must be collimated well enough to enter through a single rod face on the first pass. Thus the number of faces must increase and the width of each facet becomes smaller. We did not determine the optimum number of facets as a function of the number of arrays, although for five arrays the answer is obviously five facets on the rod. The non-circular cross-section will also distort the temperature gradients and resultant stresses and index variation near the periphery of the rod, especially for a small number of faces. This may increase the laser's divergence and decrease the fracture-limited maximum permissible pumping, but we did not calculate these effects.

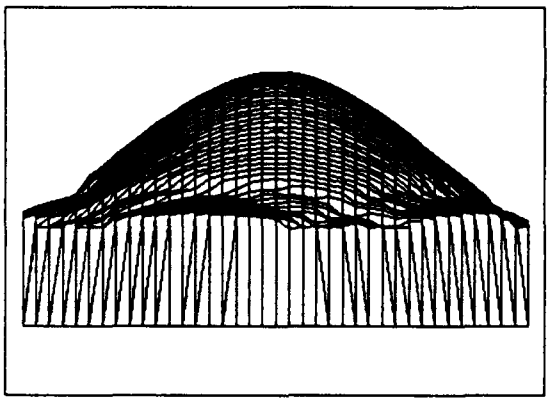

FIGURE 16
Pump Intensity Profile, 5 Diodes,
4-mm Diameter, σ = 4 cm^{-1}, δ = 0.67

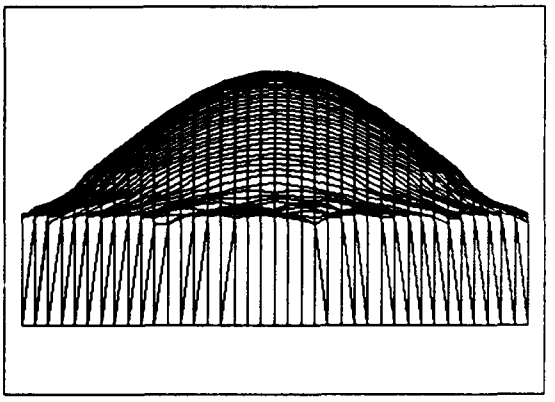

FIGURE 17
Pump Intensity Profile, 11 Diodes,
4-mm Diameter, σ = 4 cm^{-1}, δ = 1

Multiple Passes: There are two major issues to be addressed while expanding the analysis from the first pass to multiple passes, as follows:

- How does the light utilization efficiency improve?
- What happens to the uniformity?

These questions can be addressed as functions of several parameters, including the number of diodes, the absorption coefficient (σ), the ray first-pass focusing parameter (δ), the cavity geometry, and the pump reflector reflectivity. Time did not allow addressing all of these parameters; the following discussion covers a subset within these constraints:

- the number of diodes is fixed at 5, although scaling rules for the light utilization efficiency are easily estimated,
- σ is held at 4 cm^{-1},
- δ is varied, since the single-pass analyses showed that it is an important parameter in the 5-diode case,
- the geometry is held fixed with a 10-cm diameter pump cavity and a 3-mm diameter rod located in an 8-mm diameter coolant channel, and
- the pump cavity reflector's reflectivity was varied from 0.75 to 0.95 around the nominal value of 0.92.

Figure 18 shows the calculated absorption, as a function of the focusing parameter, δ, and the number of passes, for 5 diodes, pump reflectivity of 0.92, and σ = 4 cm^{-1}. The data are normalized to 1.00 for the first pass absorption with δ = 1.0. There are several caveats on the figure. Only the first and second passes were calculated, and the angular extent of the incident beams (angle A in Figure 8) differed in each case. The 0.89 times the ratio of the second pass absorption to the first pass absorption was then used to project the absorption on passes 3 through 7. The factor of 0.89 introduces an additional 11 percent loss per pass after the second pass, to allow for loss out the entrance windows in the pump cavity, and is undoubtedly pessimistic.

It is initially surprising that the absorption is a function of δ, but inspection of the calculations shows, quite reasonably, that as δ increases, the average ray path in the rod during the first pass decreases. This latter point is reasonable for the following reason: large values of δ improve uniformity by reducing the on-axis peak, which results from the fact that fewer rays pass near the rod center, and if the rays avoid the rod center, they must take a shorter path through the rod.

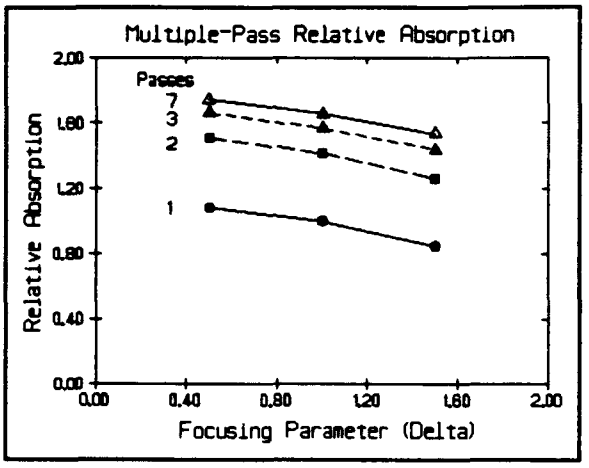

FIGURE 18
Relative Absorption for Multiple Passes versus Delta, Five Diodes

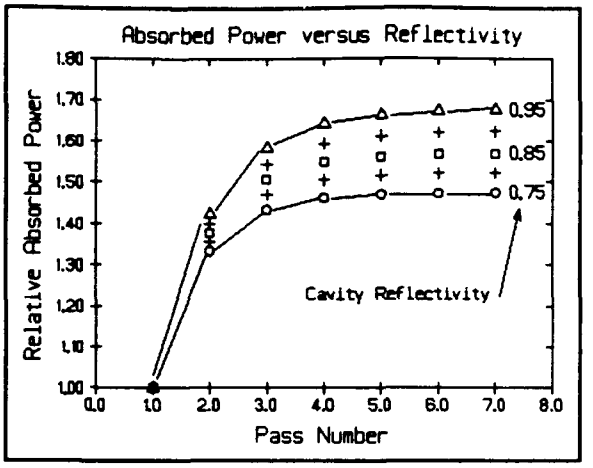

FIGURE 19
Relative Absorption for Multiple Passes versus Cavity Reflectivity, Five Diodes

Figure 18 needs to be used cautiously at this time; the extrapolation from the second pass to multiple passes is not well supported, and the variation in the angle A between cases (adjusted to avoid the formation of caustics on the second pass) should be expected to affect the curves in a manner that has not yet been determined. In particular, the roll-off of the total absorption as δ increases, for greater than 2 passes, may be under-estimated in Figure 18.

Figure 19 shows how the relative absorption is affected by the reflectivity of the pump cavity reflector surface, for the case of δ = 1.0 and 5 diodes. It is calculated in exactly the same manner as Figure 18, so the same caveats apply to the scaling of total absorption with the number of passes, for more than 2 passes. Again, the plots are normalized to the first pass absorption. The figure shows that a cavity with a reflectivity of 0.75 is 89 percent as efficient as a cavity with a reflectivity of 0.95.

An important effect not quantified in these figures is that the multiple-pass efficiency is degraded as the number of diode arrays around the rod increases. This is because the percentage of the cavity reflecting wall occupied by the windows that admit the pump light increases proportionally with the number of diodes. Thus there is a fundamental trade-off between pumping efficiency and pumping uniformity, at least to the extent the latter is determined by the number of diode arrays around the rod.

The calculations of how multiple-pass pumping affects the uniformity were incomplete during this contract period. As stated in the first contract report (referenced in Section II), one's intuition is that the second and successive passes can be no worse in uniformity than the first pass. Calculations show that this is not necessarily true,

depending on the measure of non-uniformity being used. The second and third passes are strongly focusing, so they preferentially pump the center of the rod, and slightly increase the average and RMS error from the mean intensity, because they enhance the on-axis intensity peak. This increase is small, of the order of 1 percent of the non-uniformity on the first pass. Conversely, the successive passes tend to illuminate the periphery more uniformly than does the first pass, so the ripple in intensity around the periphery of the rod is reduced, as is the total non-uniformity as measured by the peak-to-valley ratio. That is, although the second and subsequent passes enhance the on-axis peak slightly, they significantly fill in the low illumination valleys around the periphery, at least for values of $\delta > 1$. The difficulty with the calculations done to date is that the assumed diode-to-rod optics changes as a function of δ, as required to avoid the formation of pump caustics on the second pass through the rod. For cases in which the first-pass illumination has minimal ripple around the periphery of the rod, as is the case when there is a large number of diodes arrayed around the rod, this trend is probably reversed, and the peak-to-valley ratio probably is slightly degraded by the multi-pass pumping. Unambiguously quantifying the effects of multiple-pass absorption on pump uniformity will require holding the pumping optics fixed.

However, one important point does come from the analysis done. The determination of "better" or "worse" depends on the measure being used. If the measure is peak-to-valley ratio, then the multiple-pass absorption improves the "uniformity." Conversely, if the measure used is the mean (or RMS) error from the average value of the intensity, then things get slightly worse as multiple passes are considered. The determination of what measure of uniformity is most appropriate must come from analysis of the laser system. It is anticipated that the best measure of pumping uniformity may differ for oscillator and amplifier applications.

Laser Pumping--Experiment Specific

To apply the generalized calculations presented above to the laboratory experiments performed, the following must be determined:

- the intensity of the pump light reaching the rod periphery for the first pass,
- the value of the absorption coefficient, σ, that best represents the overlap of the diode spectra and the YAG absorption spectrum,
- the value of the focusing parameter, δ, that best represents the diode focusing optics used, and
- the value of the pump cavity reflector's reflectivity.

All of these can be estimated from the data available. The most unsatisfactory fit will be for δ, since the optics used to focus the diode emission patterns to the rod were simple cylindrical lenses, rather than the idealized optics assumed in the generalized case calculations presented above. Also, as discussed previously under the modeling of the laser performance, the absorbed pump power and the YAG induced emission cross section cannot be separated when operating so near threshold.

Incident Power: Throughout the experiments three types of optics were used to focus the diode light into the rod: fused quartz cylindrical rods, acrylic f/1 Fresnel lenses, and AR-coated fused quartz cylindrical lenses. Most of the laser tests were performed with the latter. Figure 20 shows these simple lenses. In addition to the type of lens used, the pump intensity at the rod is dependent on the diode emission patterns (see Figure 39 in Section IV), the alignment of the lenses to the diodes, and the alignment of the lens-diode combinations to the rod. Although we will approximate the absorption coefficient as a single number in the next few paragraphs, in fact the diversity of diode spectral distributions leads to an angular dependence of the effective value of σ around the rod. We neglect this latter effect here.

Using the lenses illustrated in Figure 20, we first measured the power transmitted through a 2.85-mm slit located at the rod center-line position. The data were taken with each diode operating at its nominal operating temperature and hence wavelength, and at its nominal current for five watts output at that temperature. The diode to rod centerline distance is approximately 6 cm. The data were expected to correlate with the diode divergence, but that didn't prove to be the case. Instead, the lens losses were found to be linearly related to the operating temperature of the diodes. Figure 21 presents this relationship. We later retook these data, with improved mounting and collimation of the diode collimation lenses. The new data were taken twice, once each with slit widths of 3.0 and 4.0 mm (Figure 23). These data show four things:

The relationship between loss, serial number, and temperature in Figure 21 remained relatively unchanged.

The relationship with transverse beam divergence became much clearer. Figure 22 shows this.

The losses were higher by an average of 15 percent, compared to the earlier corrected data. This can be attributed to the handling of the small lenses during their remounting, accumulated surface contamination, and errors introduced by the necessity of temperature correcting the initial data.

The 4-mm slit width passed little more energy than the 3-mm slit width.

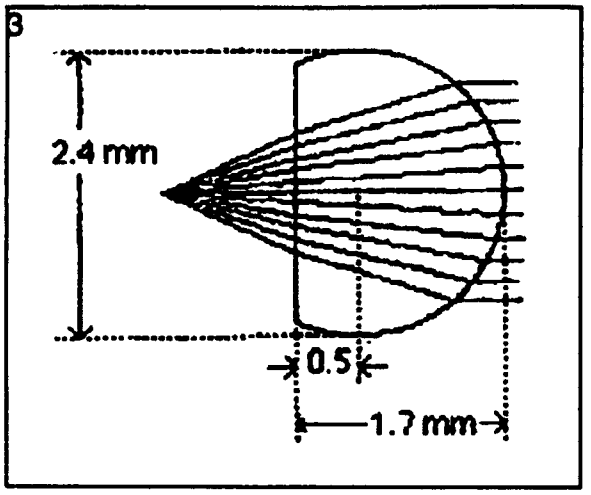

FIGURE 20
AR-Coated Cylindrical Collimating Lens

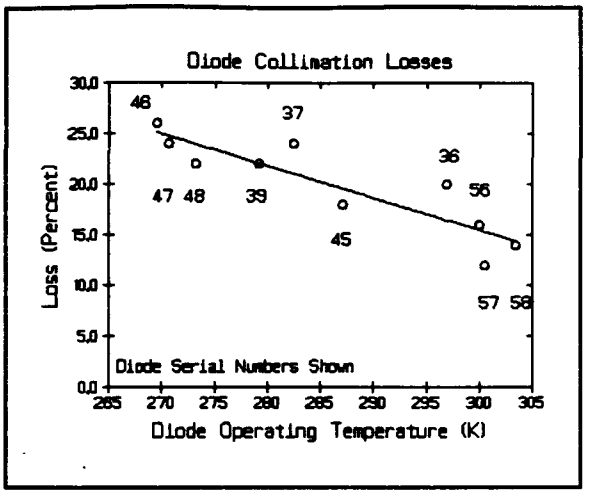

FIGURE 21
Diode-Lens Loss versus Temperature
Initial Data, 2.85-mm Slit

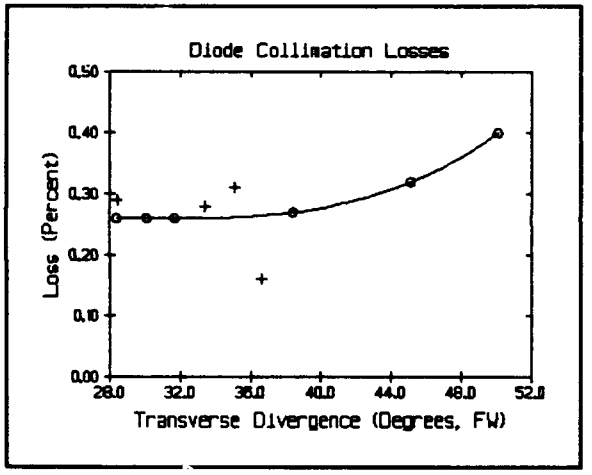

Figure 22
Diode-Lens Loss versus Divergence
New Data, 4-mm Slit

	Slit Width	
Transmission	3-mm	4mm
Average:	0.71	0.72
Maximum:	0.78	0.84
Minimum:	0.59	0.60

Figure 23
Slit Transmission at Rod Position,
New Data, Diode to Rod-Center ≅ 6 cm

The first point stands because the diode efficiency, divergence, operating temperature, and serial number are all well correlated, with the divergence and efficiency trending downward with increasing serial number. These effects are shown in Section V.

The expected correlation of loss with transverse divergence manifests itself two ways. In Figure 22, a smooth curve has been drawn through a majority of the data. The curve represents a loss of 24 percent for low-divergence diodes, and rolls off smoothly

at higher divergence. Although it has no mathematical basis, it clearly represents a reasonable fit to all the data. Secondly, correlation coefficients were calculated for the 4-mm slit transmission (1 - loss) versus a number of parameters. The result indicates that the divergence and loss are well correlated despite the small data set and experimental variations. The correlation coefficients are as follows:

Transmission to	Serial Number	r = 0.68
	Transverse Divergence	r = -0.57
	Current at 5 Watts Output	r = 0.55
	Operating Temperature	r = 0.40
	Emission Spectral Width	r = -0.18

The higher losses mean that, of the 50 watts emitted by the diodes, only 36.0 watts were available for pumping in the final experiments. Accounting for Fresnel losses in the actual pump cavity (Figure 1), reduces P_{avail} to less than 38 watts in the initial experiments and 33.5 watts in the final experiments. That the 3-mm slit had about the same transmission as the 4-mm slit indicates that the diode outputs were, perhaps, too strongly collimated for the larger rod. However, the laser performance data do not show a related adverse effect.

Absorption Coefficient (σ): Nine of the 10 pumping diodes were operated at the center wavelength of 806 nm, and one diode at 813 nm. The diodes have various spectral widths, as illustrated in Section IV, Figure 32. A measurement of Nd:YAG's highly structured absorption spectrum is shown in Section IV, Figure 29. We estimated the effective value of the absorbance, σ, of 3 cm^{-1} for use in most of the pumping analyses throughout this contract. We infer, from the experimental results in Section V, that the average σ in the experiments was lower, nearer 2 cm^{-1}. The effect of variation of σ on first-pass pump intensity profiles is as follows (δ=0.67):

σ, cm^{-1}	Rod OD, mm	RMS Variation, %	Mean Abs. Var., %	Peak/Valley
2	3	35.5	30.4	3.92
4	3	31.2	26.9	3.01
2	4	34.6	29.7	3.59
4	4	28.4	24.5	2.61

Focusing Parameter (δ): We traced geometrical rays for a diode-lens pair shown in Figure 20. Figure 25 shows the calculated ray paths through the YAG rod on the first pass. Unlike the idealized cases presented earlier in this section, the use of a single, uncorrected cylindrical lens leads to the formation of caustics in the first-pass pump intensity distribution. From Figure 25 we can estimate the value of the focusing parameter, δ, defined earlier as the ratio of the angles B/A in Figure 8, as $\delta = 0.35$.

S/N	Operating Temperature	Center Wavelength	Wavelength Spread
36	297 K	806 nm	1.9 nm FW
37	282	806	2.0
39	279	813	1.6
45	287	806	1.0
46	270	806	1.5
47	271	806	2.6
48	273	806	2.8
56	300	806	2.0
57	300	806	2.0
58	303	806	1.2

FIGURE 24
Diode Operating Parameters

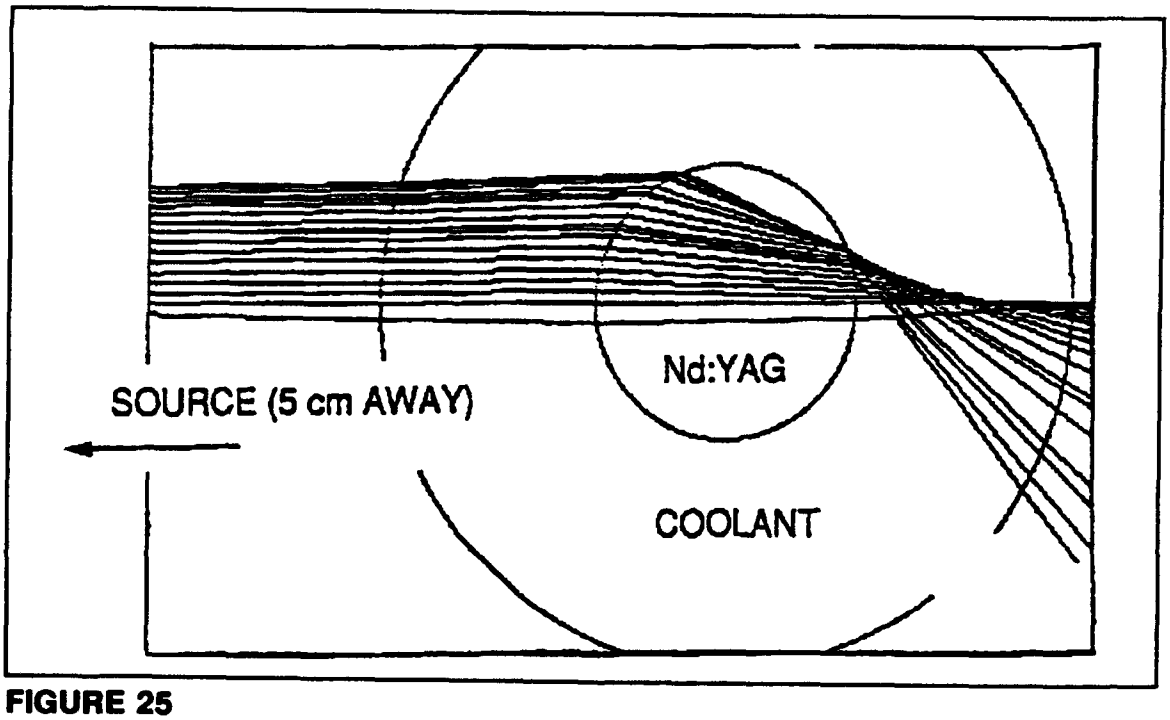

FIGURE 25
Pumping Ray Trace Through 3-mm YAG Rod

Pump Cavity Reflectivity: The pump cavity was sputtered silver on fused-silica "pumping-wheel's" exterior (Figure 1). The dominant surface in the multi-pass pumping calculations is the periphery of the wheel, not the parallel ends of the wheel, as discussed earlier. Because of the complex surface chemistry at the silver-quartz interface, it often takes a few practice runs to achieve the desired combination of adherence and internal reflectance. Our reflector is an internal one, and whereas the theoretical reflectance of silver on fused quartz is a few percent less than bare silver in air, it is still an excellent choice, and an internal reflectivity of 92 to 95 percent should be achievable. The coater (Scientific Coating Laboratory, San Jose, Calif.) achieved excellent adherence on the first attempt, but the internal reflectance is lower than optimum. It is likely a second attempt would produce substantially superior internal reflectance, without sacrifice of adherence, but time constraints dictated that we utilize the reflector as coated in the first attempt.

Figure 26 shows the reflectivity versus wavelength of a flint witness from the sputtering run. The external surface reflectance (labeled "first surface") is typical of silver before oxidization, and the lower internal reflectance (labeled "second surface") of this first attempt. Because of the geometry of the pumping cavity, direct measurement of the peripheral surface of the fused-silica wheel was not attempted. The witness internal reflectance is 74 percent at 800 nm, uncorrected for Fresnel losses, corresponding to an internal reflectance of about 82 percent for the pumping cavity. The silver coating was not over-coated to enhance durability or prevent external oxidation.

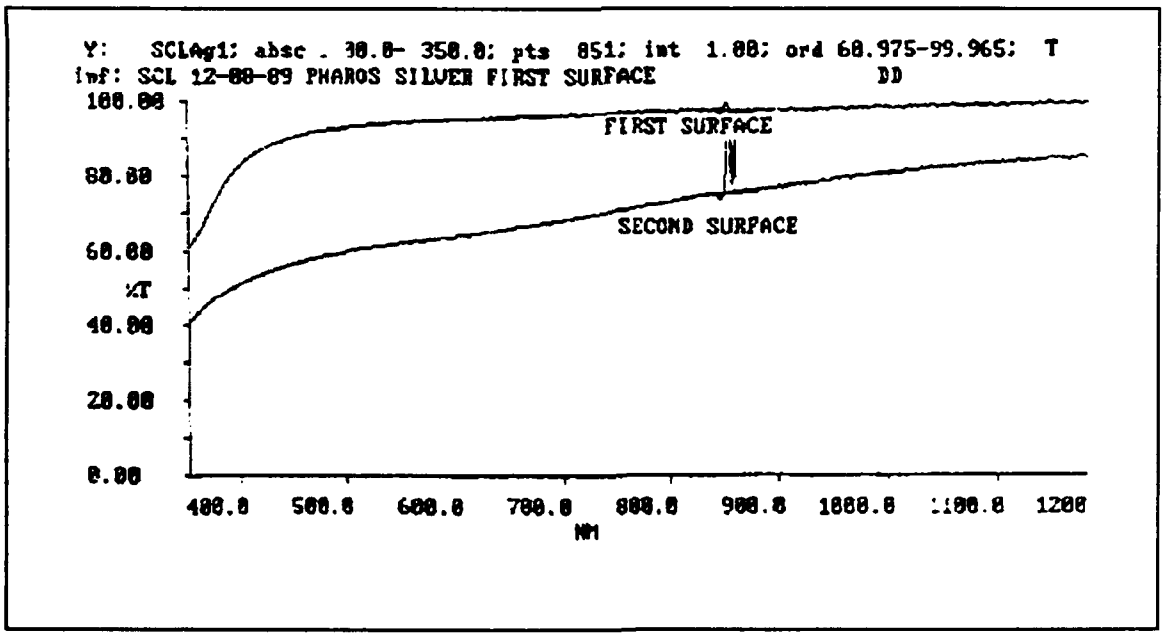

FIGURE 26
Witness Reflectivity versus Wavelength

SECTION IV

DIODE LASER CHARACTERISTICS

This section discusses the diode lasers utilized to pump the Nd:YAG laser rod. The diodes, from Spectra Diode Laboratories, were characterized for wavelength, efficiency, temperature dependence, and radiation pattern. One diode was damaged during the experiments, and the failure analyzed.

Source Selection

Because of the high cost of laser diodes, it was anticipated that the experimental program would be severely constrained by low available pumping power. This has two adverse effects: only a short length of laser rod can be pumped to a low inversion, resulting in low gain, just above threshold operation, and low over-all efficiency; and the thermal benefits of the low heat deposition inherent with diode pumping cannot be macroscopically evident and will be difficult to measure. Initial calculations showed that a minimum of 50 watts of pump power was needed to conduct even a minimal experimental program.

Two sources of diode lasers were explored: Spectra Diode Laboratories, Inc. (SDL), and Lawrence Livermore National Laboratory (LLNL). Spectra Diode Laboratories was selected as the supplier, for the following reasons:

- during this phase of the contract they announced price reductions which made it possible to purchase 60 watts of pump diodes with the available funds,
- they offered assured delivery consistent with the project schedule, and
- they offered wavelength tolerance of ± 5 nm that, although inadequate for systems designs, are adequate for this laboratory phase of the project.

Lawrence Livermore National Laboratory, doing in-house packaging of purchased metalized laser bars, anticipated having higher power devices available, with more satisfactory wavelength tolerances (± 1 nm), and at lower cost. However, fabricating devices for NRL and TTC would be inconsistent with their R&D charter, and the mechanism for delivering the diodes to TTC and reimbursing LLNL for them was unclear. This uncertainty made any assurance of a delivery schedule impractical, which would have put the entire experimental effort at risk.

SDL offered two suitable devices, models SDL-3080-L and SDL-3090-S, rated at 5 and 10 watts output power respectively. The current data sheets are in Appendix A. Note that the SDL "S" package outline went through three revisions in 1989. Both are cw devices, 1-cm in length, rated at 30 mW per emitting aperture. The primary differences are the number and density of emitting apertures along the 1-cm length of the bar, and the details of the heat sink and mounting provisions.

For these experiments, 5-watt devices were selected. Ten were wavelength selected and two were not. There were three reasons for selecting 5-watt devices:

- since the 10-watt devices were a new product, their guaranteed delivery schedules were inconsistent with our schedule,

- the use of 5-watt devices would allow pumping a 2-cm length of rod with diodes spaced at five locations around the periphery, the minimum number calculated to give useful pump uniformity, and

- although 10-watt devices were cheaper per watt, we could afford the needed total power, and meet our schedule, by waiting until after a price reduction and ordering the 5-watt devices.

Figure 27 shows the manufacturer's typical input-output relationship for these devices, and Figure 28 shows the package outline. The laser bar is attached, p-side down, at the right edge of the top surface of the large, heat-spreading mount. The electrical leads enter from the left; the positive lead connects to the heat sink and the negative lead extends over the top of the laser bar. The cathode connection to the bar is made by multiple parallel bond wires from the negative lead. All the diode channels are electrically paralleled.

Diode Emission Wavelength

As discussed in Section III, "Laser Design and Pumping Analysis," tailoring the profile of pump energy deposition in the laser rod is important in order to achieve a usable far-field beam quality from the laser. Control of the pumping profile is strongly dependent on the product of the laser rod diameter and the absorption coefficient. Although the details vary with the laser host material and the lasing ion, crystalline solid-state hosts are characterized by narrow absorption peaks and steep slopes of absorption coefficient versus wavelength. Nd:YAG, used for the experiments in this program, shows these characteristics. Figure 29 is the measured transmission (uncorrected for reflection

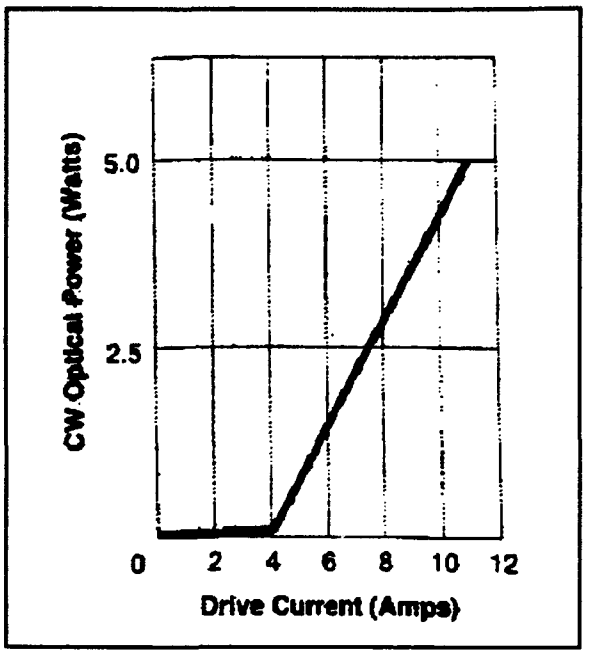

FIGURE 27
Typical SDL-3480-L Input-Output Curve

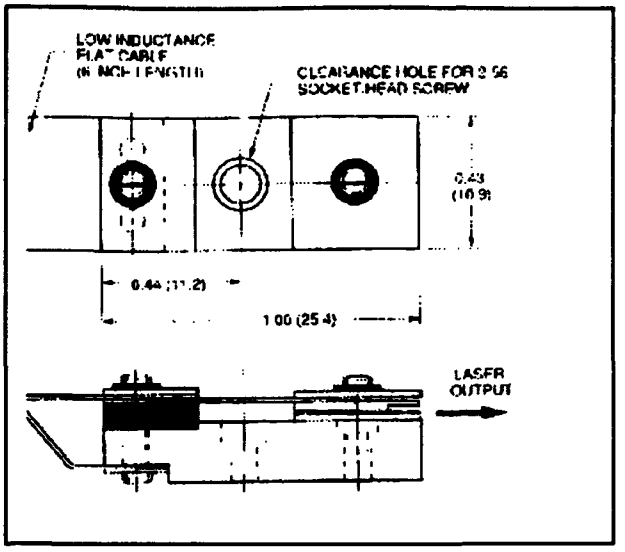

FIGURE 28
SDL-3480-L Mechanical Outline

losses) through a 2.92-mm diameter rod used in some of these experiments. Utilizing SDL's special selection to $\pm$5 nm, and ignoring the finite spectral width of each diode, if the diodes were specified at 805 nm, they would scatter from 800 to 810 nm, and Figure 29 shows the absorption coefficient of the rod in this wavelength region varies between about 1.3 cm^{-1} and 4.1 cm^{-1}. Several things are apparent:

- the diode center wavelengths must be controlled more closely than SDL is willing to specify or select for the designer to control the radial gain profile of the rod,
- the design should focus on a spectral region where the slope of the absorption-versus-wavelength curve is relatively gentle, in order to reduce sensitivity of the final design to variations in devices and environment,
- all variables affecting the diode emission wavelength must be understood in order to design a laser system and understand its performance, and
- the system designer must cope with a total wavelength spread equal to the sum of the spread in center wavelengths and the spread inherent to the bars. Anything the diode fabricator can do to reduce either helps the system engineer.

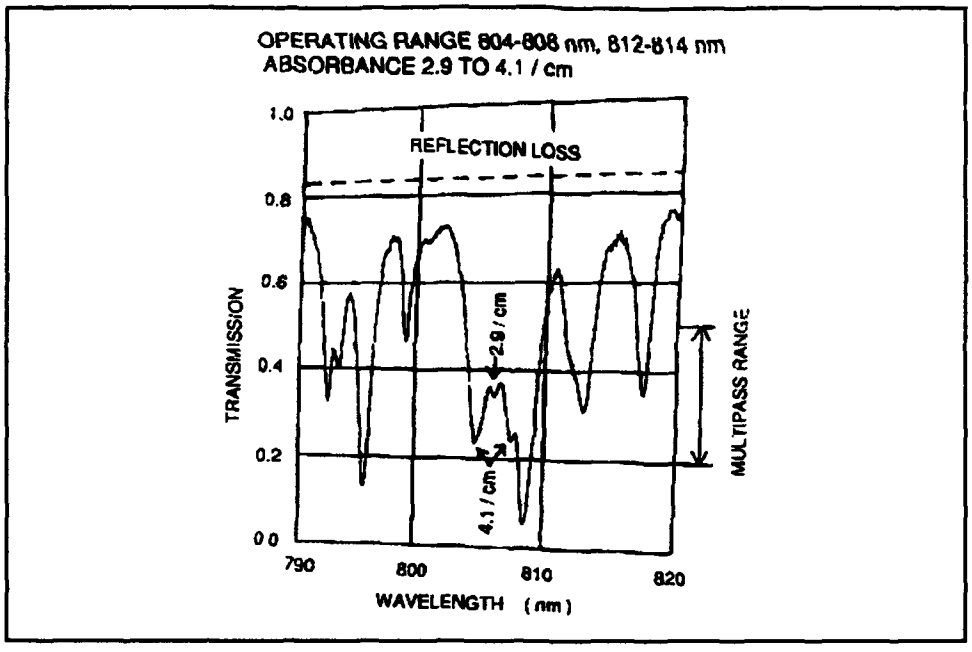

FIGURE 29
Measured Transmission Through
0.292-cm Rod Diameter, 1.1% Nd:YAG

Fortunately, Nd:YAG, Nd:YLF, and Nd:BEL have significant absorption in the region of efficient operation of aluminum-gallium-arsenide diode lasers. Other laser systems of interest, for example, Tm:Ho:YLF, require pumping in the range of 785 to 770 nm. These shorter wavelengths have proven more difficult for diode manufacturers to reach with efficient, high-power devices. However, progress is being made and a variety of solid-state lasers should be candidates for diode-pumping in the near future.

In addition to the nature of the laser material's absorption spectrum, and the diode manufacturer's ability to control the emission wavelength and/or willingness to select diodes, other variables enter into the diode wavelength issue. Among them are the following:

- the inherent spectral width of each emitting channel, or group of channels, in the diode array structure,
- the temperature dependence of the emission wavelength, and
- the spread in center wavelengths, either systematic or random, amongst the groups of channels along the length of the bar.

The first factor mentioned, the inherent spectral width of each group of emitting channels, arises from the physical structure of the diode array. The 5-watt SDL-3480-L array consists of 20 discrete emitting regions, usually called diodes, distributed along the 1-cm length of the emitting face of the bar. The arrangement is one of perhaps 20-percent packing density, that is, the "diodes" are spaced on 500 micrometers centers and are of the order of 50 to 100 micrometers in width. The emission from each of the 20 "diodes" is 250 milliwatts. Each emitting region is made up of a number of parallel channels diffused into the bar. SDL data show that each channel is rated at 30 mW, so there must be 8 channels per emitting region. The channels are packed within the group with about the same density as the groups are packed along the bar, being 1 to 2 microns in width on about 10 micron centers. The 10-watt SDL-3490-S has 30 groups, achieving the higher output power by increasing the number of groups, increasing their packing density, and presumably increasing the number of channels per group and perhaps the emission per channel.

The channels within each group are physically close enough together that their emissions are coherent, a point we will return to in the discussion of vertical far-field radiation patterns. This means that each group (or "cluster" or "diode") has a discrete center wavelength and distribution function around it, the width being determined by the mode structure of the individual channels, the coupling between them, and (in some applications) the impressed electrical modulation. SDL specifies the spread in wavelength from a bar, including both inter- and intra-group effects, is no more than 3 nm. For the purposes of this work, the spectral width of any group of channels, dominated by the channel mode structure, is significant compared to the other effects, e.g., the spread along the bar between the groups and the temperature effects. The spectrum of one group of channels (out of 20 along the bar) is shown in Figure 30. The full width shown is 2.0 nm. The width is determined by the mode structure of the coupled group of channels, and perhaps by temperature gradients within the group.

The emission wavelength of diode lasers has a significant coefficient of change with temperature, typically greater than +0.2 nm/^{o}C. This fundamental phenomenon results from the temperature dependence of the bandgap voltage. As in all semiconductors, the bandgap voltage has a negative temperature coefficient, being about -0.4 to -0.5 meV/^{o}C for GaAs, depending on the temperature and aluminum concentration. This fundamental temperature effect affects the design of diode-pumped solid-state lasers in two ways:

- temperature gradients in the diode laser bar, dependent on the bar topology, heat sink design, and bonding technology of the manufacturer, broadens the distribution of wavelengths from the different emitting region along the bar; and

- maintaining the diodes at fixed temperatures, within small limits, imposes severe requirements on the system thermal design and significantly reduces the over-all system efficiency to far below expectations based purely on laser physics considerations.

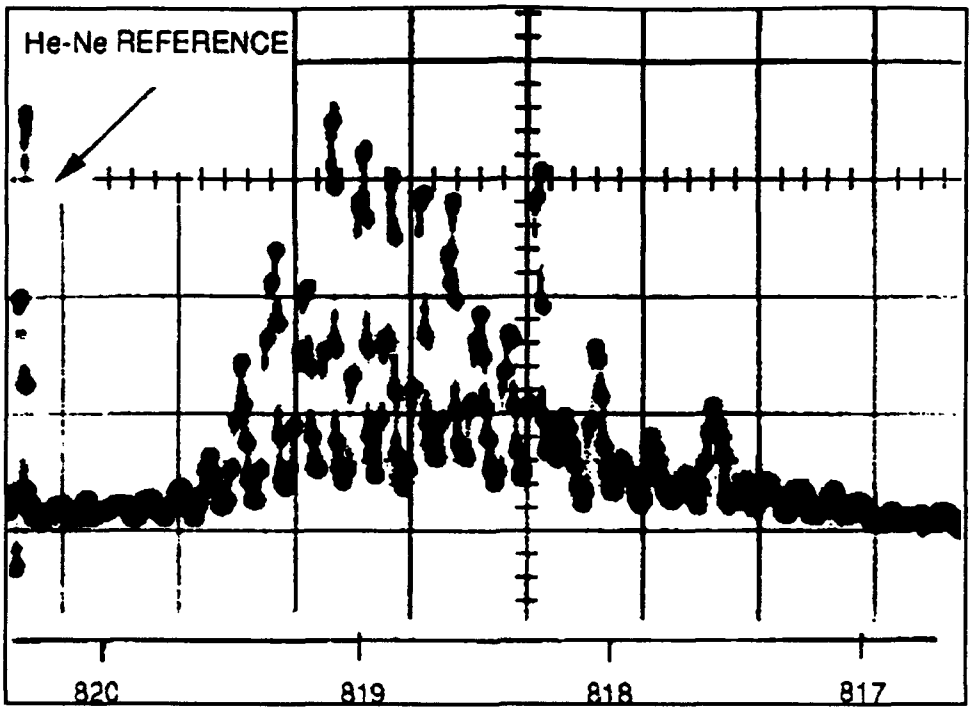

FIGURE 30
Multi-Mode Spectrum, One of 20 Lasers in a 1-cm Diode Array Bar
(Relative Intensity versus Wavelength in nm)

Indeed, system thermal management requirements can reduce the over-all system efficiency, and increase its weight, to the extreme that flash-lamp pumped laser systems are lighter, smaller, and more efficient. This system-level reality takes little consolation from the fact that the flash-lamp pumped system deposits it's excess heat in the laser rod while the diode pumped system deposits its excess heat in the diode cooling system. In the laboratory, however, this temperature dependance is readily put to advantage. Since diodes with closely selected center wavelengths were not economically available from SDL, each diode array was mounted on an individually adjustable water cooled heat sink, allowing the center wavelength of each diode array to be temperature tuned to the desired wavelength in the Nd:YAG absorption spectrum. Figure 31 shows representative temperature tuning curves for three of the SDL diode arrays used for this work. The unsuitability of this approach in militarized systems is apparent. The narrower the spectrum of emission from each laser bar, and the broader the acceptable region of operation in the laser's absorption spectrum, the greater the margin remaining to accommodate temperature drift. A large margin for temperature drift simplifies the cooling system design, reduces complexity, increases reliability, improves the over-all system efficiency, and generally increases the credibility of the final design. Conversely, it is easy to devise designs with no or negative margins for temperature

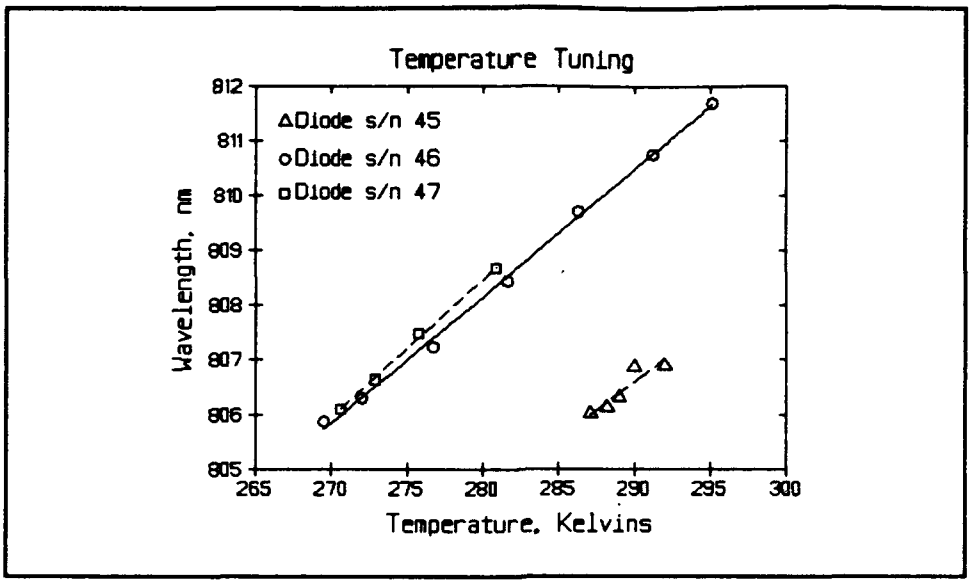

FIGURE 31
Diode Emission Wavelength versus Temperature

drift, requiring sub-degree temperature control and use of thermal-electric cooling stacks. TTC has taken the position from the beginning of this program that any militarily useful design must provide a sufficiently large margin of diode temperature drift to be compatible with direct liquid cooling systems. We believe that this program is the first such demonstration of significant scale operation of a solid-state laser with direct liquid cooling of the diodes.

The center wavelength variation along the bar due to temperature gradients may be negligible, parabolic, linear, or a combination of the latter two. If the bar is bonded to its heat sink with a uniform layer of metallization, and the heat sink has negligible gradients at the edges, negligible thermally induced wavelength variation would be experienced. LLNL, for example, is striving for this condition with their microchannel coolers and bonding technology. Significant thermal gradients at the heat-sink edges would yield a parabolic shape to the center wavelength along the bar. Conversely, a systematic wedge in the thickness of the metallization bonding the bar to the heat sink would produce a linear wavelength shift along the bar.

In addition to the spread in emission spectrum of each group of diode channels due to the laser mode structure within the channels and the coupling between physically adjacent channels, and the spread due to temperature non-uniformities along the length of the bar, other mechanisms may be expected to broaden the emission spectrum of a compete diode laser bar. One such mechanism is variation of the gallium-to-aluminum ratio along the bar, due to slight process variations across the surface of the wafer during the MOCVD processing. Such variations would be random, unless there existed a systematic gradient in the composition of the MOCVD reactor gases across the wafer.

If a linear shift in center wavelength along the bar is observed, and physical examination of the bar-to-heat sink bond shows no significant wedge, then systematic doping variation across the wafer is to be suspected. As recently as two years ago, it was not uncommon to find linear gradients in center wavelength along the length of diode bars, with shifts of greater than 5 nm from end to end being seen. Manufacturers have improved their process controls so that these obvious gradients are no longer inevitable, but thermally induced and random variations along the length of bars are still common.

We measured the wavelength spread of our diodes twice during the experimental program. Figure 32 shows the variation in center wavelength along the 1-cm length of each of the 12 diode arrays purchased for this program. The full width of the distribution caused by the mode structure (Figure 30) is shown for by the open squares and triangles. The total wavelength spread of each device is the total range between the extreme lowest and highest wavelengths of the mode distributions of all of its groups of channels taken together. It is apparent that there are process variables that are not fully under control. Some devices show narrow distributions along the bar, some show random distributions, and some show end-to-end gradients indicative of either composition gradients or a linear taper to the thickness of the metallization between the diode bar and its heat sink. (Note that serial numbers 39 and 41 were not wavelength selected devices.) The data in Figure 32 are taken at the temperatures indicated, nominally room temperature.

Because we temperature tuned the diodes to the desired absorption band of Nd:YAG, we measured the spectral width at the desired operating wavelength and temperature. Comparing the two sets of spectral width data, we found it to be temperature dependent. Figure 33 presents the change in spectral width with change in temperature. The scatter is not surprising, considering the difficulty of defining the "width" for a device consisting of 20 emitting regions. The spectral width in Figure 33 increases about 0.06 nm per K.

Diode Efficiency

Figure 34 shows the efficiency of diode s/n 45 as a function of output power. The data are at room temperature. The temperature correction of the data is insignificant.

Figure 35 shows the temperature effect on diode efficiency. The open squares show the effect at constant input power, 13.4 $\pm$ 0.1 watts, also for diode s/n 45. CW diode data are usually presented at constant output power because cw operation is relatively near threshold. Using Figure 34, Figure 35 is corrected to a constant output power of 4.0 watts, and shows a best-fit slope of -0.7 percent per K. For comparison, Figure 36 is SDL preliminary life test data for their SDL-3490-S devices at 10 watts output. The "Number 2" array was operated at both 20 and 40°C. The change of the P_{out}/I ratio is about -0.6 percent per kelvin, relative to the room temperature value, in good agreement with the our data.

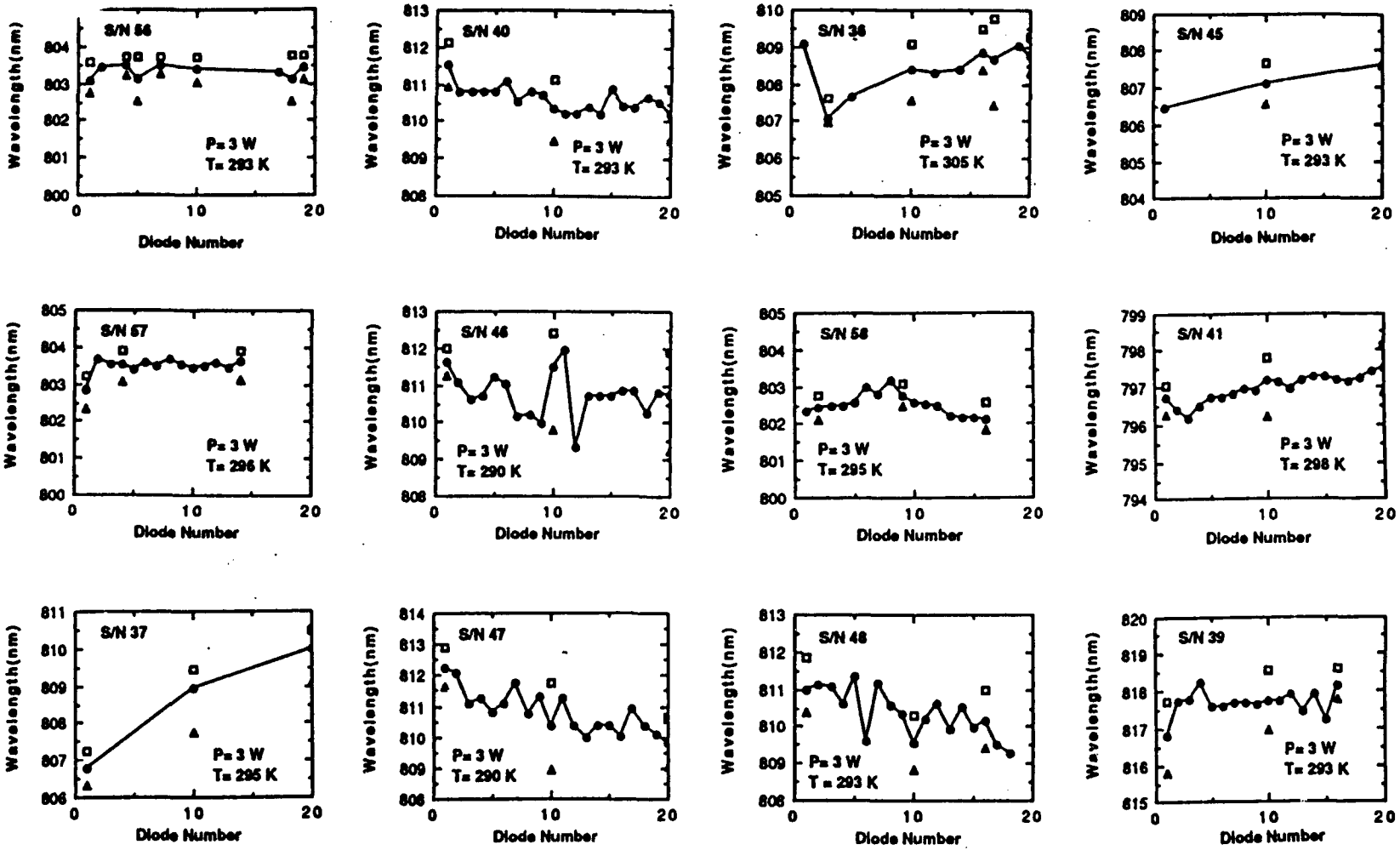

△ Lower Wavelength ● Center Wavelength □ Upper Wavelength

FIGURE 32
Diode Laser Wavelength versus Position Along Bar

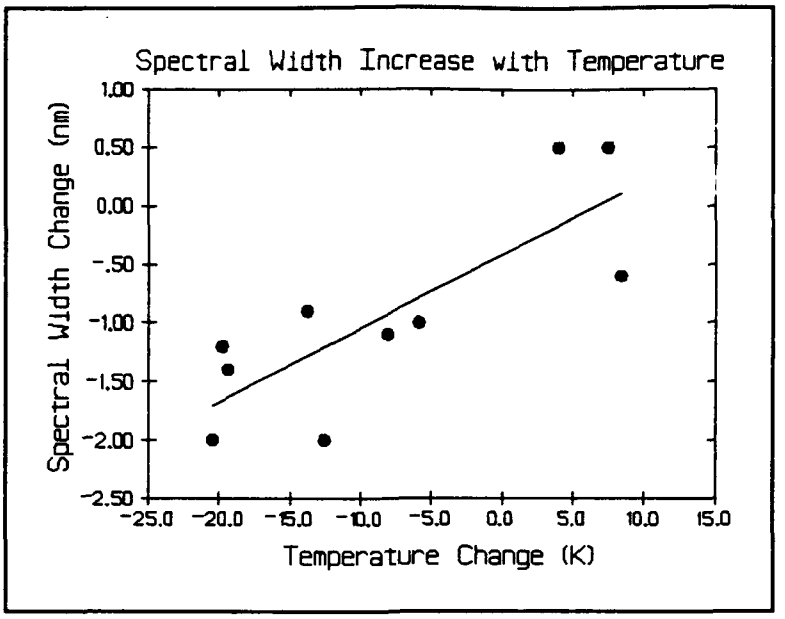

FIGURE 33
Change in Spectral Width with Temperature

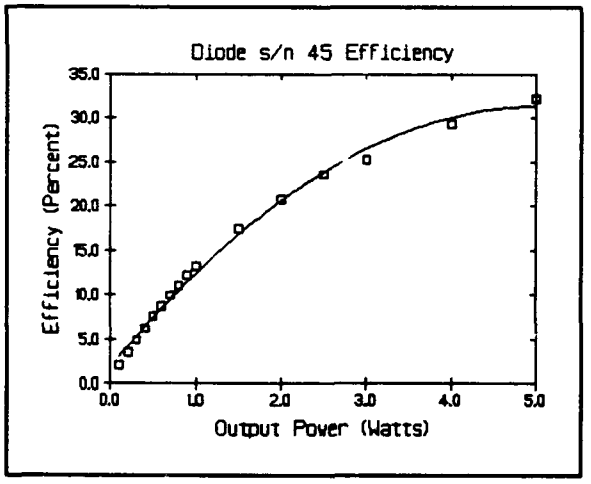

FIGURE 34
Diode Efficiency versus Output Power at Room Temperature

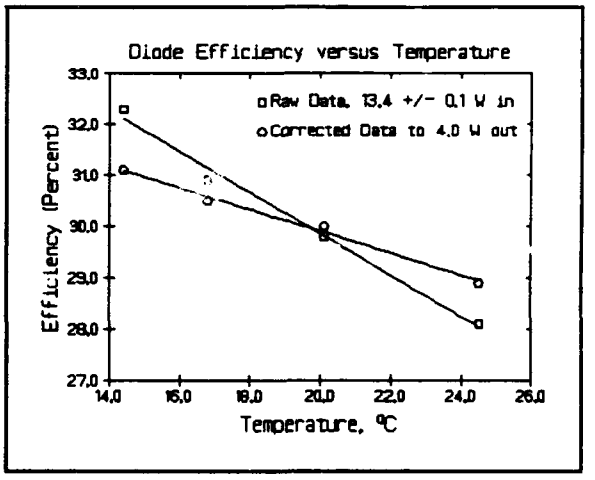

FIGURE 35
Diode s/n 45 Efficiency versus Temperature at 4.0 Watts Output

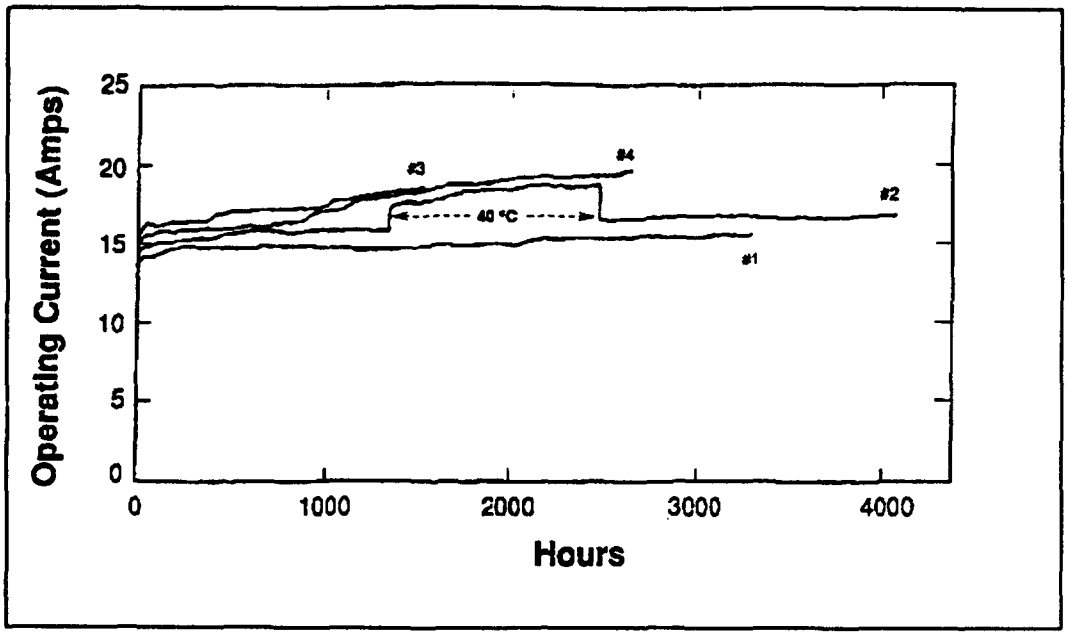

FIGURE 36
Diode Current versus Age and Temperature (Courtesy SDL)

Figure 37 shows the Input-Output (current to optical power) relationship of the diode arrays used on the program. The lasers split into two groups, with lasing thresholds of 3.16 and 5.97 amperes. The slope efficiencies of the two groups were 0.79 and 0.95 watts per ampere, respectively. Figure 38 shows the efficiency of the diode lasers at a constant 5 watts output (solid circles). The mean efficiency is 32.3 percent. The three devices showing the higher threshold in Figure 37 all cluster at low over-all efficiency in Figure 38. Figure 37 shows the distinction between the two groups of devices much more clearly than does Figure 38. The efficiency data were taken at differing case (heat-sink) temperatures, from 277 to 298K. No significant trend of efficiency with temperature can be deduced from these data alone, although it is well established that device efficiency and temperature are inversely related. Figure 38 is plotted with this correction (open circles) for comparison with the raw data (closed circles). The mean of the corrected data is approximately 30.5 percent.

The voltage-current curves of the devices are indicative of an apparent device series resistance of about 0.012 $\pm$0.005 ohms, less than one-half SDL's specified maximum of 0.030 ohms. The device series resistance is a significant factor in determining the over-all diode laser efficiency.

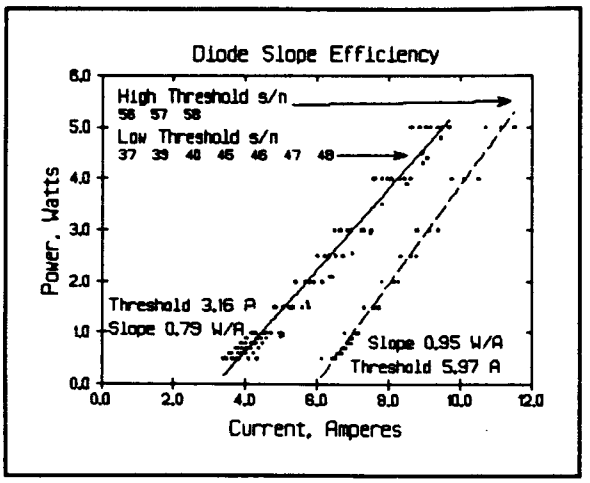

FIGURE 37
Diode Laser Power versus Input Current at Room Temperature

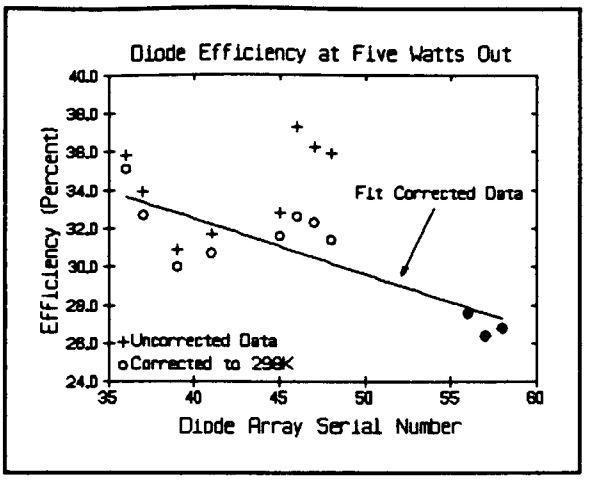

FIGURE 38
Diode Laser Efficiency versus Serial Number

Diode Radiation Patterns

Linear diode arrays commonly have significantly different far-field radiation patterns in the two directions, parallel and transverse to the long axis of the bar. In the direction perpendicular to the long axis the apertures along the diode bar have a dimension of about 1 micrometer. The resultant far-field pattern is approximately Gaussian with a FWHM angle of 30 to 50 degrees. In the experimental setup for this program, the diodes were arranged with their long axes vertical, so this transverse direction is referred to as "horizontal" here. Figure 39 shows Gaussian fits to the horizontal far-field patterns of diodes used for this project. The average divergence angle is 36.1 degrees FWHM.

The transverse divergence must be collimated into the laser rod; a $(1/e)^2$ intensity half-angle of 22 degrees was used in the pumping analyses described Section III of this report. It is taken as a good approximation that the source point lies on the surface of the output facet of the diode for the perpendicular divergence.

Figure 40 shows a systematic, although not strong, trend toward decreasing transverse beam divergence with increasing device serial number. Comparing with the temperature-corrected efficiency-versus-serial number data in Figure 35, we can see that the serial number, transverse beam divergence, and efficiency are correlated. Higher serial-number devices purchased in this project show both lower efficiency and transverse beam divergence. These variations in divergence and efficiency indicate that significant improvements are possible in manufacturing process control. Device fabrication issues,

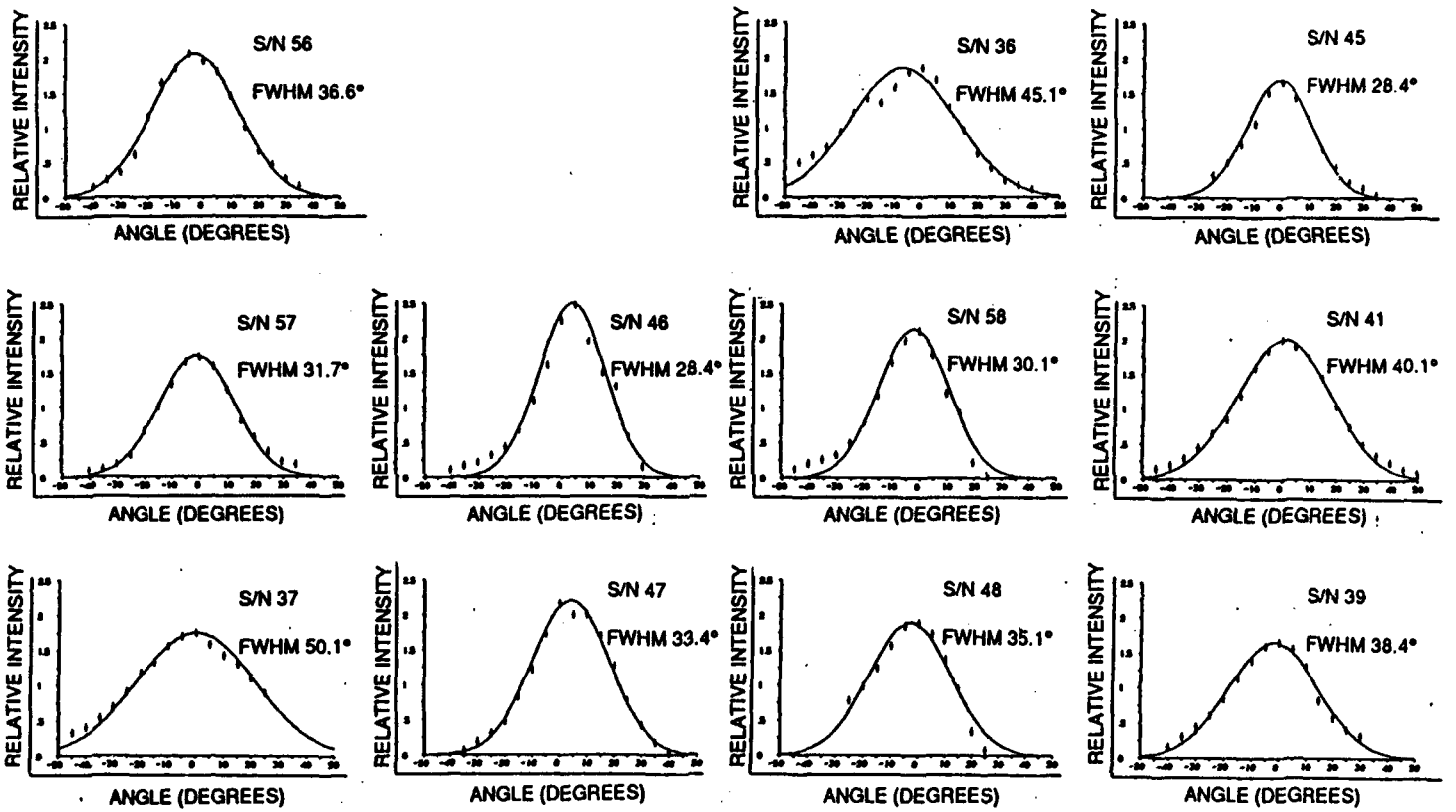

FIGURE 39
Horizontal Diode Beam Profiles with Gaussian Fits

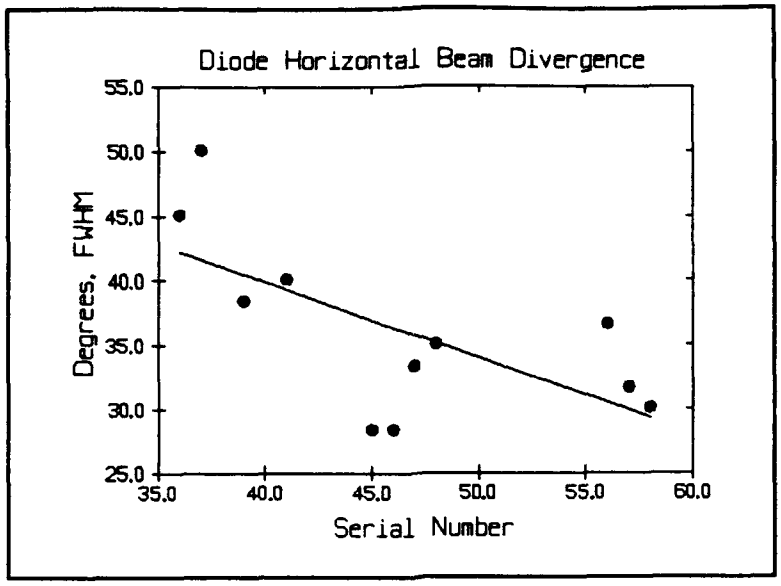

FIGURE 40
Diode Horizontal Beam Divergence
versus Serial Number

however, are beyond the scope of this project. They and cost issues are being addressed in parallel DoD-funded programs with device manufacturers, including SDL.

The diode arrays are made up of hundreds of individual channels along the length of the diode bar. Is it then fair to represent the transverse divergence as a single number for each device, as we have done in Figures 39 and 40? Figure 41 shows the transverse beam profile at three positions along one device: 2.5, 5.0, and 7.5 mm from one end. The data were taken 3.2 cm from the device. It is apparent that the assumption of a single angle to describe the transverse divergence of this device is justified. Similarly, the longitudinal (vertical) beam profiles were found to be insensitive to horizontal angle.

While the large transverse beam divergence of the diode arrays is a major challenge to the designer attempting to maximize the utilization of the available pump light, the longitudinal divergence is much more tractable. Because of the clustering of channels into groups along the length of the diode bar, the channels within each group are optically coupled. The effective aperture in the longitudinal direction is several microns, and the quoted far-field divergence is typically 10 degrees. This coherence among the adjacent channels in each group produces a second effect; the longitudinal beam profile usually shows a pronounced two-lobed pattern with a deep notch on axis. This two-lobe pattern

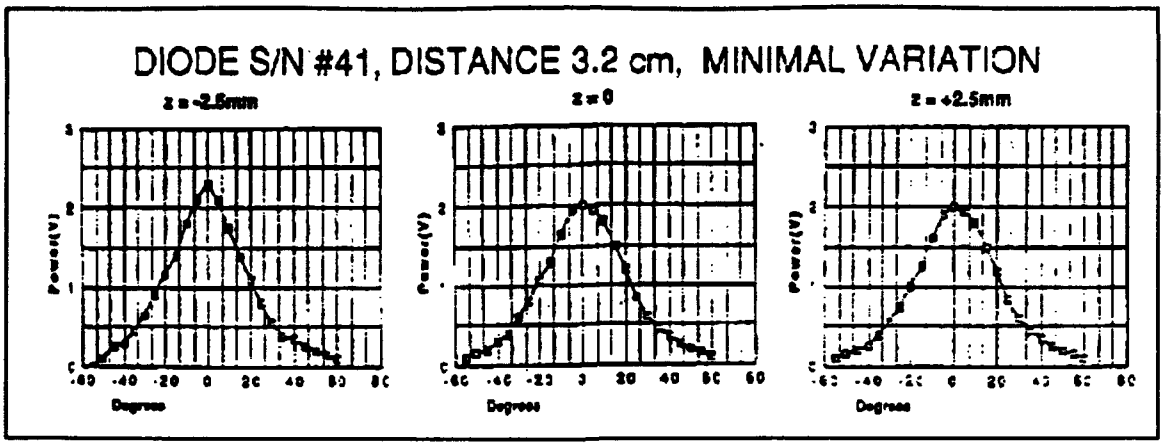

FIGURE 41
Horizontal Beam Profile at Three Positions Along Array

is inherent to the phase distribution of the fields across the total effective aperture. Spectra Diode is among the manufacturers more successful at minimizing the depth of the notch on-axis in the longitudinal direction. Figure 42 shows the vertical beam profile, as a function of distance from the diode, for one of our diodes. Although the beam develops the expected two-lobe profile at distances over one-half meter, it is distinctly flat-topped and uniform at distances of 6 cm or less. Figure 43 shows that all of our diode arrays had similar longitudinal beam profiles at a distance of 5 cm.

The small divergence in the longitudinal direction means the resultant Fresnel losses at the interfaces are negligibly larger than for the collimated case. As a result, only cylindrical optics are required to collimate the diode outputs to illuminate the laser rod. The ends of the pump cavity need to be highly reflective to maximize utilization of the light from the diodes located at the ends of the laser rod.

Diode array outputs show both different divergences in the two directions and the apparent source positions are usually found to be different. The rays for the transverse divergence are usually characterized from a source at output facets of the diode, while the source for the rays representing the longitudinal divergence usually lies a few microns inside the diode. This astigmatism is unimportant here and was not characterized.

The diode radiation is usually well polarized, with the electric field vector parallel with the long axis of the bar. For the TTC/NRL transverse-pumped rod geometry, this makes the pump field predominately "S" polarized at the interfaces along the pump light path. The degree of polarization of the diode emission is relatively unimportant in these experiments and was not characterized.

- REMAINS FLAT WITH 1 cm WIDTH TO ABOUT 6 cm DISTANCE, THEN DEVELOPS PEAKS --> KEEP DIODES WITHIN 6 cm OF LASER ROD (POWER 3 W AT 3 cm, 5W FOR REST, 8 mm x 1mm SLIT ON DETECTOR)

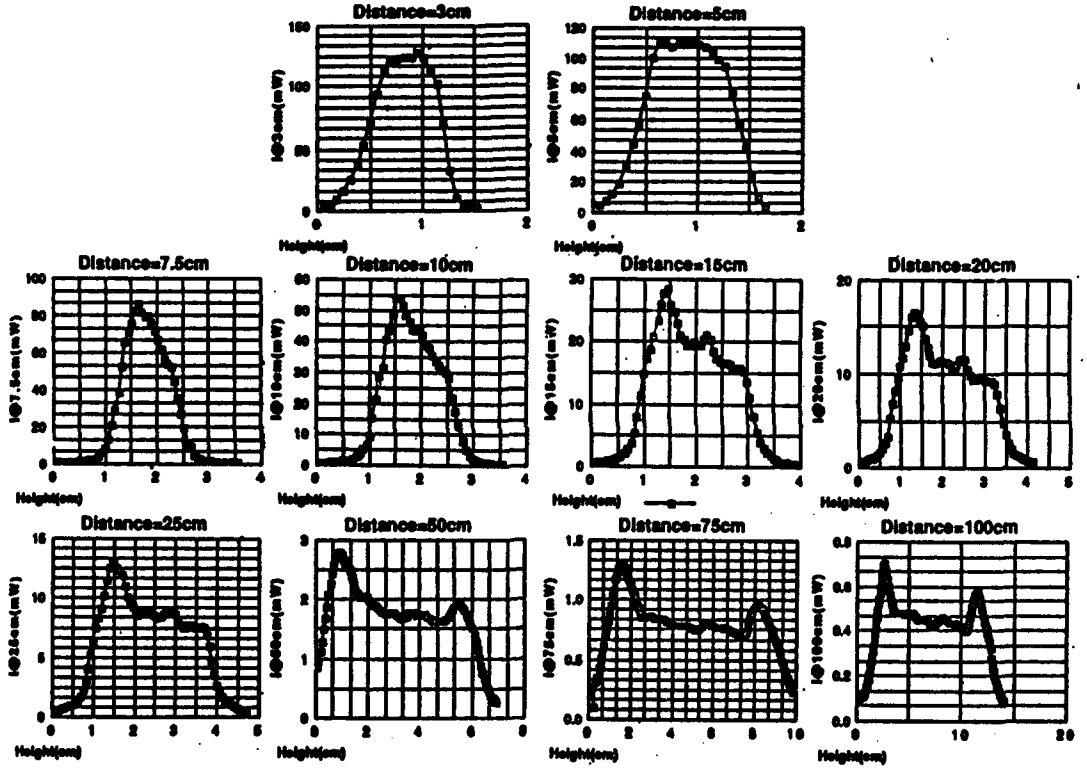

FIGURE 42
Vertical Beam Profile versus Distance, Diode s/n 39, on Center Line

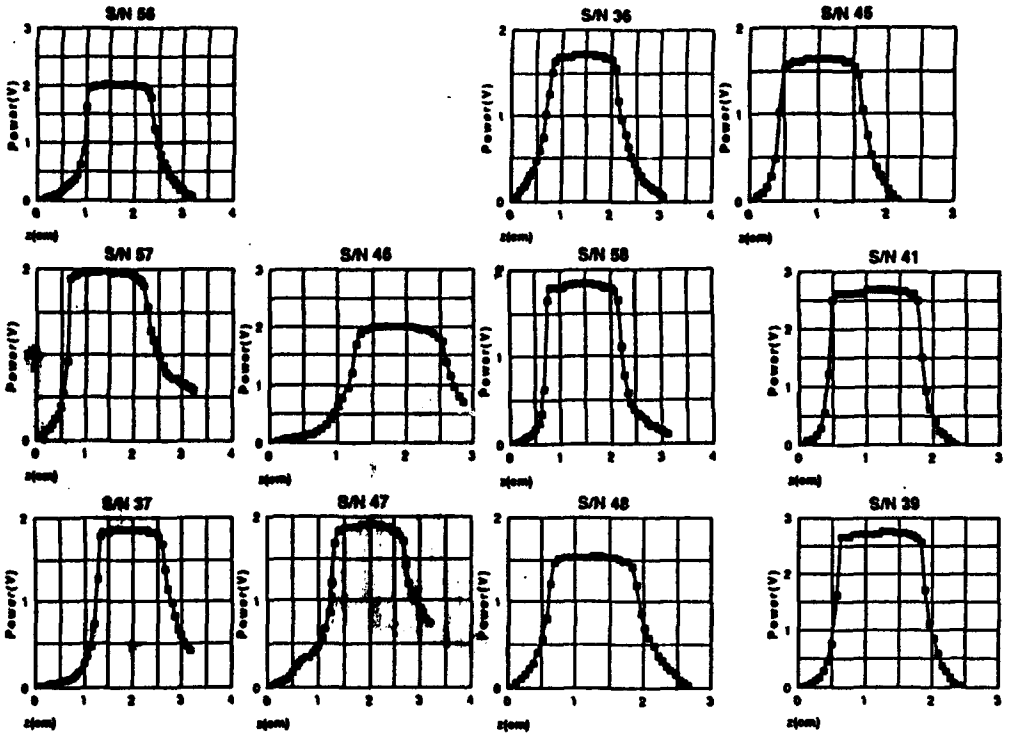

Measurements at 0 degrees angle, 5cm distance
Power = 3W, Temperature = 290K

FIGURE 43
Diode Laser Vertical Beam Profiles

Diode Mounting and Cooling

Spectra Diode Labs offers thermoelectric, but not liquid, coolers for their high-power diodes. As discussed earlier, because of eventual system efficiency considerations, TTC is committed to designs based on direct liquid cooling of the diodes. Thus SDL's cooling options were deemed unsuitable for this project, even for the laboratory demonstration experiments funded in this increment of the project.

TTC has done extensive work in the field of adaptive optics, including the development of active mirrors capable of sustaining high power loadings. As part of those efforts, TTC has developed a small (one-half inch square), light weight, liquid cooler with high heat transfer capability and small thermal gradients across its surface. These coolers have several distinct features, leading to their selection for this program:

- they meet or exceed all requirements for heat transfer rate and thermal uniformity,
- they are readily available in quantity, with minimal lead time, and
- they cost us about $60 each in small quantities.

Maximum temperature issues are important in handling diode laser arrays. Gallium and aluminum have large diffusion rates in the structure, and the laser performance is critically dependent on their concentrations. Nominally the junction (not the heat sink) temperature must be held to the order of 30°C in order to not adversely affect the laser lifetime or efficiency. SDL estimates that they "use up" ten percent of the lifetime of the device during processing and accelerated burn-in at elevated temperature before shipping. Although SDL did not identify the alloy used to braze the diode bars to the heat sink, they indicated that it would be safe to use brazing temperatures of up to 135°C when mounting the diode assembly to the cooler. We chose a low-temperature alloy (below 100°C) with excellent wetting properties, since voids in the braze would lead to temperature gradients in the diode heat sink. The brazing of the diode arrays to the coolers was done at TTC in a small oven, with no indications of difficulty. SDL indicated that this is the first time that they are aware of a customer doing their own brazing to the device or using liquid cooling.

The thick heat sink utilized by SDL increases the thermal impedance between the coolant and the junction, but it also makes the device mounting to the cooler a relatively non-critical step. Optimization of future systems designs, especially at high average power per diode array, may require significant reduction of the thermal impedance in the SDL package, and greater attention to the details of the junction-to-coolant thermal path. Figure 44 shows a side view of the diode mounted on the cooler. Figure 45 shows cross section of the liquid cooling unit and views of diode lasers soldered in place.

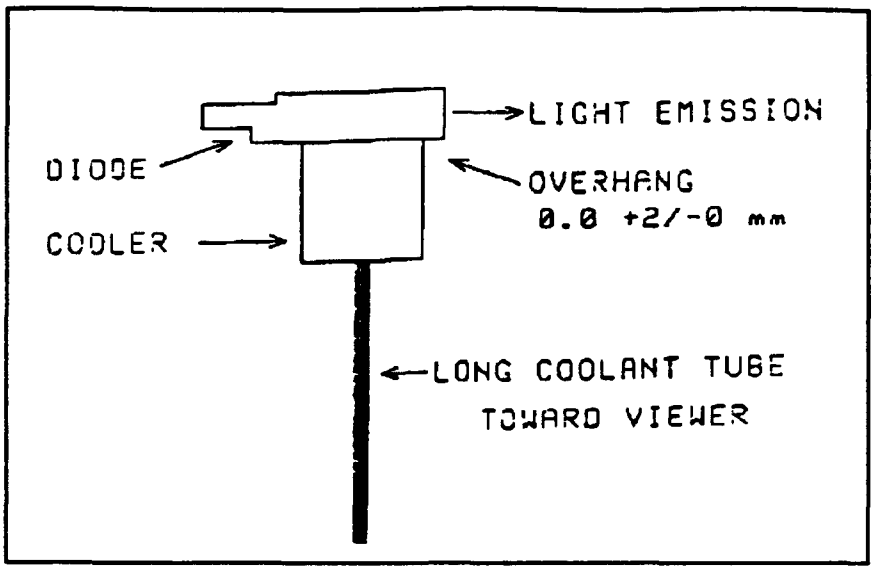

FIGURE 44
Diode Mounting on TTC Cooler

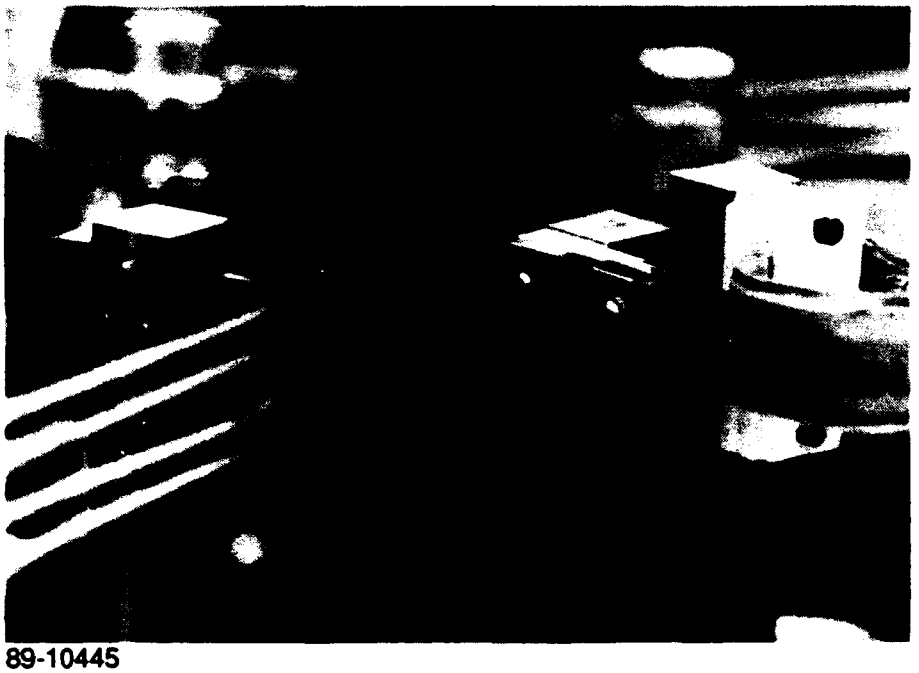

89-10445

FIGURE 45
Cross-sectioned Liquid Cooler and Views of Mounted Diodes

Failed Diode

Because of the limitation on the junction temperature in Ga:Al:As diodes to an absolute maximum of 35°C, temperature tuning of the diodes requires that their emission wavelengths be specified to be above the desired operating wavelength and they be cooled to tune their emission to the desired absorption band of the solid-state laser being pumped. The resultant operation below room temperature has two side benefits: it increases the lifetime and reliability of the diodes, and it increases their efficiency slightly. However, if the resultant operating temperature is below the dew point, then the diode is susceptible to condensation of atmospheric moisture. If the diode is operating, it is unlikely that condensation would form on the optical facets. However, if the diode is cooled before operation, or turned off while cooled, or operation is interrupted, then condensation on the optical facets can occur. To prevent this, we enclosed our laboratory experiment is a large plexiglass enclosure and purged it with dry air. With this setup, no condensation problems were encountered.

Construction of the dry-air enclosure was concurrent with initial testing of the diodes. Prior to completion of the box, care was taken to operate the diodes at all times they were cooled below ambient temperature. However, on one occasion, steps got out of sequence and a diode was cooled below ambient before being powered, and then power was applied. The diode failed immediately. Examination by SDL showed the failure to be unrepairable, so the device, s/n 40, was scrapped.

The nature of the failure was tin plating over the faces of the facets of the diodes in the array. Presumably the mechanism was that, with condensation on the facets, the application of power caused to current flow between the region where the bond wires are attached (diode N side) and the heat sink (diode P side). The current flow caused tin from a metallization layer to grow out over the facets, obscuring the optical apertures. This growth, shown in Figure 46, must have occurred rapidly, and electrically shorted the diode. Once the diode shorted, there was then no optical power to drive the condensation off the facets, and subsequent operation simply caused additional tin growth and damage. It is interesting to conjecture if the diode might have been undamaged if it had been warmed and thoroughly dried before power was applied.

Unfortunately, serial number 40 was one of the wavelength selected devices, of which we had exactly 10, i.e., there were no spares, and of course no funds to procure a replacement. The rest of the experiments were performed by replacing it with serial number 39. The latter diode lases at 817 to 818 nm at room temperature, and we were able to temperature tune it to the 813 nm absorption band of Nd:YAG. As a result, the diode failure had no significant effect on the experimental effort.

90-13588

FIGURE 46
Tin Plated Over Failed Diode Facet (Courtesy LLNL)

SECTION V

EXPERIMENT RESULTS and COMPARISON to ANALYSES

This section presents the results of the experimental program. These results also are compared with the analyses in Section III.

Experimental Setup

Figure 47 shows the experimental laser with the rod in a cooling jacket for single-pass pumping experiments. The laser rod is mounted vertically, as shown in Figure 48, with the resonator optics above and below it. The output beam exits upward. Figure 45 showed a close-up of mounting of two of the ten diode arrays. Figure 49 shows the multi-pass pumping cavity, a silver-coated wheel of fused silica, and Figure 50 shows it in place surrounding the laser rod. The entire experiment was housed in a dry-air-filled plastic enclosure to protect the diodes and optics from water condensation. The cover is removed in Figure 47 for clarity. Figure 51 diagrams the optical cavity.

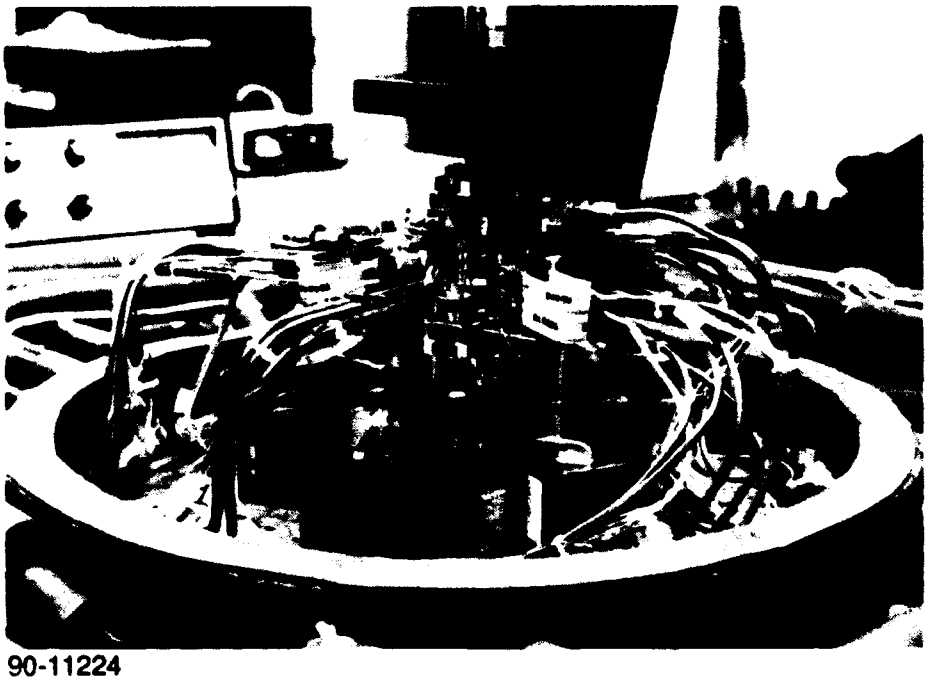

90-11224

FIGURE 47
Single-Pass Experimental Setup

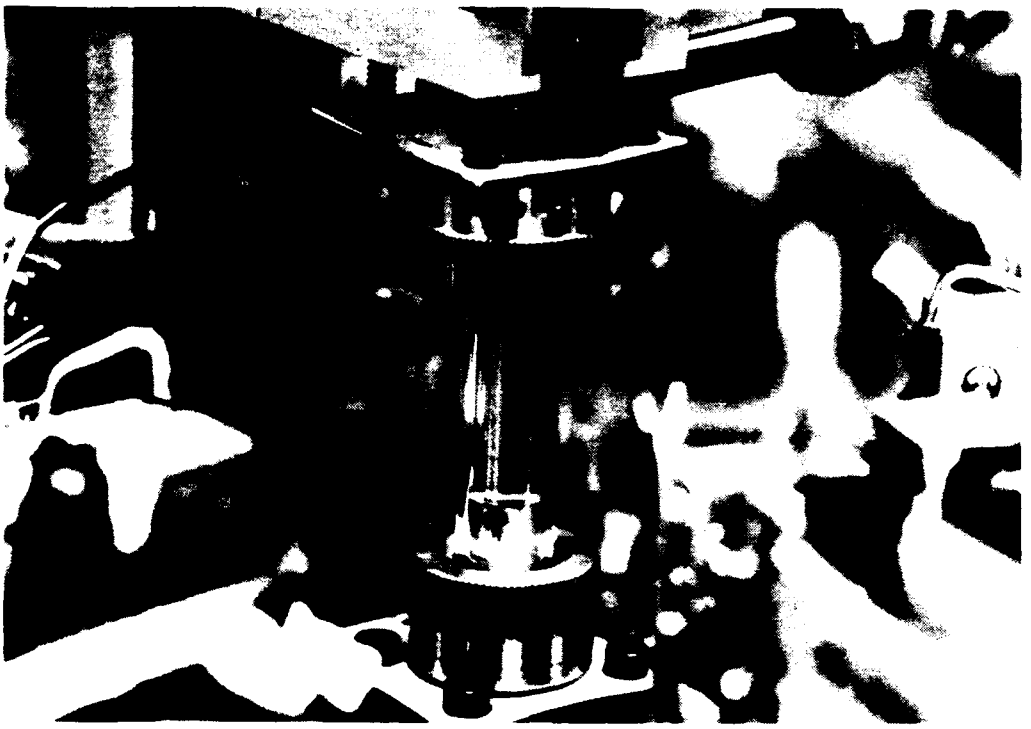

90-11223

FIGURE 48
Rod Mounted in Cooling Jacket for Single-Pass Pumping

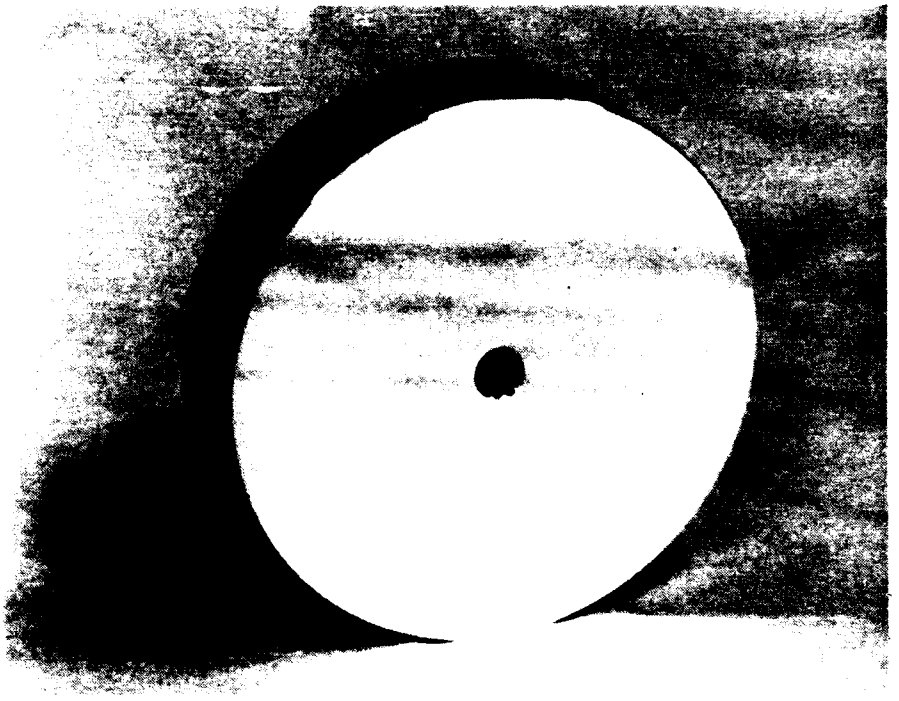

90-11226

FIGURE 49
Silver-Coated, Fused Silica Multi-Pass Pumping Cavity

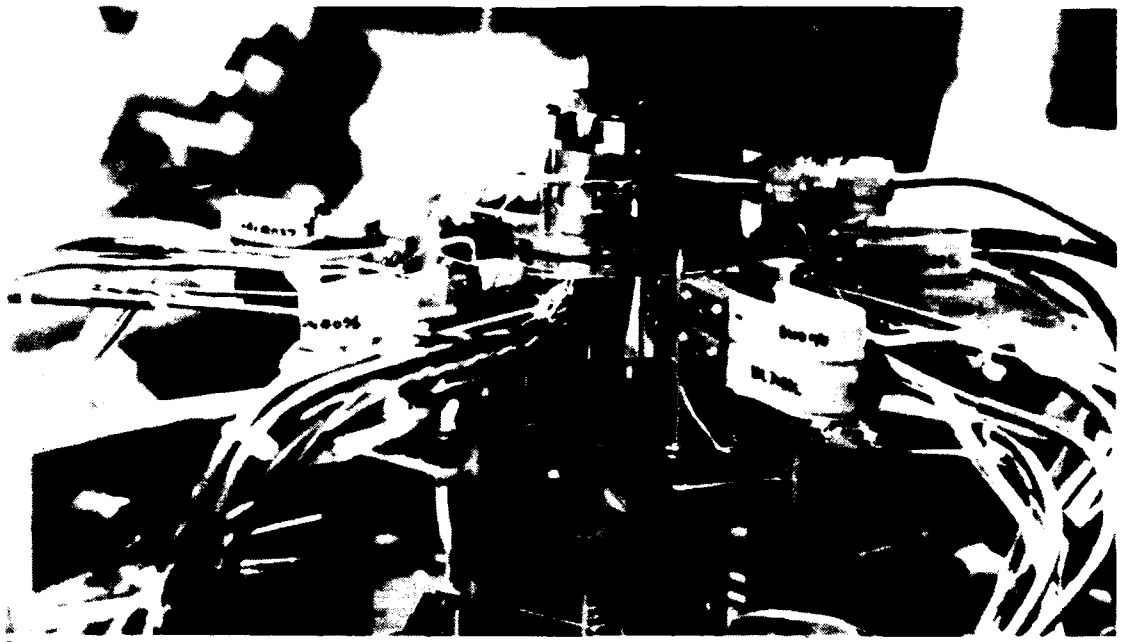

90-11228

FIGURE 50
Assembled Multi-Pass Experiment

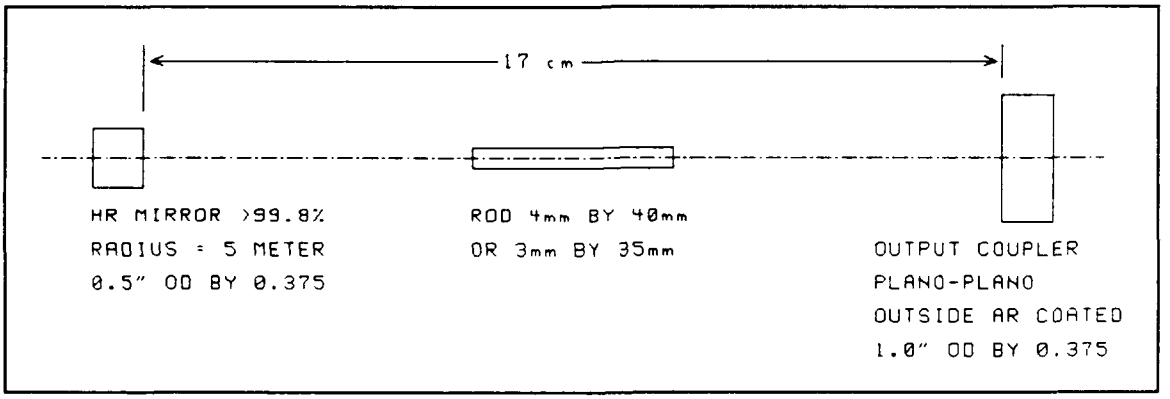

FIGURE 51
Laser Cavity Configuration

4-mm Diameter Rod Results

Figures 52 and 53 show the output of the 4-mm laser rod, as a function of diode array current, with 4 output couplers. Figure 52 data were taken with only a single pass of the pump light through the laser rod, that is, without the pumping-wheel multi-pass cavity in place. Figure 53 data are for the multi-pass pumping configuration.

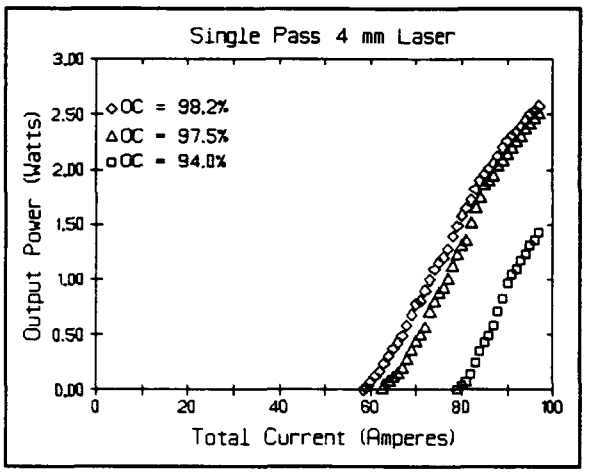

FIGURE 52
4-mm Rod, Single-Pass Pumping

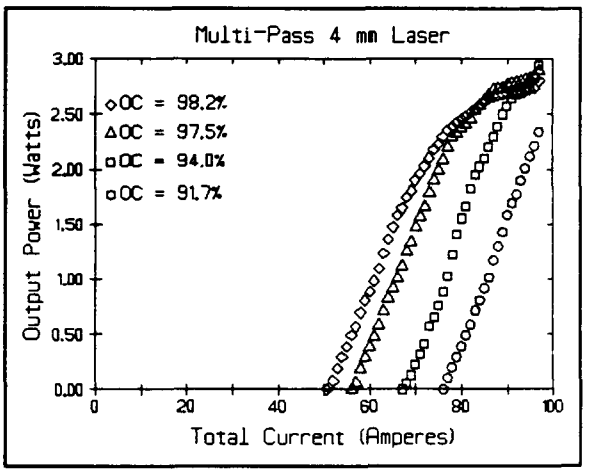

FIGURE 53
4-mm Rod, Multi-Pass Pumping

The single-pass data in Figure 52 shows a slight knee in the curves as they approach threshold from the right. This is indicative of slight pumping non-uniformity, reflecting that the diode optics were adjusted to maximize the light into the 3-mm rod, rather than attempting to achieve a uniform gain profile. Calculations in Section III indicate that the gain is expected to be peaked on axis. The x intercept indicates where the rod center went over threshold, while the straight-line projection of the laser output to the x-axis indicates the true threshold condition for the laser. The multi-pass data in Figure 53 show this effect much reduced, consistent with the reduction in peak-to-valley ratio expected from Section III.

Figure 53 shows a more serious effect, the asymptotic limitation of the output to less than about 3 watts. This indicates the turn-on of an output-limiting mechanism, such as ASE, excited state absorption, or parasitic oscillations. Excessive ASE (without feedback) can be reasonably ruled out, the gain is simply too low at these low pump powers. Indeed, we measured gains of the order of 10 percent per pass. Excited state absorptions have been reported in YAG with diode pumping, from both the upper and lower laser levels. Single-photon effects would lower the slope efficiency, but not cause the sharp roll-over shown in Figure 53. We more seriously considered parasitic modes, thermal effects, and multi-photon absorptions as possibilities.

Parasitic modes could be transverse, longitudinal, and circumferential. Transverse parasitic modes can be ruled out because the gain is too low; the transverse gain is perhaps 2 percent, while the loss at the pump cavity wall is at least 7 times greater. Longitudinal parasitic modes are in two classes: diamond modes entirely within the rod and modes off spurious reflections in the cavity. The rod is AR coated and we know from transmission loss measurements that the coatings must average at least 99.3 percent transmission, so the diamond mode would see a single-pass gain of 10 to 12 percent and a corresponding loss of over 99 percent. Off-axis cavity modes are geometrically possible; reflections are encouraged by metal tubes on the ends of the rod. However, with the cavity mirrors having a worst-case reflectance of nearly 92 percent, a competing mode in the same cavity is unlikely. Additionally, simple searches for off-axis output, with or without the output coupler in place, showed nothing unusual.

The fluorescence output, with and without the HR mirror in place, was measured at the location of the output coupler mount. Figure 54 shows these data, plotted against the best estimate of the available pump power incident on the 4-mm rod, as discussed in a later paragraph. If longitudinal parasitic modes were running off the HR mirror, the two curves would be substantially different in shape. If no gain-dependent losses were present, the curves would both turn upward with increasing pumping, reflecting the exponential nature of the small-signal gain process. These data, however, show good straight line fits. Any scattered pump light in the data in Figure 54 would tend to mask any gain depletion effects, but pump light was effectively filtered from the detector in the experiment. These data, although they do not strongly support the parasitic mode argument, do absolutely rule out any parasitic mode that includes the cavity HR mirror.

That leaves the circumferential mode as the only 1.064-micrometer parasitic candidate. Figure 55 shows the ray path. Two requirements exist for these modes, and our configuration meets both: the rod periphery is polished, and there is an index mismatch at the rod edge. Figure 56 shows the fraction of the rod cross section swept out by this mode. With water coolant (n = 1.33), the mode occupies nearly half the volume. This mode, if present would be expected to roll over the fluorescence output, and Figure 54 does not show that to be occurring. Thus we must be skeptical of any effect of a circumferential parasitic mode in the data Figures 52 and 53.

Parasitic oscillations at wavelengths other than 1.064 micrometers could occur, oscillating between the cavity mirrors, especially if the 4-mm rod AR coatings are peaked off-wavelength. However, most Nd:YAG lasing transitions are from the same upper level, the $^4F_{3/2}$ R2 level, so the 1.064 micrometer lasing limits the available population and gain, and the cavity mirrors are unlikely to have the requisite low losses off 1.064. Lastly, we would have detected light out the output coupler at the most likely transition, to the $^4I_{13/2}$ level at 1.319 micrometers.

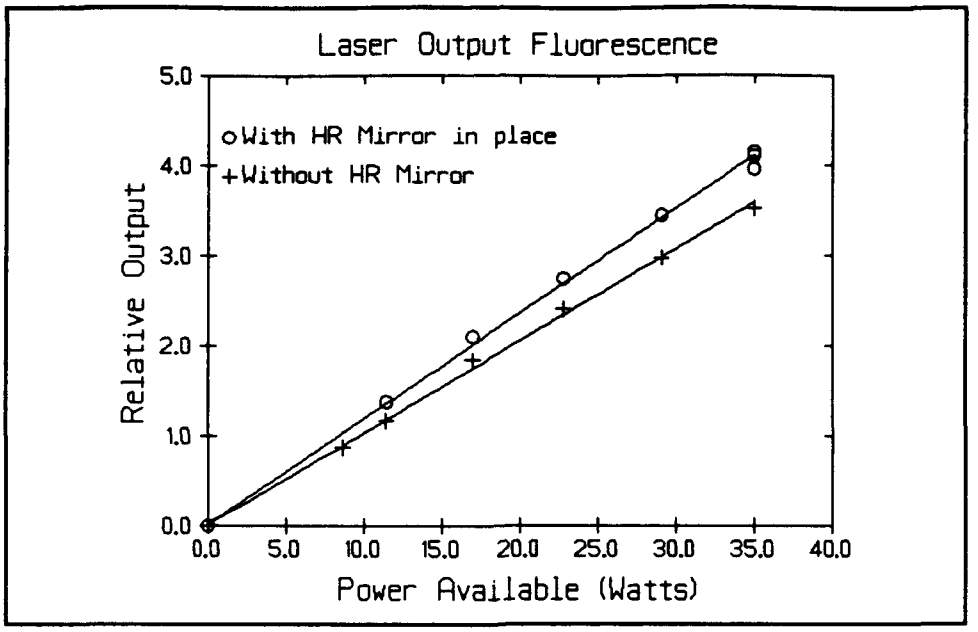

FIGURE 54
4-mm Rod Fluorescence Output

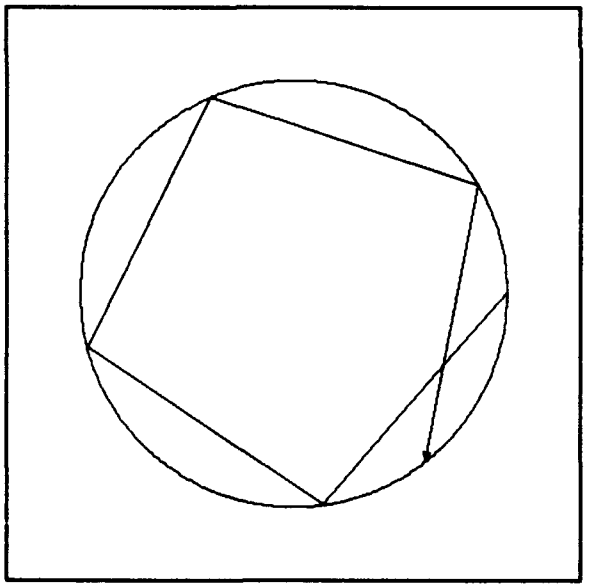

FIGURE 55
Circumferential Parasitic Mode

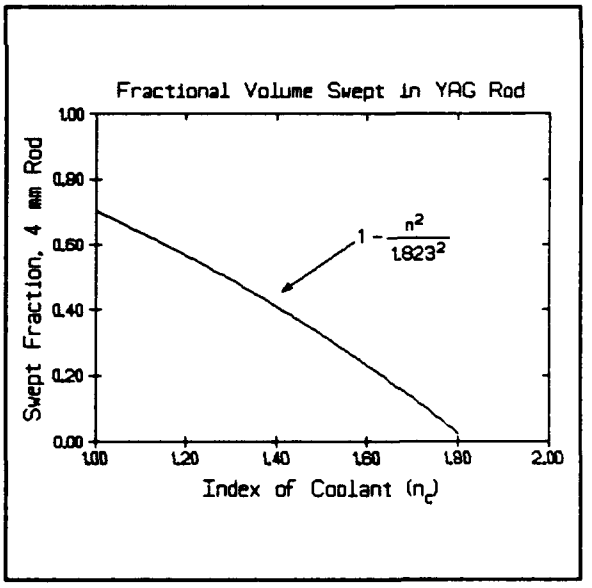

FIGURE 56
Fraction of YAG Rod
Swept by Circumferential Mode

Thermal effects are not likely candidates. We looked for gross output beam defocusing, and saw none, although monitoring for beam depolarization would have been more sensitive. More importantly, thermal effects would be dependent solely on pumping power, and the roll-over in Figures 52 and 53 is clearly output coupler dependent.

Single- and multi-photon absorption of the laser light in YAG would have been discovered a long time ago, so we can dismiss that. Similarly, single- and multi-photon absorption of the pump light would roll over the fluorescence output in Figure 54, so we can rule that out too. An absorption responsible for the roll-off in Figures 52 and 53 must involve the laser light, or else it would appear in the fluorescence output, and it must include the narrow-band diode pump light, or else it would have been observed before. Thus, the only possible absorption processes must be two-photon, encompassing both laser and pump light. The sum frequency is at about 21,805 cm^{-1}. Because the diode emission has a spectral width of about 2 nm, an absorption must be of comparable or greater width to have a significant effect on the system. Such an absorption could be either from the ground state, or an excited state. A ground-state absorption would be at about 458 to 459 nm. This corresponds to a moderate $^4G_{11/2}$ absorption at 460 nm. Without an intermediate level, there would be no enhancement of the absorption due to parity considerations in this two-photon case.

There are three possibilities for excited-state two-photon absorptions: from the lower laser level and from the R1 and R2 levels of the upper laser level. We can dismiss an absorption, at about 21,890 cm^{-1}, from the lower laser level, because the population in it is insignificant at this low power. We estimate the population of the lower laser level, at our maximum pumping rate, to be of the order of 10^{-7} to 10^{-9}, exclusive of the thermal population. The upper laser level is split by 85 cm^{-1}, so two-photon absorptions from either of them would lie at about 31,280 or 31,370 cm^{-1}. Either absorption would need to be of the order of 100 cm^{-1}, or greater, wide. There are two nearby levels, a $^2H_{9/2}$ O level at 31,600 cm^{-1}, and a $^2L_{17/2}$ N level at 30,800 cm^{-1}. Additional experiments, performed with the diode wavelengths tuned to another YAG absorption, might test this fairly readily. Thus, although we cannot rule out two-photon absorption, the case for it being the culprit on Figures 52 and 53 is far from complete.

Despite the circumferential parasitic mode being an unlikely candidate as a problem in these data, there is future interest in techniques for suppressing it. One, suggested by Figure 56, is to index-match the coolant to the YAG rod. Instead of index matching the coolant, the rod may be surrounded by a sleeve of sapphire sufficiently thick that the mode is confined entirely to the sleeve, where there is, of course, no gain. Another way to suppress this mode is to cut narrow grooves longitudinally or spirally in the edge of the rod, introducing additional loss to the circumferential mode.

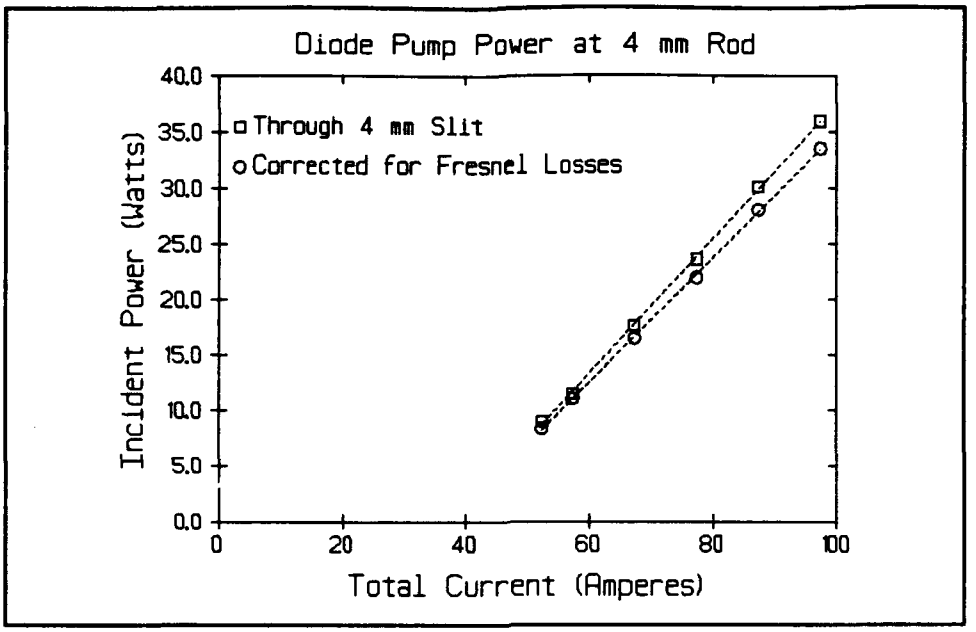

FIGURE 57
Diode Pump Power Through 4-mm Slit

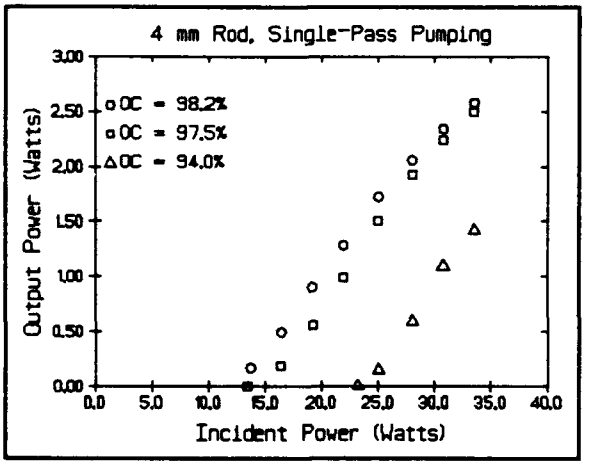

FIGURE 58
Laser Performance, 4-mm Rod
Single-Pass Pumping

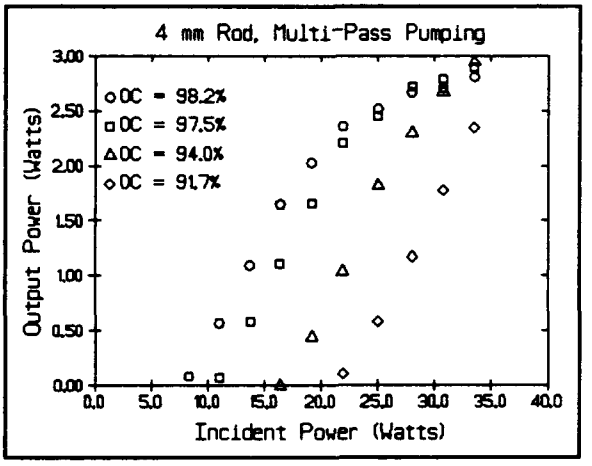

FIGURE 59
Laser Performance, 4-mm Rod
Multi-Pass Pumping

Figures 52 and 53 are plotted against the diode current. Figure 57 presents the optical power measured through a 4-mm slit at the rod location, but without the pumping wheel in place, as described in Section IV. Also presented is an estimated correction for Fresnel losses, to show the total incident pump power in the rod on the first pass. With that, we can replot Figures 52 and 53 against incident pump power, which is done in Figures 58 and 59. Figures 58 and 59 include only points from Figures 52 and 53 that correspond to points in Figure 57 where the linear interpolation is known to be valid.

In addition to the threshold data from Figures 58 and 58, the passive losses in the laser cavity are needed. The measured losses are as follows:

3-mm x 35-mm rod	0.68%
4-mm x 40-mm rod	1.36%
97.5% (nominal) output coupler	1.79% (98.2% R)
95.0% (nominal) output coupler	2.56% (97.4% R)
92.5% (nominal) output coupler	5.96% (94.0% R)
90.0% (nominal) output coupler	8.33% (91.7% R)

The 5-meter radius HR mirror loss was unmeasurable by our technique; we take it as less than 0.5 percent. Figure 51 showed the laser cavity configuration. Because of the large Fresnel number (>40), the diffraction losses are taken as zero. In the Rigrod calculations we use the round-trip loss of (2 x 1.36) + <0.5 as 3.25 percent. The results are not sensitive to small variations in this loss. Figure 60 shows the calculated threshold for the 4-mm rod plotted with the best-estimate of the thresholds from Figures 58 and 59. The experimental thresholds are projections of best-fit lines through the output data near threshold, avoiding the knees near zero output caused by pumping non-uniformity.

The 4-mm rod used had excessive passive losses, measured at 1.36 percent per pass. This is a combination of internal absorption, scattering, and imperfect AR-coating losses. The internal absorption is limited to about 0.05 percent per cm, while the scattering and coating losses can approach nil. For comparison purposes, Figure 60 includes the Rigrod-calculated thresholds for a more realistic passive loss of 0.2 percent per pass, 0.4 percent round trip.

From Figure 60 we can directly deduce the efficiency of utilization of the available diode-output pump light in both the single-pass and multi-pass configurations. The slopes of the best-fit lines in Figure 60 are in the ratios 1.84 : 1.42 : 1.00 (single-pass : multi-pass : calculation). The values at 94-percent output coupler reflectance are consistent with this, being in the ratios 1.88 : 1.33 : 1.00. These imply the single-pass configuration utilizes 54 percent of the available pump light, and the multi-pass configuration is about 1.35 times as efficient, utilizing 74 percent of the available pump light.

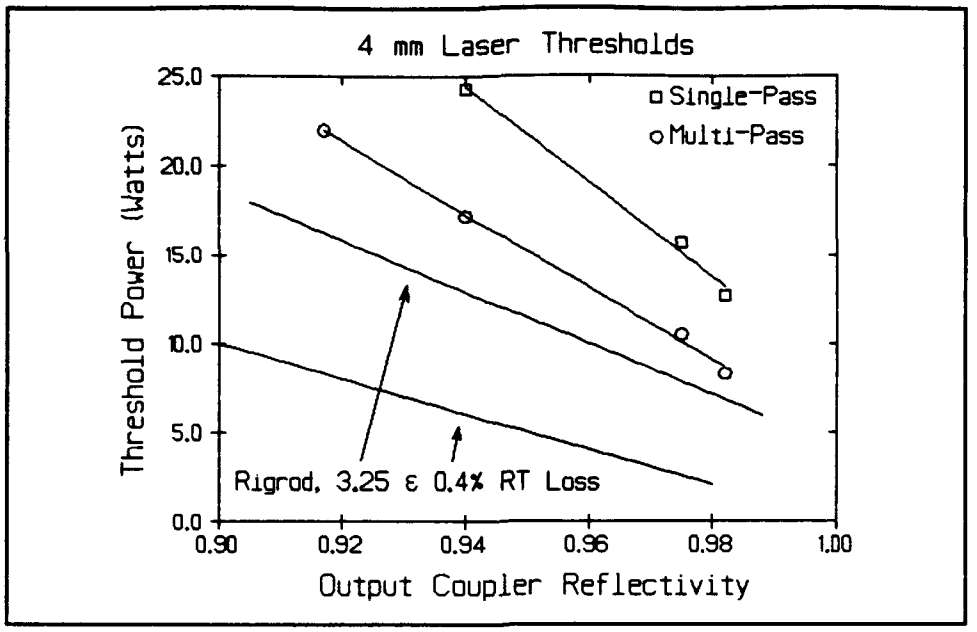

FIGURE 60
Calculated and Experimental Laser Thresholds
4-mm Rod, 3.25- and 0.5-Percent Round Trip Loss

In the first year analysis (TTC-1529-R, page 40) the over-all pumping efficiency of the multi-pass geometry was estimated at 75 percent, with the first-pass efficiency being about 63 percent (1.20-fold multi-pass improvement). This was for a 3.2-mm diameter rod and an average σ = 3 cm^{-1}. The experimental data in Figure 60 differs from this calculation in that the calculation included some of the losses between the diode and the rod, while Figure 60 is based on measured power at the rod location, with additional correction for estimated Fresnel losses.

For the pumping-wheel geometry used here, Figures 18 and 19 showed the multi-pass improvement expected to be about 1.5 improvement expected. The experimental results, with an efficiency of over 70 percent, and a multi-pass improvement factor of 1.35, are consistent with these expectations. Lower first-pass absorption, which raises the multi-pass improvement factor, implies a lower σ-l product in the rod. These experimental data indicate an average value of σ of 3 cm^{-1} or less, as assumed in the first-year multi-pass pumping calculations and much of the Section III analysis.

From Figures 58 and 59 we can also determine the slope efficiencies. For the multi-pass pumping case the average of the four slopes, below the roll-over, is 20.7 percent. In the single-pass case, it's 15.5 percent (3 estimates). This also reflects a 34 percent improvement in pump light utilization in the multi-pass geometry.

We can write

$$P_{Threshold}\alpha\ell - \gamma\ell = -\frac{1}{2}\ln(R)$$

where R is the reflectivity of the output coupler, $\exp(-\gamma\ell)$ is the single-pass loss term, and $\exp(+P_{Threshold}\alpha\ell)$ is the single-pass gain. For the multi-pass configuration, we have four output couplers and four threshold powers, as follows:

A. (R=0.982) (8.3 watts)$\alpha\ell - \gamma\ell = 0.0091$

B. (R=0.975) (10.5 watts)$\alpha\ell - \gamma\ell = 0.0127$

C. (R=0.940) (17.2 watts)$\alpha\ell - \gamma\ell = 0.0309$

D. (R=0.917) (22 watts)$\alpha\ell - \gamma\ell = 0.0433$

From the six possible pairs of these equations, we get six estimates of $\alpha\ell$ (in units of watt^{-1}), as follows:

A-B	0.00164	A-C	0.00245	A-D	0.00250
B-C	0.00272	B-D	0.00266	C-D	0.00258

Because the reflectivity in cases A and B are very close, the errors are relatively large compared to the difference between the two. Thus, it is not surprising that the A-B difference equation falls significantly away from the other five pairs. It is also fair to exclude it from the analysis. The mean value of $\alpha\ell$ for the other five pairs is 0.002582 $\pm$0.000111 ($\pm$4%) per watt.

With the same four equations, we can get four estimates of the single-pass loss. The average value is 0.01344 $\pm$0.00085 ($\pm$6.3%). Thus, it would appear that our estimate of 3.25 percent round-trip loss, used to calculate the Rigrod approximation line in Figure 60, is too high, lying 3.3σ above the mean. Indeed, the value calculated here is almost exactly equal to the measured passive loss in the 4-mm rod (0.0136), implying the assumption of zero diffraction losses is right (which we knew) and the HR mirror may be substantially better than the assumed 0.5 percent loss. But the 3.25 percent original estimate is close enough to the mean (best estimate), and we know the best estimate (mean) calculated here must be a bit low, so we won't change the 3.25-percent baseline in Figure 60. Decreasing the round-trip loss in Figure 60 from 3.25 percent to 3.0 percent decreases the estimated efficiencies by about 0.984, which is an insignificant correction.

The single-pass threshold data (Figure 58) give four equations, as follows:

A. (R=0.982) (12.7 watts)$\alpha\ell - \gamma\ell = 0.0091$

B. (R=0.975) (15.7 watts)$\alpha\ell - \gamma\ell = 0.0127$

C. (R=0.940) (24.3 watts)$\alpha\ell - \gamma\ell = 0.0309$

From the three pairs of equations, we get estimates of $\alpha\ell$ per watt, as follows:

A-B 0.00164 A-C 0.00245 B-C 0.00272

Not surprisingly, the estimate is poorer than in the multi-pass case. Our best estimate of $\alpha\ell$ is 0.00173 $\pm$0.000477 ($\pm$28%) per watt and of $\gamma\ell$ is 0.0128 $\pm$0.0017 ($\pm$13%).

In summary, the threshold data for the 4-mm rod indicate an effective single-pass loss of $\gamma\ell$ = 0.0134 and a single-pass gain of $\alpha\ell$ = 0.0026 per watt incident multipass and $\alpha\ell$ = 0.0017 per watt incident single pass.

Figure 61 shows the multi-pass 4-mm output data and the Rigrod theoretical performance for three conditions with σ = 3.4E-19 cm^2, a quantum efficiency of 0.9, and a quantum defect of 0.76:

34 watts absorbed power with 3.25 percent round-trip losses
(lower curve, representative of the experimental conditions),

34 watts absorbed with 0.2 percent round-trip losses
(representative of a low loss 4-mm rod), and

40 watts absorbed with 0.2 percent losses
(representative of better diode collimating lenses).

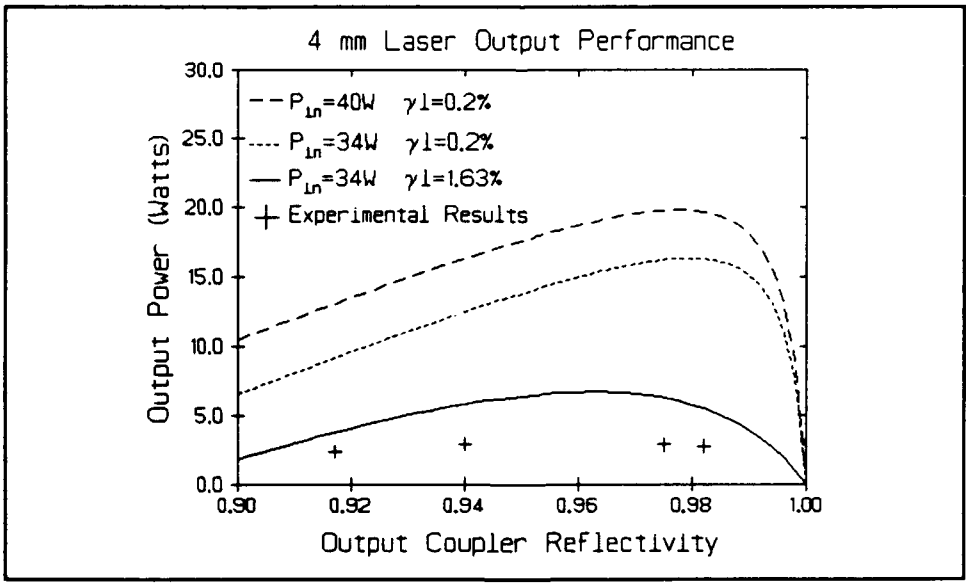

FIGURE 61
4-mm Laser Output Performance, Calculation and Experiment

From these data we can conclude the following:

- The use of diode-lens pairs allows standoff from the laser rod while maintaining efficient utilization of diode output light.
- Multi-pass transverse pumping allows efficient utilization of diode pump light with small diameter rods of low σd product.
- Diode arrays can be water cooled with adequate temperature control and heat transfer rate.

There are some shortfalls too, as follows:

- There is some, not fully explained, mechanism limiting the laser output.
- The 4-mm rod had excessive losses for these tests, the losses being of the order of 10 times achievable levels.
- The low available diode output power for pumping limited the extent of testing of thermal effects.
- The multi-pass pumping chamber requires refinement, including optimized entrance window size, AR coating of the windows, and enhanced internal reflectivity.
- The diode-lens pairs require refinement, including optimization of the lens type and figure, and improved AR coating.

Despite these limitations, the 4-mm multi-pass pumping achieved a slope efficiency of 20 percent and an over-all efficiency of over 11.5 percent in these experiments. The results would improve significantly with more pump light, a lower-loss crystal, and solution of the output roll-over most evident in Figure 53. Figure 61 shows that up to a five-fold improvement in output should be possible with the diodes used.

3-mm Diameter Rod Experiments

The same laser configuration was run with the 3-by-35 mm rod in place, using the same pump configuration and laser cavity mirrors. Figures 62 and 63 present the experimental results.

As with the 4-mm case, the diode output light was measured at the rod position through a 3-mm slit. Figure 64 presents these data, along with an estimated correction for Fresnel losses in the first pass of the actual pump geometry. Figure 64 differs insignificantly from the 4-mm data, Figure 57. Combining Figures 62 and 63 with Figure 64 gives the laser performance shown in Figures 65 and 66.

It is apparent that the 3-mm rod data suffers from more gain-profile non-uniformity than the 4-mm data. Also, the multi-pass data in Figure 66 looks particularly suspect, and suffers from the output-saturation evident in the 4-mm data. Figure 67 shows the thresholds for lasing versus output coupler reflectivity. Also shown is data for the Rigrod approximation with 2 percent round-trip losses. Figure 67 indicates that the experimental setup with the 3-mm rod did not perform as well as the setup with the 4-mm rod (Figure 60). This is probably due to the greater alignment sensitivity of the smaller rod. The cooling channel was the same for both rods, thus the cooling channel inside diameter was larger than optimum with the 3-mm rod. Despite our interest in laser systems with 3-mm rods, we believe these data do not merit further analysis.

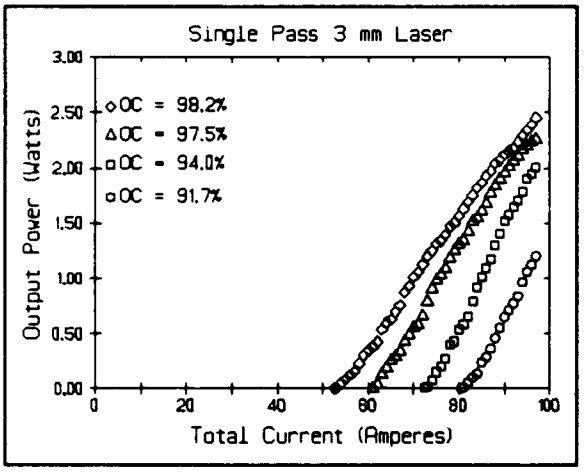

FIGURE 62
3-mm Rod, Single-Pass Pumping

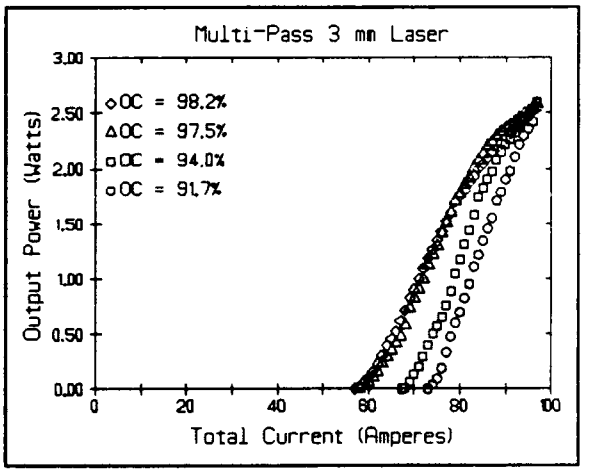

FIGURE 63
3-mm Rod, Multi-Pass Pumping

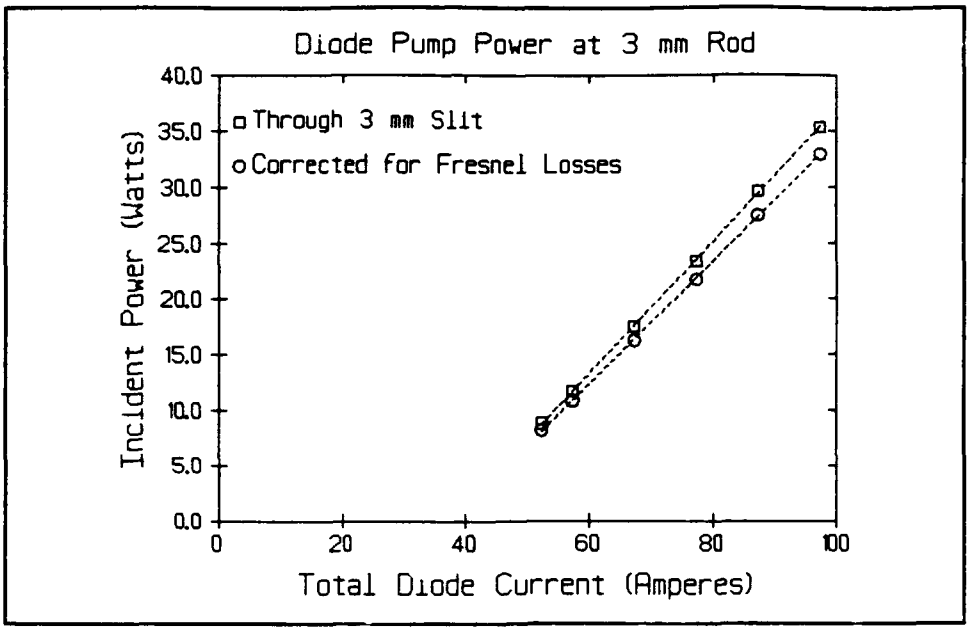

FIGURE 64
Diode Pump Power Through 3-mm Slit

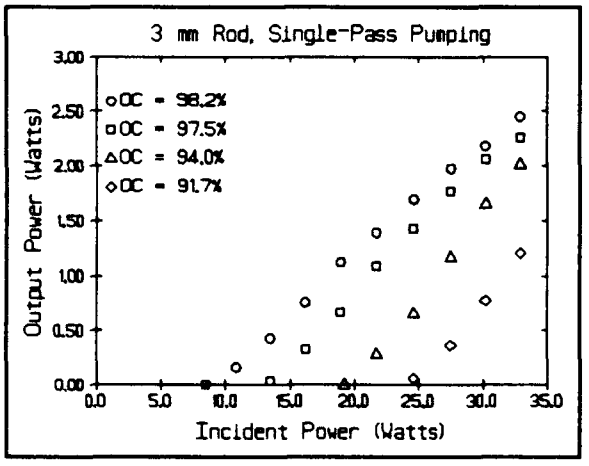

FIGURE 65
Laser Performance, 3-mm Rod
Single-Pass Pumping

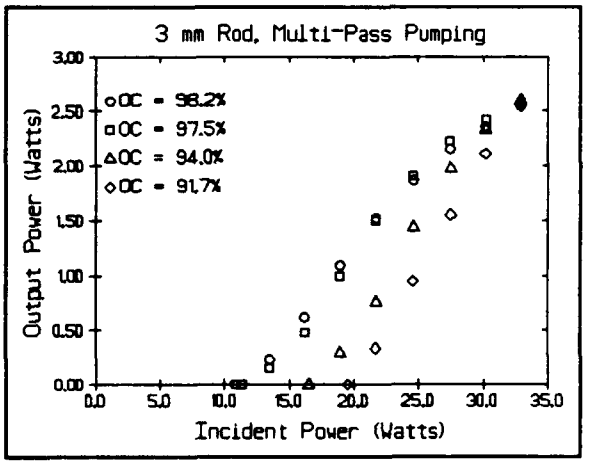

FIGURE 66
Laser Performance, 3-mm Rod
Multi-Pass Pumping

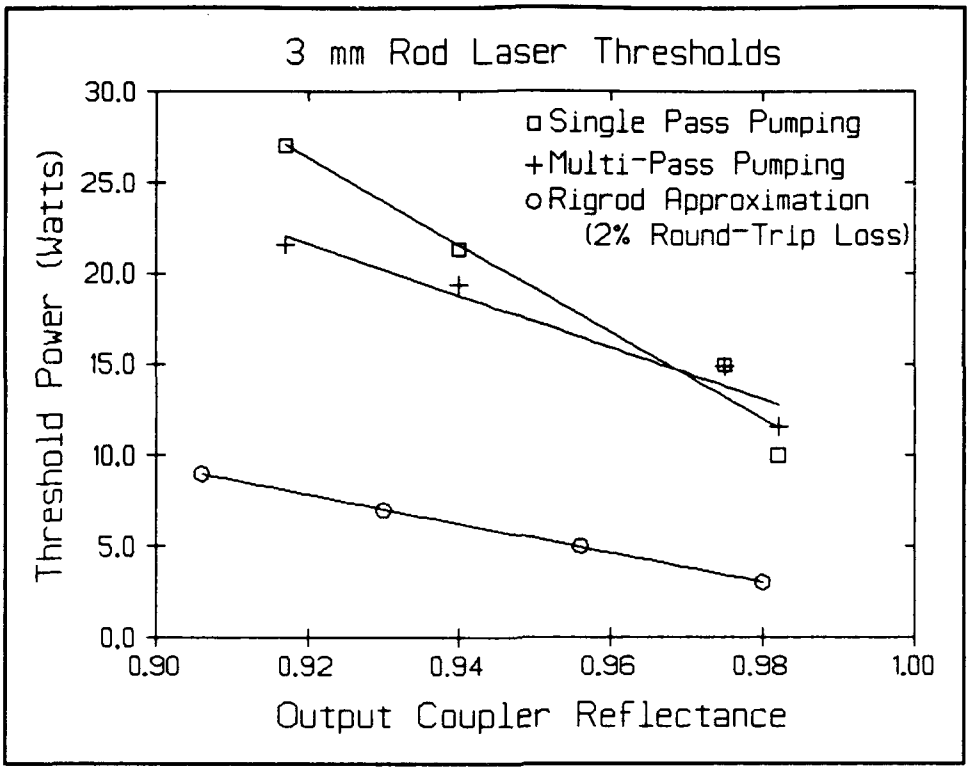

FIGURE 67
Laser Thresholds with 3-mm Rod

SECTION VI

LASER SYSTEM CONSIDERATIONS

This section is a brief discussion of systems implications for transverse-pumped solid-state lasers. With the basic pumping concepts validated, systems analyses will assume greater significance, with appropriate use of program resources, during the next contract period.

Electrical Efficiency

Individual diode arrays present an unacceptably low electrical impedance, for example, 2 volts at 10 to 15 amperes is of the order of 150 to 200 milliohms. Driving such low impedances incurs two penalties: low electrical efficiency and excessive weight. The low efficiency occurs because the practical impedance of the power supplies and connecting wiring will be of the same order of magnitude as the diode load, so the circuit losses would be comparable to the power delivered to the load. The weight penalty comes from the amount of conductor required to route around the high currents with even moderate losses. Practical systems require multiple diode arrays and optimization of the strategy for powering the diodes. Considerations of reliability and complexity must be weighed along with efficiency and weight.

The diode channels within each bar are electrically paralleled. This is a consequence of the channels being diffused into a single bar. The inherent parallel nature of the electrical flow within each bar results in the low impedance cited above, and explains why the impedance gets lower (i.e., worse) as the power of diode arrays increases. Two questions arise when devices are paralleled, concerning reliability and current sharing.

The reliability question involves the failure mechanisms intrinsic to the devices. The electrical power grid is an example of a parallel-load network of high reliability; loads either intrinsically fail open, or if they short-circuit, they are quickly isolated by individual isolation devices (fuses or circuit breakers). If neither of these conditions were satisfied, the failure of any light bulb would bring down the entire electrical grid. There is no reasonable opportunity to fuse individual diode channels on a bar, so the question of intrinsic failure mechanisms must be addressed. If diode channels fail by becoming electrically shorted, then a bar can have a useful lifetime no longer than its least reliable channel, and parallel

connected arrays would require over-current isolation for each array. Conversely, if diodes fail electrically open, then operation of individual bars is unaffected by failure of a few channels, but serious system reliability questions must be addressed if bars are to be connected in electrical series. Fortunately, based on data from Spectra Diode Laboratories, other manufacturers, and users, neither of these failure modes appear to occur. Diode laser channels appear to fail by simply ceasing to emit light. This leads to a thermal design issue, since if the channel is not emitting light, then its efficiency is zero, and all of its electrical input must be dissipated locally as heat. Electrically, however, the failure of a channel, or even a whole bar, appears to have little consequence.

The current sharing issue is more complex. Semiconductor devices do not inherently share current equitably when connected in parallel. The underlying physical cause is the negative temperature coefficient of resistivity of all semiconductor materials. If the current in some region becomes slightly higher than in the neighbors, the region is heated slightly, the band-gap decreases slightly, and the current increases there. This run-away cycle has no intrinsic limit within the device. Early experience with DCTL (Direct-Coupled Transistor Logic) showed that the problem is impossible to solve with discrete devices. More recent experience with IIL (Integrated Injection Logic) shows that over small regions of a single chip, with good thermal coupling, and clever circuit design, semiconductor devices may be effectively paralleled and share current effectively. Some large power transistors were also fabricated in the past, but they usually incorporated enough bulk resistance to swamp out the thermal change in the band gap, at the expense of high losses and hence low efficiency. Present-day large-scale thyristor structures show that large-area uniform current distributions can be achieved in semiconductor structures, although the attendant gate structures are exceedingly complex and these designs are based on three decades of experience, some of it not so pleasant. Present-day high-current MOS-FET structures often include hundreds of paralleled devices within a single package, showing, like the IIL case, that the problems of parallel operation of semiconductors are soluble within prescribed limits. Diode array bars appear to depend on a combination of techniques. As in early high-power transistors, there is enough electrical resistance in the structure to force current sharing, at the expense of efficiency. Additionally, since the channels in a bar are fabricated at the same time, they have properties that closely track in current and temperature, so that there is an inherent degree of capability to operate in parallel, such as in IIL. The downfall in paralleling channels within a diode bar is in the thermal management. The bar has such a large aspect ratio, and the heat dissipation density in the channels is so great, that there is little effective thermal coupling along the bar intrinsic to its structure. The device fabricator must control the thermal environment, and provide the thermal coupling between areas of the bar, with the package. This requires thin, uniform metallization layers, void-free brazes, high thermal conductivity heat spreaders, and close attention to thermal gradients and edge effects. In many respects the advances in laser diode arrays focus on exactly two areas: achieving uniform properties across the wafer and providing a mounting and

packing technology that assures an isothermal environment for the bar. If those conditions can be achieved, the electrical resistance of the bulk material in the bar can be decreased without sacrificing thermal stability and lifetime, and the over-all efficiency will then improve all by itself. The data presented in Section IV would indicate that SDL has made substantial progress in these areas, but there is still much room for improvement.

The argument above indicates that the channels on a bar may be operated in parallel, which we knew. That leads to the low device impedance mentioned. However, these arguments both weigh against parallel connection of multiple bars. If current sharing among the channels of a bar is a problem, attempting to current share among paralleled bars is likely to have a significant efficiency penalty. Further, if one bar has a distressingly low impedance, paralleling bars just makes it worse.

There are two alternatives to parallel connection of bars: series connection and separate power supplies. Series connection is the only viable system concept, since a separate supply for each diode array is unrealistic in at least cost, size, and weight. The first fundamental requirement of series operation is that the individual bars do not fail electrically open. As indicated above, this requirement is satisfied. There are two additional requirements: that the series-connected bars operate at the same current and that they be electrically isolated from the common structure. These requirements are discussed below.

During the experiments this year the diodes were operated from individual power supplies. This allowed the operating currents to be individually adjusted for five watts output. Although the operating currents are not tabulated in Section IV, Figure 37 shows the current spread among the devices. We can see that, for the high-efficiency (low threshold) group of devices, a current of 8 amperes would produce 4 to 5 watts output per device. Thus, even with this group of devices that were selected for wavelength only, the system designer could achieve constant-current series operation with only a ± 10 percent spread in power output. Presumably, this spread will be reduced with further development and production experience.

Electrical isolation is more difficult. The channels are diffused into the "p" side of the bar, so thermal conductance requirements dictate that the bars must be mounted with their "p" in close thermal (and mechanical) proximity to the heat sink. There are two ways to achieve electrical isolation between bars: use of an electrically insulating heat spreader in the thermal path, or electrically isolating the individual heat sinks. The electrically insulating heat spreader is very attractive to the systems designer. Three materials have been considered or used. The most attractive is diamond, which has excellent thermal conductivity and is an excellent electrical insulator. Bonding to diamond is also not a major problem. Diamond is, however, expensive. Only a small piece is required per bar,

so the cost is tolerable, but continued improvements in the costs of laser diode bars will put increasing pressure on package costs, making diamond increasingly unattractive. Beryllia is a second choice, with a long history of use in high power vacuum tubes and integrated circuits. Although inferior to diamond, its thermal and electrical properties are very good. However, beryllia in powder or dust form is highly toxic, so handling and machining it is expensive. Because of the toxicity, the DoD is placing considerable effort on eliminating it from integrated circuits. A complete ban of its use in military systems is not improbable. The best alternative to beryllia identified to date is cubic boron nitride. Its thermal properties are less desirable, but it appears feasible to fabricate integrated circuit packages with it. Diode laser arrays, however, operate at significantly higher thermal power densities than do microwave and VSHIC ICs. Optimum diode designs may become incompatible with the heat transfer capabilities of cubic boron nitride (or similar) heat spreaders in the thermal path.

The alternative to electrical isolation of the bar is electrical isolation at the heat sink. This means a separate heat sink for each bar, an electrically non-conductive coolant, and mechanical complexity. On the positive side, the system voltages are small, and the currents large, so electrical isolation is not difficult. There is one approach that may represent a solution to this. LLNL has developed, from Stanford University work for IC cooling, silicon microchannel coolers of high heat transfer capability (of the order of 1 kW/cm^2). High purity silicon has a bulk electrical resistivity of the order of 0.1 ohm-cm. Although this resistivity is still low enough to classify silicon as a metal, it is 3 to 5 orders of magnitude greater than that of other metals. LLNL's techniques of direct-bonding of the GaAs diode bars to the Si cooler chips leaves a relatively small package to be electrically insulated from the structure, with virtually no thermal requirements placed on the insulator material. As with any water-cooled electrical system, galvanic corrosion issues must be considered and resolved. We anticipate no intractable problems in this area.

Importantly, series operation of significant numbers of diode arrays addresses the issue that brought us to this discussion of connection methods: efficiency. The impedance of the load that must be handled by the power supplies and the wiring increases linearly with the number of devices series-connected. The losses in the wiring, and the weight of the wiring, however, remains relatively constant per circuit. So the circuit losses are a decreasing fraction of the diode power as the number of diodes in each series connected circuit increases. As with all such things, the greatest improvement is with the first few, and the improvement is asymptotic. Series connection of array pairs halves the system wiring losses and weight, and reduces the power supply losses too. The optimum number of series connected devices is likely to depend on the vehicle power bus and system power supply details.

In summary, the low impedance of diode arrays is an efficiency and weight issue, but not a reliability problem. Series connection of the arrays addresses this problem, and appears completely feasible. And, LLNL's cooler technology may allow decoupling of the thermal and electrical constraints in the design process, although there could be galvanic corrosion issues. TTC's liquid coolers, demonstrated in this contract, require more attention to electrical isolation. The use of electrically insulating heat spreaders on the diode bars is an electrically attractive option with all cooling technologies, but carries cost and perhaps thermal penalties.

Grounding

MIL-STD-1541 requirements for ground isolation have served well for simple systems, especially with DC power buses. The trend toward larger spacecraft will lead to AC power distribution, following the trend first set in urban power distribution, then aboard ships, and in the past 45 years aboard aircraft. This trend may be expected to lead to the growth of more stringent ground isolation requirements, as have been already developed for the proposed space station. As discussed previously, electrical efficiency and weight constraints will drive the designer to series electrical connection of multiple diode arrays in laser systems. Solution of the ground isolation requirements dictated by series connection of the diodes will automatically address the major grounding issues imposed by the vehicle power distribution system. There is no inherent reason why diode-pumped laser systems should be in conflict with present or future DC grounding requirements.

In addition to DC grounding requirements, future specifications may impose limitations on the flow of displacement currents in the grounds and structure. Purely cw diode-pumped systems would be unaffected by such requirements (except, of course, in the power supply design). Quasi-cw operation poses more concern. The relatively long pulses expected to be characteristic of quasi-cw operation will minimize displacement currents coupled to the grounds. Conversely, laser diode efficiency and power switch efficiency arguments will encourage relatively fast turn-on and turn-off times, increasing capacitive displacement currents. Switching the large diode currents also contribute to larger AC ground currents. The degree of difficulty will be strongly system dependent, but the designer may be faced with an efficiency versus ground current trade off that does not appear in the pure cw case. In general, ground current specification limits are absolute, and are expected to become more restrictive as systems become more complex.

Diode-Laser Reliability

Laser diodes do not have standard failure rates in MIL-HDBK-217E, which is not surprising. The technology and fabrication techniques are rapidly evolving, and lifetime and failure rate data are sparse. With the future applicability of present data in question, it is clear that the reliability and lifetime of future devices will be better than for present devices. Much of the conventional thinking about the reliability and failure modes of electronic systems is not applicable to diode-pumped solid-state lasers, because of the high level of redundancy and the lack of catastrophic failure mechanisms. Diode pumping subsystems are highly redundant, both on each diode array bar, and as a system as a whole. A transversely pumped laser rod will be pumped by thousands of diode channels located in tens of bars arrayed around the rod. Degradation or failure of individual channels will have negligible effect on the total pump light available, or on the uniformity of its deposition in the rod. Within limits, total system input power can be increased to offset the loss of channels.

Diodes are known to degrade with age. Figure 36 (Section IV) is representative of the data available. In it, the devices are operated at constant output, and the required input current is monitored. In essence, the device efficiency decreases throughout its lifetime. At some point one must declare that end-of-life has occurred. This may be when there is limitations of the power supply or the supply bus are reached, or when the power dissipation in the diodes reaches the package thermal design limits, or when the cooling system is no longer able to hold the devices to the proper temperature and wavelength, or (with power-limited input) when the pump light available to the laser is inadequate to sustain the necessary inversion.

Although the system efficiency will degrade as the diodes age, the additional input power is not dissipated in the laser rod. Indeed, the laser rod is completely isolated from diode efficiency, power, and cooling issues. Thus the system optical design and performance will be invariant to the changes occurring with diode aging. This simplifies the system design, and also simplifies the design process in that the laser optical design can be completely decoupled from system issues resulting from diode aging and efficiency degradation. This decoupling of design and performance issues from a major system ageing mechanism is not typical of flashlamp or direct electrically pumped lasers.

As a result of these considerations, determination of the effect of diode array aging on standard measures of system performance and reliability will be highly design and system dependent. Also, the conventional measures of reliability, which have proven so suitable for most electronic systems, must be applied very carefully to highly redundant subsystems like the diode laser arrays.

Laser Maintainability

When the failure modes are gradual, measurable, and predictable degradations of performance, the system will benefit significantly from scheduled maintenance procedures, if feasible. Although this consideration is usually not relevant for space-based assets, it is very attractive for ground- and ship-based and especially airborne systems. Whereas a flashlamp pumped laser system fails totally and catastrophically when the flashlamp fails, the equivalent diode-pumped system can be expected to degrade gracefully over hundreds to thousands of hours of operation. Maintenance can be performed when convenient, or postponed when inconvenient, and completion of the current mission is never an issue. Although this argument doesn't apply to the entire laser system, it applies to the diode subsystem, which replaces the flashlamp in a conventional laser system. Flashlamps are a life-limited, often catastrophic, single-point failure in most laser systems. Recent engineering practice of limiting the energy input to the lamps, and high standards of quality control in production, have reduced the frequency of premature or catastrophic flashlamp failures, but the lamp is always a single-point failure component in the system. Laser pumping with diode arrays fundamentally changes that.

Applications where maintenance is feasible require realistic assessments of the system design to assure that the potential benefits are realized. MIL-HDBK-472 provides several well-tested methods of evaluating the maintainability of system in the design and prototype stages. The TTC-NRL transversely pumped rod geometry provides opportunities to improve the system maintainability as defined by accepted measures set forth in MIL-HDBK-472. One improvement we have identified is use of prealigned diode-lens modules as sealed, slip-in SRAs. Prealignment and sealing reduces maintenance time and protects the diode facets and all but the final lens surface from contamination. The ruggedness and simplicity of such a module should simplify designing the system to meet environmental (vibration, shock, temperature, altitude, and humidity) requirements.

The solid, filled pumping cavity is also a maintenance asset. It reduces the number of parts by eliminating the coolant jacket, which is a fragile piece. The use of diodes automatically eliminates the flashlamp cooling jacket also. Additionally, the pumping reflector becomes an internal surface, protected from coolant leaks, atmospheric contamination, and maintenance-induced failures.

Another potential improvement inherent to this design is the use of the solid pump cavity as a major structural piece, supporting either or both the pumping diodes and the laser cavity optics. Supporting the laser optics may require the use of very-low expansion materials in place of the fused silica utilized in our demonstration experiments this year. Two very low expansion materials were examined for this application, Corning ULE 7971 and Schott ZeroDur. Both are titanium silicates and are available in grades meeting or exceeding the optical requirements for the pump cavity.

Diode Wavelength Control

Wavelength control is a significant systems issue in the application of diode arrays for laser pumping. In the past, diode emission wavelength was controlled by precise temperature control with thermoelectric cooling. This has a significant system's efficiency penalty, as well as adding weight and complexity. In this program we demonstrated two technologies addressing this issue: multi-pass pump cavity design and direct liquid cooling. Multi-pass pumping allows operation off the pump absorption peaks, with a small rod diameter, and without sacrificing pump-light utilization efficiency. This pumping geometry thus reduces wavelength control requirements slightly, sufficient to allow use of TTC's direct liquid coolers, as we demonstrated. The resultant elimination of thermoelectric coolers simplifies the system and boosts over-all system efficiency.

Certainly, the system would benefit from even further relaxation of wavelength and/or temperature control requirements. Combinations of laser ions and hosts with broader absorption characteristics than Nd:YAG, but with comparable absorption depths, would simplify the designs further. Alternatively, the use of injection-locking techniques to stabilize the diode laser output frequency in the presence of temperature pulling, would also relax temperature control requirements while maintaining wavelength control. We did not seriously examine the use of injection locking for wavelength control, since it is beyond the scope of this program. However, NRL has performed numerous experiments defining the injection-locking gain and pull-in range of diodes operating under a variety of conditions. In general, there will be a tradeoff between required injection power and required temperature stability to hold a specific diode array design within a specified wavelength window. There are too many variables in a system design to give specifics at this point.

SECTION VII

CONCLUSIONS and RECOMMENDATIONS

This section discusses the conclusions reached with the analyses and experiments done to date. The most important tasks for further experimental verification and analysis have been reevaluated in light of the additional progress this year, and are presented. They lead naturally to identification of specific additional equipment, experiments, and calculations recommended for future work. Completion of the recommended program will present the comprehensive understanding of tradeoffs, limitations, and strengths of the transversely pumped rod geometry for diode-pumped solid-state lasers needed to support future systems studies and point designs.

Conclusions

We conclude the use of cylindrical collimating lenses paired with laser diode arrays allows effective standoff of the diodes from the laser rod, allowing more diode arrays to be installed around the rod for increased pumping.

The use of the multi-pass pumping geometry allows effective pumping of small-diameter laser rods with limited σ-d product.

Direct liquid cooling can effectively cool diodes and maintain adequate temperature control, negating the need for thermoelectric cooling devices.

Our laser rods, especially the 4-mm rod, have excessive passive losses for efficient use in low-power, low-gain cw oscillators.

Our laser configuration would be subject to circumferential parasitic modes at higher pump rates, requiring introduction of effective suppression techniques.

Some mechanism, as yet unidentified, limited the unsaturated gain and output power of the experimental laser to very low levels. This precluded demonstration of the efficiency and output power expected for this experiment.

Analysis of laser threshold data shows the multi-pass pump cavity was about as effective as expected.

Recommendations for further work

Additional work is required to improve the light distribution patterns of the diode collimating optics, including examination of reflecting options, use of Fresnel lenses, and/or use of multi-element lenses.

Additional work is required to reduce losses in the diode collimation optics, including improved AR coatings and Fresnel/reflecting/multi-element designs.

The entrance windows to the pumping cavity wheel require optimization, including minimizing the window area and AR coating.

Coating techniques for the pumping cavity wheel require further development to achieve high reflectivity (>90 percent) and high adherence simultaneously. Sputtering, electron-beam evaporation, and chemical deposition techniques merit further investigation.

The coolant channel and rod diameters require optimization in addressing specific system designs.

An effective technique must be applied to suppress the circumferential parasitic mode, which would occur at higher pumping rates.

Very low-loss laser rods with excellent AR coatings are required to improve the slope and total efficiencies in low-gain cw designs.

The mechanism causing the roll-over of the gain in these experiments must be unambiguously identified and suppressed.

Laser cavity design must be optimized to demonstrate the best achievable far-field emission pattern.

A complete power flow showing all losses must be prepared and reconciled in detail with experimental data.

More comprehensive thermal modeling is appropriate to understand and optimize laser performance with more realistic levels of pump power.

The multi-pass pumping analysis should be extended from the 3 to 11 arrays around the rod analyzed here to up to about 25 arrays around the rod, identifying efficiency and total pump rate tradeoffs.

More pump power is required to explore and understand thermally induced limits to diode-pumped oscillator and amplifier performance.

More useful lasers than Nd:YAG need to be demonstrated with this technique.

A method of injection-locking the emission wavelengths of the diode arrays should be devised for this configuration and demonstrated to be feasible.

For a selected laser ion and host, a complete tradeoff model should be prepared for wavelength control issues, including system efficiency, cost, and weight.

Diodes with narrower emission spectra and closer wavelength matching than demonstrated by the SDL devices procured for these experiments should be used in future systems.

A design manual providing clear tradeoff methods leading to optimal systems designs using multi-pass transverse diode pumping should be prepared.

The geometry should be extended to cw-pumped, repetitively Q-switched systems, as well as to quasi-cw pumped systems.

APPENDICES

Diode Data Sheets, SDL-3480-L and SDL-3090-S